Structural studies of *trans*-translation

Christopher D. Rae

MRC-Laboratory of Molecular Biology

Robinson College

University of Cambridge

This dissertation is submitted for the degree of Doctor of Philosophy

April 2019

To my sister Michelle

Declaration

This dissertation is the result of my own work and includes nothing, which is the outcome of work done in collaboration except where specifically indicated in the text. It has not been previously submitted, in part or whole, to any university of institution for any degree, diploma, or other qualification. In accordance with the Faculty of Biology guidelines, this thesis is does not exceed 60,000 words, and it contains less than 150 figures.

Christopher D. Rae

April 2019

Abstract

Structural studies of *trans*-translation

Christopher D. Rae

Ribosomes translate messenger RNA (mRNA) into protein in all living cells. The faultless production of protein is critical for a vast array of catalytic and structural roles and is essential for the survival of the cell. Ribosomes themselves are made up of both RNA and protein, and are composed of two subunits, each with a separate function. The small subunit reads the mRNA message, directing the large subunit to synthesize a sequence of amino acids to form a protein. In many cases, mRNA may be damaged or truncated in such a way that ribosomes reach the end of the message and become trapped. Rescuing stalled ribosomes is essential as an otherwise lethal build-up of unproductive ribosomes diminishes the translation capacity of a cell.

This study focuses on an essential pathway called *trans*-translation, which resolves stalled ribosomes in nearly all bacteria. Two factors, transfer-messenger RNA (tmRNA) and small protein B (SmpB), form a complex that rescues the ribosome by terminating translation and releasing the ribosome from the mRNA message. *In vitro* biochemistry in conjunction with cryo-electron microscopy (cryo-EM) was used to visualize frozen snapshots of the ribosome undergoing *trans*-translation. The structures reveal the coordinated movement of tmRNA and SmpB through the ribosome.

Binding interactions between tmRNA-SmpB and the ribosome explain why *trans*-translation only begins on ribosomes that reach the end of an mRNA and not for actively translation ones. SmpB plays an essential role in positioning tmRNA as together they mimic both a tRNA and mRNA. The movement of tmRNA-SmpB results in a stepwise message swapping from the original mRNA to tmRNA, facilitating the rescue of stalled ribosomes. Overall, this structural study advances our atomic level understanding of the mechanism of *trans*-translation.

Acknowledgements

This thesis is a product of opportunity and privilege; I am merely fortunate enough to put my name on it. It is a product of the people who have guided me, both known and unknown, and I hope to recognize them here.

Thank you Venki for giving me a chance to work in your lab. I am inspired by your respect and generosity, you care about us as people and give us the freedom to pursue our interests with unending support. The example that you set has shaped me in the most positive way, both as a person and a scientist.

To all my teachers and mentors, I am forever grateful. To Mrs. Hanna, in whose classroom I first learned about the microscopic world within a cell, your commitment to teaching and your passion for nature motivated my younger self to pursue biology. And to my undergraduate supervisor Ken, your rigorous pursuit of science and teaching fostered my curiosity about the ribosome and directed my interests in molecular biology in ways I could not have imagined. To a dear friend and mentor, Song, thank you for everything. Your guidance helps me tremendously, especially when I first started at the LMB, and your continued friendship and advice have kept me going. Your attention to detail inspires me to pursue science with relentless diligence.

To all the members of the lab, you are more than co-workers; you have become friends. Thanks to Jason, Alan, José, Tanweer, Nathan, Alexey and Israel. I came into the lab lost and you pointed me in the right direction. To those who came after, Seb, Hanting, Jailson, and Aswini, you have brought warmth and enthusiasm to the group and have made our lab the friendly and ambitious place that it is. And of course, to those who were here all along, Nirupa, Vish, Yuliya and a great friend of the hallway Jonida, you are the core, always well resolved. To Nirupa, for fish knives and black ties, and for showing me that adolescence never has to end. To Vish, I have seen you grow into who will become and undoubtedly fantastic young supervisor, you inspire me to help others with the same commitment and patience as you have helped me. To Yuliya, for taking care of anything and everything to keep the lab running, without your support none of us would progress. And to Jonida for your unrelenting pursuit of thought and rejection of the dull, although I still enjoy the train, I always seek the ripest tomatoes.

Thank you Lori and Jason, my secondary supervisors, your critical opinion has always kept me in line and given me confidence in the direction of this work. To Manu,

Reynald and all those who have donated reagents toward this project, your sharing has greatly accelerated the pace of this work. Thank you to Kayla Friedman and Malcolm Morgan for producing this template and to Vish, Song and especially Alina, for your critical reading and review of this document, without you this thesis would be illegible. To my funding sources Gates-Cambridge and the LMB, thank you for putting a roof over my head and food on the table.

To the scientific and support staff at the LMB, you made this work possible. The microscopes, computing power, media kitchen, IT support, biophysics facility and mass spectrometry, among others, are essential for the success of a project and no individual scientist could enjoy these resources without your expertise. And for our clean lab space, the food we eat, the deliveries we receive, the paperwork we don't have to see, the front doors we walk through every day, and undoubtedly all of the things that are taken care of on our behalf; to the LMB staff, thank you. You are the real heroes.

Lastly thank you to my friends, especially to those with whom I've shared a home, your integrity is unmatched and your compassion is unconditional. You have made living in Cambridge more healthy, tasty, cosy, caffeinated, adventurous, interesting, classy, not-classy, and fun than I could have ever hoped. And to my family, from whom I've been far away for far too long, you always support me with your love and I know you will always be there for me. Thank you.

Contents

List of Tables

List of Figures

List of Abbreviations and Acronyms

2D	two dimensional
3D	three dimensional
A site	aminoacyl site
AlaRS	alanyl-tRNA synthetase
ArfA	Alternate ribosome release factor A
ArfB	Alternate ribosome release factor B
ASF	A-site finger
ASL	anticodon stem loop
ATP	adenosine 5'-triphosphate
CP	central protuberance
cryo-EM	cryoelectron microscopy
DNA	deoxyribonucleic acid
DTT	dithiothreitol
E site	exit site
E. coli	Escherichia coli
EDTA	2,2′,2″,2‴-(ethane-1,2-diyldinitrilo)tetraacetic acid
EF-G	Elongation factor-G
EF-Tu	Elongation factor-Tu
EMDB	Electron Microscopy Data Bank
FCwSS	focused classification with signal subtraction
fMet	formyl-methionine
FSC	Fourier shell correlation
GDP	guanosine 5'-diphosphate
GDPCP	guanosine 5′-(β,γ-methylene)triphosphate
GMP	guanosine 5'-monophosphate
GTP	guanosine 5′-triphosphate
GTPase	guanosine 5′-triphosphatase
H. marismortui	Haloarcula marismortui
H2	tmRNA helix 2
H5	tmRNA helix 5
HEPES	2-(4-[2-hydroxyethyl]piperazin-1-yl)ethylsulphonic acid
IC	initiation complex
IF (1,2,3)	Initiation factor (1,2,3)
IPTG	isopropyl β-D-1-thiogalactopyranoside
MLD	mRNA-like domain

mRNA	messenger RNA
NTP	nucleoside 5′-triphosphate
P site	peptidyl site
PDB	Protein Data Bank
Pi	inorganic phosphate
PK	pseudoknot
PTC	peptidyl transferase center
RF (1,2,3)	release factor (1,2,3)
RNA	ribonucleic acid
RNase	ribonuclease
RRF	Ribosome recycling factor
RRF	ribosome recycling factor
rRNA	ribosomal RNA
SD	Shine-Dalgarno
SmpB	Small protein B
SRL	sarcin ricin loop
SspB	stringent starvation protein B
T. thermophilus	Thermus thermophilus
TBE	tris–borate–EDTA
TLD	tRNA-like domain
tmRNA	transfer-messenger RNA
Tris	tris-(hydroxymethyl)-aminomethane
tRNA	transfer RNA

1 Introduction

1.1 A general overview of the ribosome

1.1.1 The ribosome translates the genetic code

The ribosome is responsible for the crucial task of translating one chemical language into another. Organic life depends on messages coded by nucleotides in the form of DNA and RNA to be successfully converted into a sequence of amino acids that forms a protein (Figure 1.1). The intricacies of this process, centered on the ribosome, are the focus of this thesis. Specifically, the work presented concerns a mechanism in bacteria that is responsible for salvaging ribosomes when aspects of translation go wrong. It builds on an extensive body of work examining normal and aberrant translation, which are reviewed briefly below.

Early ideas from Beadle and Tatum suggested that a single gene encodes one functional molecule, or enzyme (*1*). The molecule encoding genetic information was contentious until an elegant series of experiments by Avery, Hershey and Chase established it as DNA (*2*, *3*). Later studies by Schramm and Williams revealed that RNA has a similar genetic capacity (*4*, *5*). Their experiments showed that transformation of viral RNA into bacteria causes infection and results in the formation of new viruses. Isolated viral protein could not act in this way, however, protein was known to form the viral capsule surrounding RNA, suggesting a connection between nucleic acids and protein synthesis.

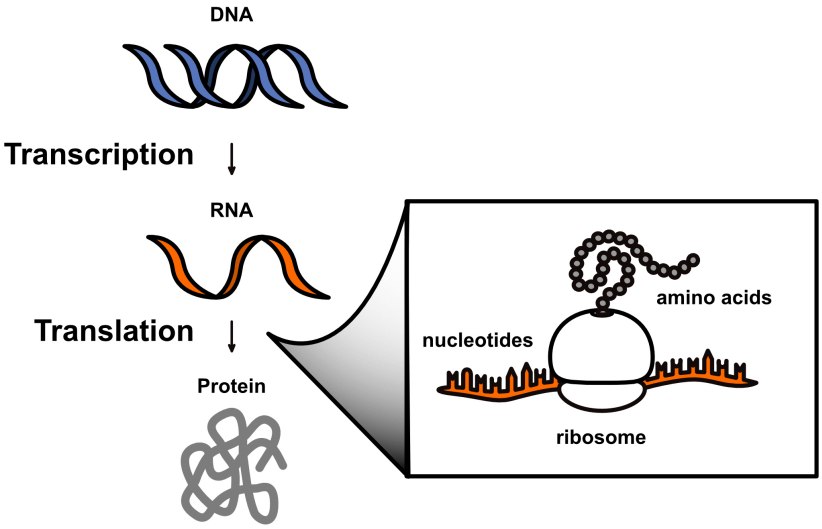

Figure 1.1 The flow of genetic information from nucleic acid to protein. DNA contains genes, which are transcribed into an RNA message that the ribosome translates into protein. (Inset) The ribosome synthesizes a polymer of amino acids as dictated by a sequence of RNA nucleotides.

In 1953, Watson and Crick used data from Franklin and Wilkins to describe the structure of DNA (*6*). The structure immediately suggested a mechanism for DNA replication based on a strict one-to-one nucleotide correspondence between complementary bases (*7*). Base pairing is dictated by hydrogen bonding, which had previously been inferred biochemically by Chargaff and Wyatt (*8*, *9*), showing that adenine (A) complements thymine (T), and guanine (G) complements cytosine (C) (Figure 1.2). Although the structure of DNA creates an obvious template for replication, how the genetic information within DNA directs protein synthesis was not immediately apparent. One of the first steps toward understanding this was the recognition of an intermediary message between DNA and protein, called RNA. RNA is transcribed from a DNA template and has two chemical differences compared to DNA: the sugar in the backbone is ribose instead of deoxyribose, and the base uridine (U) replaces thymine (T). Validating this connection, Berg showed that when enzymatically synthesized RNA was added to protein synthesis reactions, there was a pronounced increase in peptide formation (*10*). In what way genetic information was encoded within nucleic acids, however, was still unclear. The following decades were marked by numerous theories addressing this problem, along with the desire to understand the machinery that performs the decoding process.

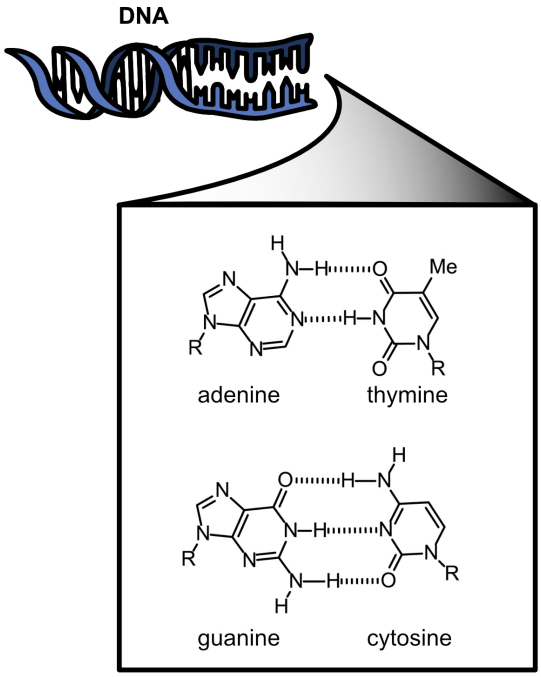

Figure 1.2 Nucleotide bases are complementary. Hydrogen bonds dictate complementarity between bases and this base pairing creates a template for replication.

We now know that four nucleic acids must encode 20 different amino acids. This mandates that a set of multiple nucleotides, called a codon, must specify a single amino acid. To adequately specify all 20 amino acids requires at least a three-nucleotide code, since each nucleotide can take any of four possible forms (4x4x4=64). This results in excess codons, meaning the genetic code is degenerate. Based solely on theory, the mathematician Gamow put forth one of the first possible interpretations which, though ultimately incorrect, assumed that the code was triplet, overlapping and degenerate (*11*). Crick later showed genetic evidence for the code's triplet nature (*12*), while work by Brenner established that the code was not overlapping, as a triplet overlapping code would require more than 64 codons (*13*). By the 1950's, understanding which codons corresponded to which amino acids, and the mechanism by which they were read was the focus of intense research.

A major breakthrough in understanding the genetic code came when Nirenberg and Matthaei determined experimentally that RNA composed entirely of uridine nucleotides encodes stretches of the amino acid phenylalanine (*14*). With this they conclusively showed that RNA containes the code for protein synthesis and uncovered the first codon, UUU, encoding phenylalanine. Nirenberg and Leder then used a newly developed translation system to further show the nucleotide triplets coding for Phe, Lys, and Pro (*15*). This study optimized a filter-binding assay for the systematic

determination of amino acid-codon correspondence with a sequence of repeating RNA nucleotides. These experiments allowed the full genetic code to be rapidly determined experimentally and the remaining code (Figure 1.3) was deciphered in 1966 by Khorana and colleagues using chemically synthesized RNA sequences that could be unambiguously matched to a corresponding amino acid sequence (*16*).

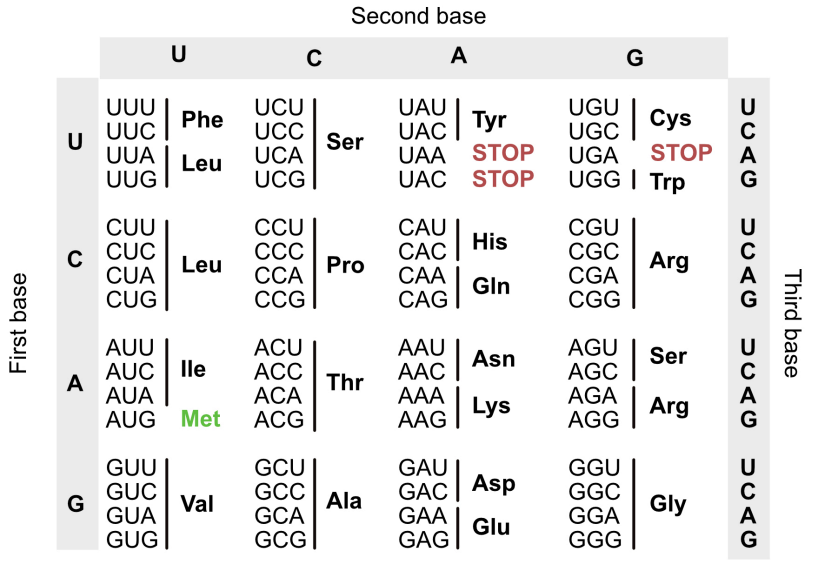

Figure 1.3 The genetic code. Each amino acid is specified by one or more sets of three nucleotides called codons.

As the code was being deciphered, the mechanism by which an RNA message is translated into the chemical language of amino acids was of increasing interest. Given the relative size of a single amino acid compared to a nucleotide, Crick recognized the need for an adaptor molecule (*17*). The adaptor hypothesis was supported by Hoagland, Zamecnik and Stephenson's discovery of small RNA molecules, now known as transfer RNA (tRNA), which were shown to be covalently bound to amino acids (*18*). tRNAs are typically about 75 nucleotides in length and form four helical domains that fold into a distinct L-shape (*19*, *20*). We now know that each tRNA has a set of three nucleotides, called an anticodon, which is complementary to an mRNA codon, while the 3' end is covalently bound to an amino acid (Figure 1.4). Aminoacyl-tRNA synthetases catalyze the coupling of a specific amino acid to the 3' end of a tRNA. Some aminoacyl-tRNA synthetases specifically recognize the anticodon of tRNA, whereas others recognize the acceptor stem to which the amino acid is attached. In either case, synthetases use energy from ATP hydrolysis to form the bond between the tRNA and its corresponding amino acid. This bond is broken during translation to fuel peptide bond formation between

amino acids in the growing polypeptide. Attachment of an amino acid to a tRNA is therefore in itself, a form of translation.

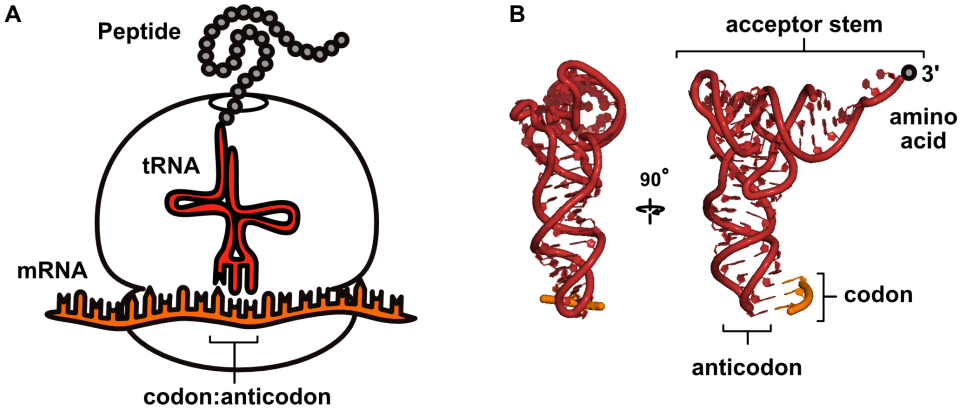

Figure 1.4 tRNA acts as an adaptor between mRNA and amino acid. (A) tRNA links the code within RNA to the synthesis of peptides (B) tRNA folds into a distinct L-shape. On one end an anticodon pairs with the mRNA codon and on the 3' end an amino acid is attached.

The macromolecule responsible for decoding an mRNA message and catalyzing protein synthesis is the ribosome. The initial identification of the ribosome began with the isolation of membranous small granules called 'microsomes' by Claude (*21*). These were small, globular particles recognized as hubs for protein production. Peterman and Hamilton were able to isolate specific, smaller granules from these microsomal fractions and show that these particles had a distinct sedimentation coefficient (*22*). Those particles were first visualized in mammals by George Palade and colleagues using electron microscopy (Figure 1.5) (*23*) and were later observed in plants (*24*). This was made possible by advances in cell culture, plastic embedding and knife design that allowed visualization of thin sections of the cell by electron microscopy. Specifically, they saw round granules of high-density contrast that were attached to the endoplasmic reticulum. Later work established that these granules were composed primarily of RNA and protein (*25*, *26*), and were responsible for protein syntheses (*27*).

At the time, the particles were referred to as "ribonucleoprotein particle of the microsome fraction", however this was replaced by the less cumbersome name "ribosome" proposed by Roberts in 1958. That year, the first prokaryotic ribosomes were characterized in *E. coli* by Tissieres and Watson (*28*). All ribosomes have a similar design and are often referred to by their sedimentation coefficient (S). The complete bacterial ribosome (70S) is made of approximately two-thirds RNA and one-third protein, and is composed of two subunits, the large subunit (50S) and the small subunit

(30S) (*28*, *29*). Despite these early important discoveries, the ribosome field was relatively stagnant in the decades immediately following the 1950s. Why the ribosome was composed of RNA was especially unclear at the time as proteins were thought to be the most important catalysts within a cell.

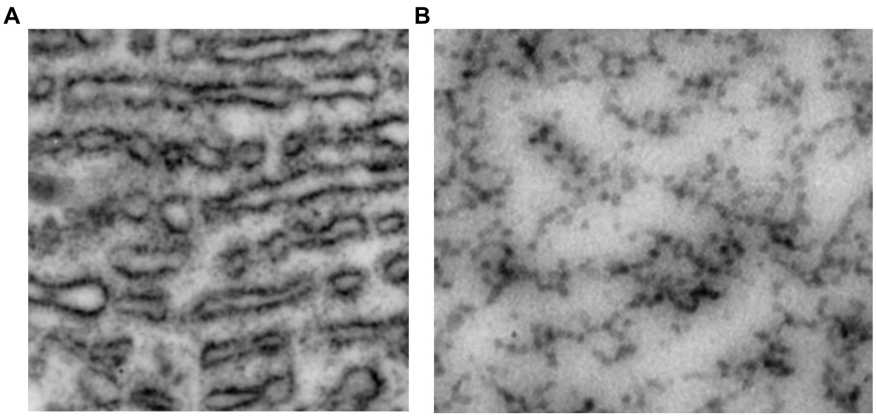

Figure 1.5 First EM visualization of the ribosome by George Palade. (A) Electron micrograph of a thin section of the endoplasmic reticulum within pancreatic cells of guinea pig. (B) Multiple rounds of pelleting endoplasmic reticulum by ultracentrifugation isolated small dense particles, which were visualized by electron microscopy. Figure adapted from (A) figure 1 and (B) figure 18 of Palade and Siekevitz 1956 (*26*).

Then in 1982 the discovery of RNA enzymes reinvigorated the field. Cech and colleagues showed for the first time that RNA could act as an enzyme, capable of breaking and forming covalent bonds (*30*). They characterized a sequence in the 26S rRNA of *Tetrahymena thermophila* and demonstrated that it could self-splice; remove parts of itself, circularize, and then join the neighboring ends. Around the same time, Altman and Pace discovered that RNA also provides the catalytic function of the ribonuclease RNaseP (*31*). These studies motivated the idea that the ribosome was a ribozyme (RNA enzyme) and could therefore be responsible for the catalysis of protein synthesis. It became apparent that if RNA was the active component of the ribosome, ribosomal proteins may not play individual catalytic roles. To understand the concerted function of all the pieces of the ribosome, it was clear that detailed structural information would be required.

1.1.2 Structural biology of the ribosome

Initial structural work with neutron scattering (*32*, *33*), cross-linking, and immune electron microscopy (*34*) was focused on establishing the relative positions of ribosomal proteins within the subunits. However, it was soon realized that spatial

arrangement alone would be insufficient to determine the mechanism of translation. Thus, work began on the structures of individual ribosomal proteins. Although high-resolution structures of ribosomal proteins would eventually be useful, in isolation they too were ultimately insufficient for understanding the function of the ribosome. For this, an atomic resolution structure of the entire ribosome would be needed.

X-ray crystallography was the first technique used to this end. As implied in the name, a necessary step for this technique is to crystallize one's sample, an inherently difficult process for a large, asymmetric molecule like the ribosome. By the late 1980's, significant developments allowed larger molecules to be crystallized and analyzed, (*35*, *36*) and in 1991 Yonath obtained the first potentially useful crystals of the 50S subunit, diffracting below 3 Å (*37*). A well diffracting crystal is not sufficient to determine the arrangement of molecules in a protein, as one must first solve the 'phase problem'. When x-rays diffract, the intensity of the signal (related to the wave's amplitude) is detected, but the phase is lost. The problem then is how to recover the lost information. The phase problem remained outstanding for the ribosome, whose complexity dwarfed all previously determined structures, making its phase determination all the more difficult.

An alternative approach toward determining the structure of the ribosome was electron microscopy (EM). In EM, instead of a diffraction pattern, an image is detected that contains both the amplitude and phase information. Although the technique doesn't suffer from the phase problem, at the time, EM technology was insufficient for determination of structures at high-resolution. EM could, however, be used to visualize the general shape of a macromolecule. A big step toward understanding the structure of the ribosome came from EM studies of ribosomes frozen in vitreous ice. Two ~ 25 Å reconstructions of the ribosome by Frank and Stark first described its three-dimensional architecture (Figure 1.6) (*38*, *39*). These maps showed a channel in the small subunit and a tunnel in the large subunit, speculated to coordinate the mRNA and the polypeptide chain, respectively. They also showed how the L-shaped tRNA could fit into the space between the small and large subunits.

At the time, atomic resolution structures had only been achieved by crystallography, and therefore most structural biologists attacked the phase problem. It was first solved for the ribosome in 1998 by Frank, Moore and Steitz, with their determination of a 9 Å resolution reconstruction of the large subunit from *Haloarcula marismortui* (*40*).

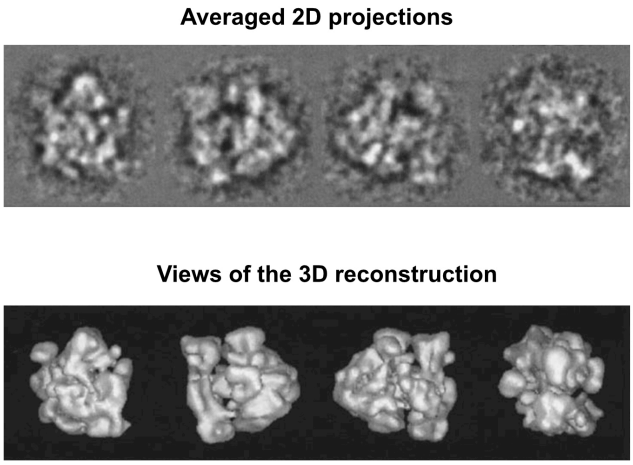

Figure 1.6 Initial EM reconstruction of the ribosome. Figure adapted from figure 1 of Stark et al. 1995 (*39*) showing micrographs averaged into 2D classes and multiple views of the map formed by reconstructing those projections in three-dimensions.

The breakthrough came by exploiting an EM map to first determine initial phases for low-resolution information, which were then used as a template to locate heavy atom clusters for high-resolution refinement. This study showed key structural elements at yet-unseen resolution, and maybe more importantly, showed that the structure of the ribosome could be solved. This instigated two years of intense competition as groups rushed to solve a high-resolution structure of the entire ribosome.

By 1999, Moore and Steitz had improved the resolution of the large subunit to 5 Å (*41*). At the same time, the Ramakrishnan group obtained a 5.5 Å resolution map of the small subunit from *Thermus thermophilus* (*42*), and simultaneously a 7.5 Å map of the entire *T. thermophilus* 70S ribosome was solved by Noller, showing the position of tRNAs in the three binding sites (*43*). The race came to an end in 2000, when a 2.4 Å structure of the large subunit of *H. marismortui* from Steitz was published (*44*). Within a month, the structure of the small subunit was published by Yonath at 3.3 Å resolution (*45*) and then three weeks later a more precise structure by Ramakrishnan at 3.1 Å resolution (*46*). These structures, as well as the full 70S ribosome (*47*) and two other 70S ribosomes in complex with mRNA and tRNA (*48*, *49*), were the founding models for ribosome structure and function, ushering in a new era of understanding the mechanism of translation.

1.1.3 An overview of translation

Ribosome structures confirmed extensive biochemical evidence suggesting that rRNA carries out the critical catalytic steps of translation. The ribosome is comprised of

roughly 2/3 rRNA, which makes up the central core and subunit interface of the ribosome, with ribosomal proteins primarily scattered around the outside. Though important, proteins are thought to mainly provide structural integrity to the complex and perform supporting functions.

Like all ribosomes, the bacterial 70S ribosome is composed of two subunits, the small subunit (30S) and the large subunit (50S) (Figure 1.7A). The 30S subunit contains a ~1500 nucleotide-long 16S rRNA and some 20 proteins that together form two major domains, known as the 'body' and 'head', which are connected by an RNA double helix called the 'neck' (Figure 1.7C). The gap between the head and the body forms a channel that holds mRNA during translation. Two closely associated areas situated between the head and body, resembling latches, prevent the mRNA from leaving the channel. The beginning of translation therefore mandates that the mRNA bypass these latches when it is loaded into the ribosome.

The 50S subunit is made of a ~2900 nucleotide-long 23S rRNA, the shorter ~120 nucleotide 5S RNA and some 31 proteins. It contains the catalytically active site of the ribosome called the peptidyl transferase center (PTC) (*50*). The 23S rRNA forms

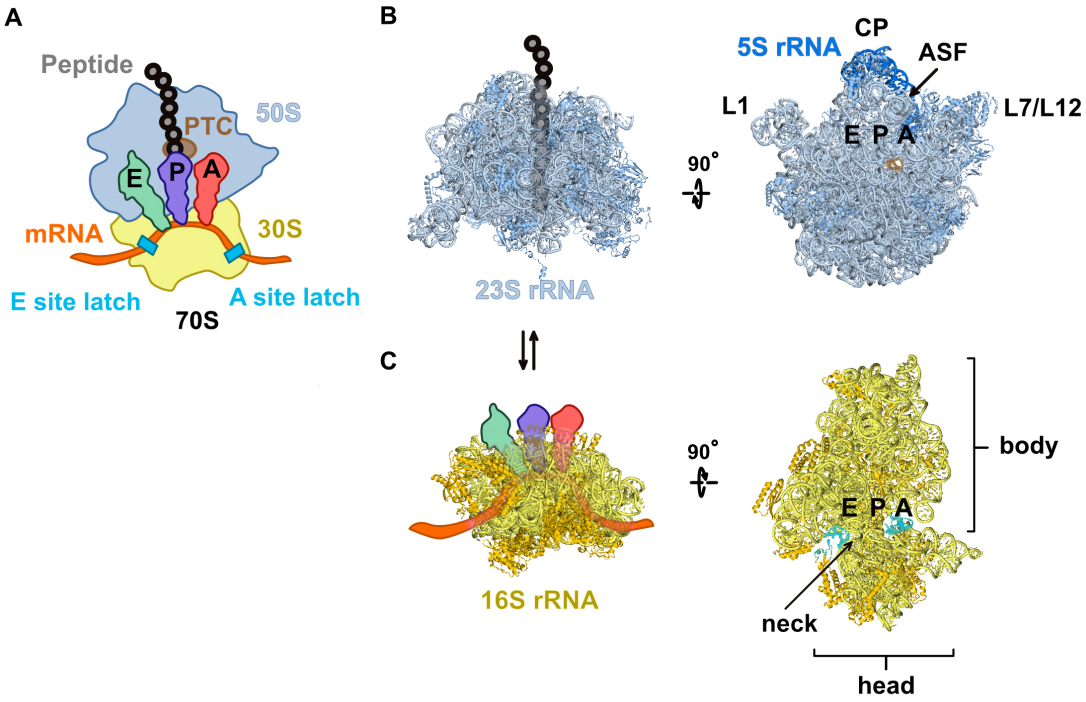

Figure 1.7 High resolution structure of the ribosome. (A) Cartoon schematic of the 70S ribosome showing the small (30S) and large (50S) subunits carrying an mRNA and nascent peptide with three tRNAs bound. (B) The structure of the 50S from the Steitz group, Ban et al. 2000 (PDB 1FFK) (*44*). (C) The structure of the 30S from the Ramakrishnan group, Wimberly et al. 2000 (PDB 1J5E) (*46*).

the PTC, a pocket where the peptide bond between subsequent amino acids is formed (Figure 1.7B). The synthesized polypeptide extends out of the peptide exit tunnel leading from the PTC to the solvent side of the 50S. The 50S also contains two stalks of RNA and protein (the L1 stalk and the L7/L12 stalk), as well as two protrusions [the A-site finger (ASF) and the central protuberance (CP)]. This architecture plays important roles in the coordination of translation, and will be discussed in more detail in section 1.2.

As translation begins, the ribosomal subunits join on an mRNA, forming the 70S complex. Ribosomes read mRNA from 5' to 3' ends, synthesizing peptide chains from the amino end (N-terminus) to the carboxyl end (C-terminus). The ribosome has three tRNA binding sites at the interface between the subunits: the aminoacyl (A) site, peptidyl (P) site and exit (E) site (Figure 1.7A) (*51*). During translation, tRNAs move successively from one binding site to another, from A to P to E, as the mRNA slides through the ribosome. As tRNA is covalently linked to the C-terminus of an amino acid, it is the N-terminus that is conjugated to the available C-terminus of the peptide chain. The ribosome therefore synthesizes proteins from the N- to C-terminus.

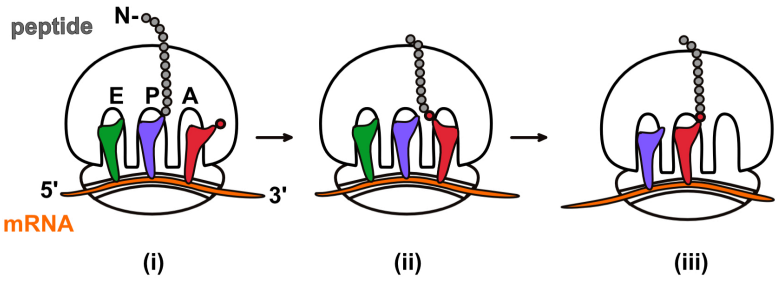

Figure 1.8 Basic overview of translation. (i) Aminoacyl-tRNA (red) enters the A site, then (ii) a peptide bond is formed with the nascent peptide bound to tRNA in the P site and (iii) the ribosome shifts by exactly one codon, and the process can repeat.

The location of a tRNA in either the A, P or E site is sufficient to know the stage of peptide synthesis in which it is participating. The first tRNA binding site, the A site, is where an incoming tRNA is first delivered and verified to match the codon specified by mRNA (*52*). The large subunit then catalyzes the formation of a peptide bond in the PTC (*53*, *54*). During catalysis, the nascent chain is transferred from peptidyl-tRNA in the P site to the aminoacyl-tRNA in the A site. The mRNA and tRNAs then shift relative to the ribosome, revealing the next codon in the A site and translation continues. The details of this process in bacteria are explored in the following section.

1.2 Translation in bacteria

Translation proceeds in three main stages (i) initiation, (ii) elongation and (iii) termination/ribosome recycling. Initiation is the process by which the ribosomal subunits join at the correct starting position on an mRNA. Elongation proceeds as the ribosome reads an mRNA, connecting successive amino acids to form a polypeptide. Termination marks the end of translation and releases the completed protein from the ribosome. The ribosome is then separated into its subunits and removed from the mRNA, allowing it to begin another round of translation.

1.2.1 Initiation

To begin translation, the ribosome must first bind an mRNA at the start of a protein coding sequence. Correctly positioning the first aminoacyl-tRNA on the mRNA sets the reading frame, and is the main determinant for the ensuing amino acid sequence. As codons are composed of three-nucleotide repeats, mRNA contains three possible reading frames. Selecting the correct frame is therefore critical as only one will result in the desired protein product. To ensure fidelity in this respect, the genetic code has evolved a signal, the start codon, to indicate the beginning of a message. A set of initiation factors (IFs) coordinates the position of aminoacyl-tRNA on this signal to initiate translation.

In bacteria, the typical start codon is AUG, which is recognized by fMet-tRNA^{fMet}, a special initiator tRNA charged with a formylated methionine (fMet). All polypeptides in bacteria initiate with fMet-tRNA^{fMet} as the N-terminal modification ensures that the amino acid cannot be incorporated within a protein coding sequence outside of the start position. To position the ribosome correctly on the mRNA, the start codon is preceded by a ribosome binding sequence called the Shine-Dalgarno (SD) (*55*). The Shine-Dalgarno sequence pairs with a complementary sequence in the 16S rRNA (the anti-SD) of the 30S subunit to place the start codon in the P site. With the help of initiation factors, fMet-tRNA^{fMet} binds to the 30S in the P site such that it pairs with the start codon (Figure 1.9).

Three specialized initiation factors (IF1, IF2, and IF3) position initiator tRNA on the 30S and assist in selection of the cognate start codon. IF1 binds in and blocks the A site (*56*), acting as an anchor for IF2 and IF3, stabilizing them in their positions on

the 30S (*57*). IF2 is a GTPase that binds to initiator tRNA (*58*, *59*), and is thought to specifically recognize the fMet group (*57*). Like other translational GTPases, IF2 binds tRNA and acts as a switch for an irreversible step in translation. IF3 takes on multiple conformations (*57*) to monitor the position of the start codon (*60*, *61*) and selects for initiator tRNA (*62*, *63*). IF3 is a dynamic, dumbbell shaped protein consisting of two globular termini connected by a mostly helical linker. One domain binds near the P site, possibly probing the codon:anticodon interaction between the mRNA and initiator tRNA, while the other domain binds to initiator tRNA directly.

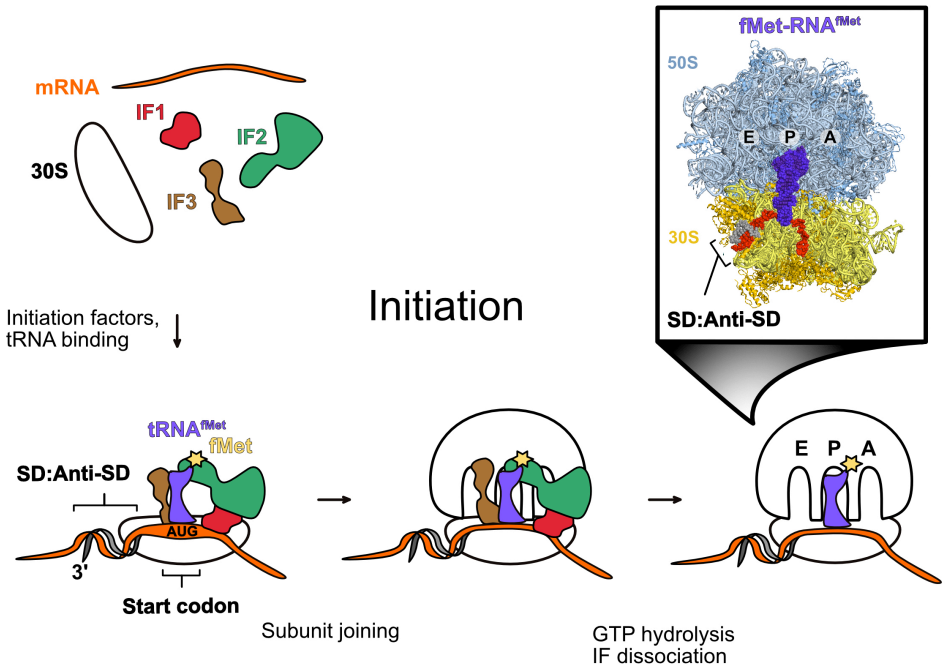

Figure 1.9 Translation initiation in bacteria. Initiation factors coordinated the assembly of mRNA and initiator tRNA (fMet-tRNA^{fMet}) on the 30S subunit. The Shine-Dalgarno (SD) sequence coordinates the position of the mRNA, placing the AUG start codon in the P site. The 50S subunit then joins and the initiation factors leave, forming the 70S initiation complex. (Inset) Structure of a 70S initiation complex from Jenner et al. 2010 (PDB 4V6G) (*64*).

The three initiation factors assemble with initiator tRNA onto the 30S subunit while mRNA is loaded into the mRNA channel. This permits initiator tRNA to interact with the start codon after both are correctly positioned in the P site. Initiation culminates in the 50S subunit docking onto the 30S complex and triggering GTP hydrolysis by EF2, resulting in an irreversible dissociation of the IFs followed by the formation of the full 70S ribosome (*65*). Here, with mRNA loaded into the mRNA channel and fMet-tRNA^{fMet} bound to the start codon in the P site, elongation is ready to begin.

1.2.2 Elongation

Translation elongation happens in three key steps: (i) decoding, (ii) peptidyl transfer, and (iii) translocation (Figure 1.10). Elongation factor Tu (EF-Tu) bound to GTP delivers aminoacyl-tRNA to the codon in the A site, where the ribosome 'decodes' the codon:anticodon interaction. EF-Tu is the first of two translational GTPases that act

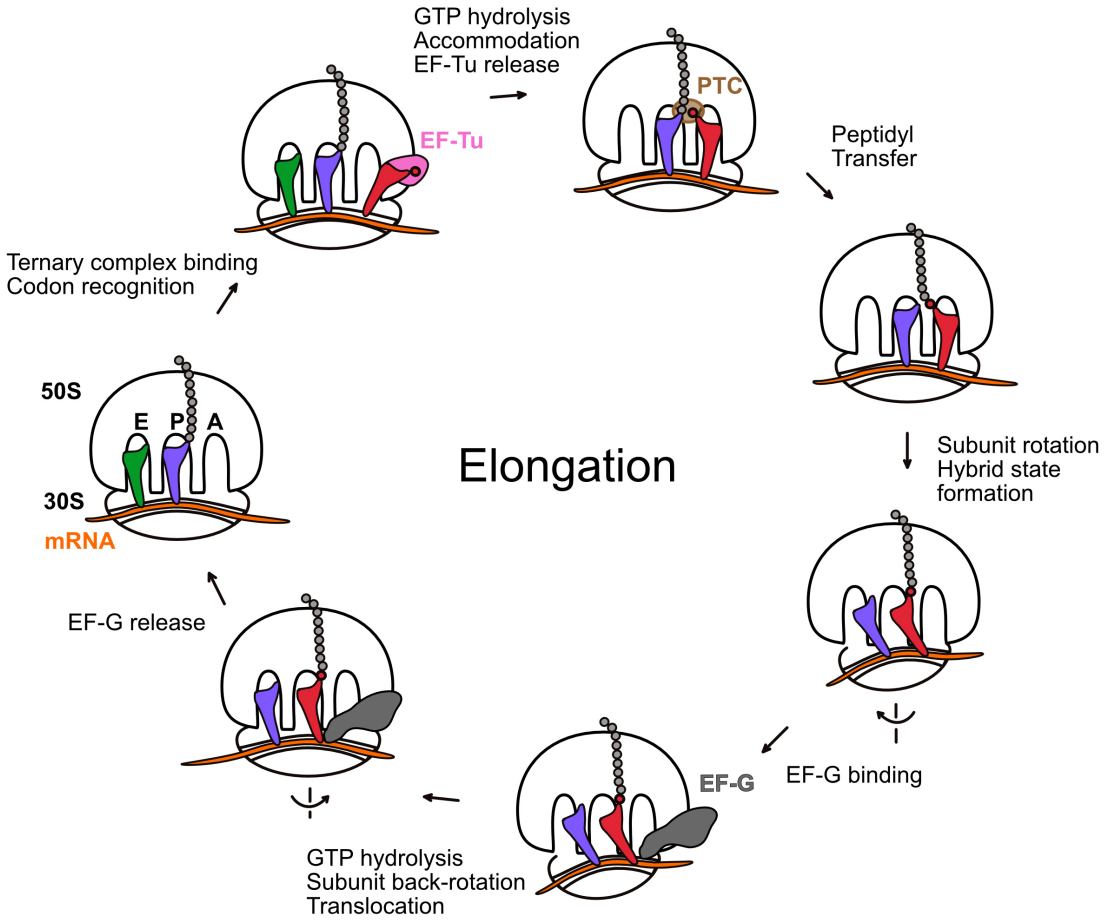

Figure 1.10 Translation elongation in bacteria. Translation elongation is a repeating cycling of decoding, accommodation, peptidyl transfer and translocation.

as switches during elongation. If a cognate codon:anticodon pair is recognized, EF-Tu hydrolyzes GTP and dissociates, licensing the accommodation of aminoacyl-tRNA into the A site. Immediately upon accommodation, the 3'end of the aminoacyl-tRNA is positioned within the peptidyl-transferase reaction center (PTC) next to the peptidyl-tRNA. Here, the nascent chain from the peptidyl-tRNA is transferred to the aminoacyl-tRNA in the A site, elongating the polypeptide by one amino acid. Subsequent movement, or translocation, of the ribosome by exactly one codon is facilitated by another GTPase, elongation factor G (EF-G). After translocation, the next codon is available in the A site and the steps of the elongation cycle repeat.

1.2.2.1 Decoding

EF-Tu delivers aminoacyl-tRNA to the ribosome in an mRNA-independent manner, binding the 50S to position aminoacyl-tRNA in close proximity to the A site (Figure 1.11A,B) (*66*, *67*). Aminoacyl-tRNA reversibly samples mRNA in the A site until a cognate codon:anticodon interaction is detected by the ribosome. The ribosome decodes the interaction by assessing base pair complementarity using three highly conserved nucleotides: A1492, A1493 and G530 of the 16S rRNA (Figure 1.11C). These 'decoding nucleotides' contact the minor groove of the codon:anticodon interaction to assess whether the geometry of the base pair is correct (*68*).

Cognate codon:anticodon base pairing induces domain closure within the ribosome (*69*), bringing the head of the 30S subunit closer to the body, which subsequently triggers GTP hydrolysis by EF-Tu. Codon recognition and ribosomal domain closure initiates a cascade of conformational changes within EF-Tu leading to GTPase activation, GTP hydrolysis and finally dissociation from the ribosome. This represents an important stage of translational fidelity as EF-Tu prevents tRNA from fully entering the ribosome until after GTP hydrolysis. A highly conserved domain of EF-Tu performs catalysis. When activated, a catalytic histidine residue (His 84) thought to coordinate a water molecule necessary for GTP hydrolysis rotates into an active conformation within the catalytic center (Figure 1.11D). Indeed, mutations of His84 have a deleterious effect on GTPase activation (*70*). After GTP hydrolysis, phosphate is released, causing a large movement of the catalytic domain of EF-Tu as it adopts a GDP bound conformation (Figure 1.11E). This movement weakens the interactions of EF-Tu with the ribosome and tRNA, ultimately inducing dissociation and permitting the accommodation of tRNA into the A site.

Following decoding, a second proofreading step occurs, increasing translational fidelity. After EF-Tu leaves, the tRNA can either enter the ribosome or dissociate. Biochemical studies suggest that accommodation is more favorable for cognate tRNA, as it requires less GTP hydrolysis than incorporating a non-cognate tRNA (*73*, *74*). Accommodation of tRNA ultimately points the amino acid on its acceptor stem into the PTC, leading to peptide bond formation.

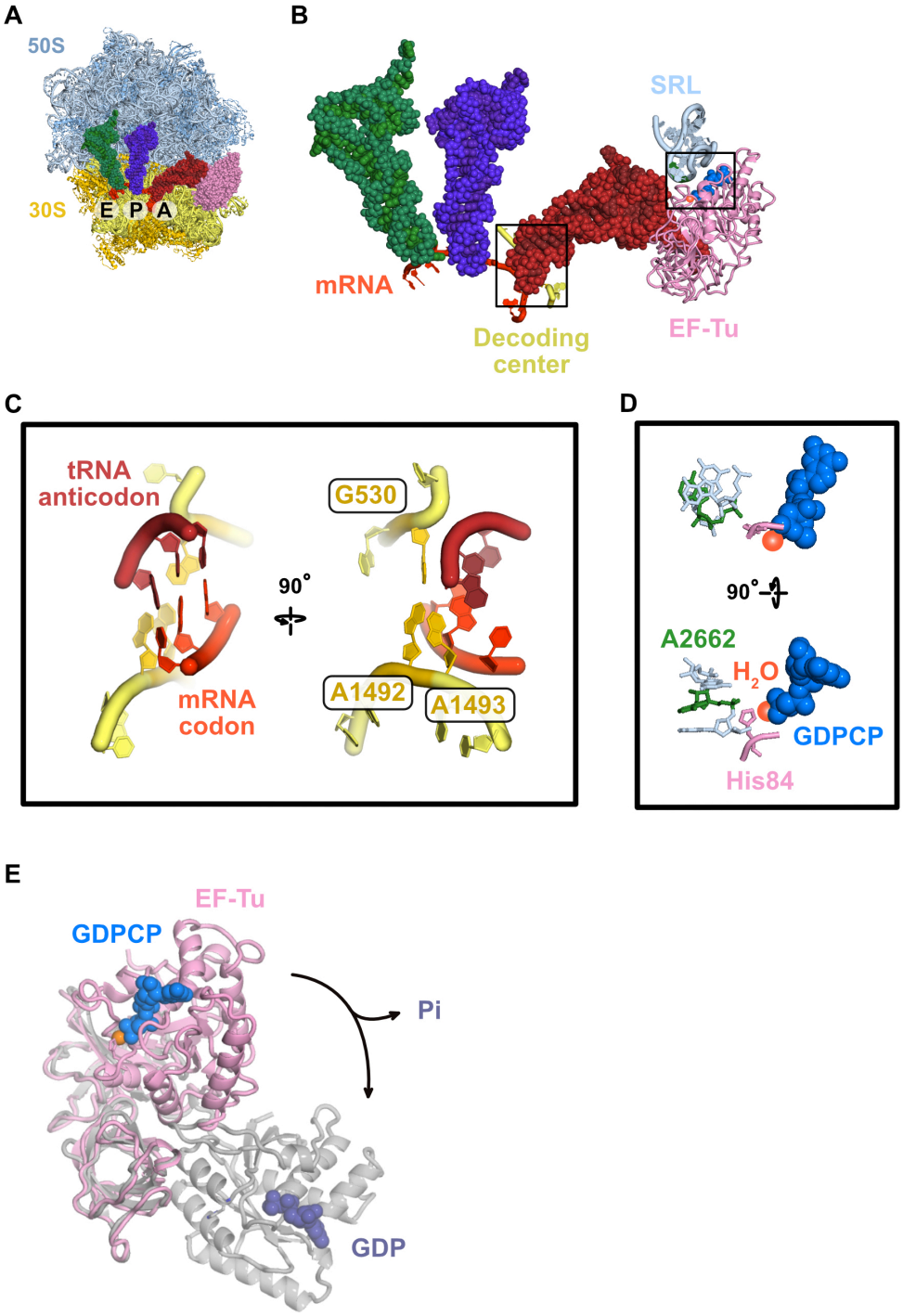

Figure 1.11 Aminoacyl-tRNA delivery and decoding. (A) Overview of a ribosome in the pre-accommodated state from Voorhees et al. 2010 (PDB 4V5L) (*71*). (B) EF-Tu (pink) interacts with the Sarcin-Ricin loop (SRL; light blue) when delivering aminoacyl-tRNA (red) to the A site where the anticodon interacts with the mRNA (orange) in the decoding center (light yellow). (C) Decoding center nucleotides assess the geometry of the codon:anticodon interaction. (D) Catalytic His84, oriented by A2662, coordinates a water molecule in the active site of EF-Tu. (E) The catalytic domain of EF-Tu rotates after GTP hydrolysis and phosphate release [gray, PDB 1TUI (*72*)].

1.2.2.2 Peptidyl transfer

Biochemical and structural evidence suggest that rRNA plays the catalytic role in peptide bond formation (*49*, *54*), increasing the reaction rate to ~10^6 times that in solution (*75*, *76*). Accommodation of the 3'CCA of aminoacyl-tRNA into the PTC (Figure 1.12A-C) exposes the ester bond that links the amino acid to the tRNA. This ester bond undergoes nucleophilic attack by the alpha-amino group of aminoacyl-tRNA, transferring the nascent chain from P-site tRNA to A-site tRNA (Figure 1.12D).

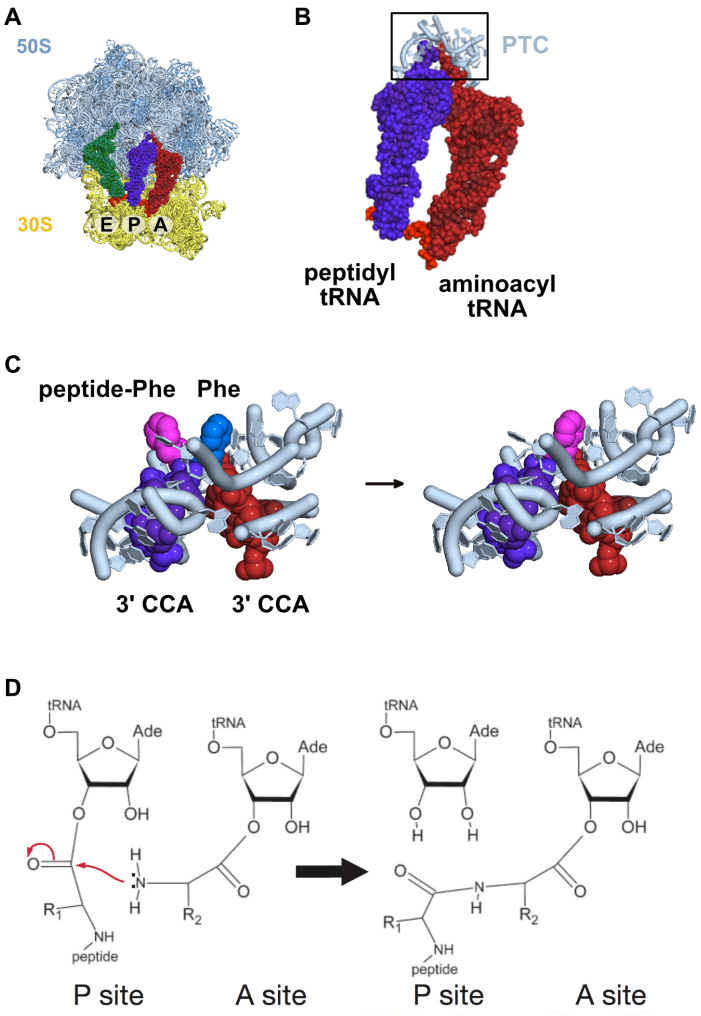

Figure 1.12 Mechanism of peptidyl transfer. (A) Overview of a non-rotated 70S ribosome with mRNA and tRNA in all three binding sites [PDB 4V5D; (*78*)]. (B) The acceptor stems of A-site (red) and P-site tRNA (purple) point into the peptidyl transferase center (PTC; light blue). (C) The 3' CCAs of A- and P-site tRNA are covalently linked to an amino acid. Peptidyl transfer shuttles the peptide bound to P-site tRNA to aminoacyl-tRNA in the A site. (D) General chemical mechanism of peptidyl transfer showing nucleophilic attack by the alpha-amino group of aminoacyl-tRNA, adapted from figure 4a of Schmeing and Ramakrishnan 2009 (*79*).

The exact catalytic mechanism of peptide bond formation is unclear, however, entropic effects and substrate-assisted catalysis have been proposed to influence this

process. Many nucleotides within the PTC are highly conserved, particularly A2602, which is within catalytic distance from the tRNA ester bond; however mutations of this nucleotide have little effect on the rate of peptidyl transfer. This is consistent with biochemical and molecular modelling evidence suggesting that substrates are positioned in the ribosome such that water is excluded. Apart from the entropic effects of the ribosome alone, the tRNAs themselves could participate in substrate-assisted catalysis. This is thought to occur via the coordination of the nucleotide A76 of peptidyl-tRNA as it is in a position that could participate in peptide bond formation. A proton shuttle mechanism for substrate assisted catalysis (*77*) has been proposed, however exactly how A76 plays a role in the shuttling and where the proton goes is unclear. In any case, the reaction within the PTC is clearly different from that in solution and the ribosome therefore plays a critical role catalyzing peptide bond formation.

1.2.2.3 Translocation

For elongation to continue after peptidyl transfer, the peptidyl-tRNA in the A site must move into the P site while deacylated tRNA in the P site shifts into the E site. This movement occurs in two main steps: first the ribosome rotates, and second EF-G hydrolyzes GTP to catalyze the translocation of tRNAs and mRNA relative to the ribosome during back rotation (Figure 1.13). The resulting ratcheting motion slides the mRNA and tRNA by exactly one codon relative to the ribosome, making the next codon available in the A site.

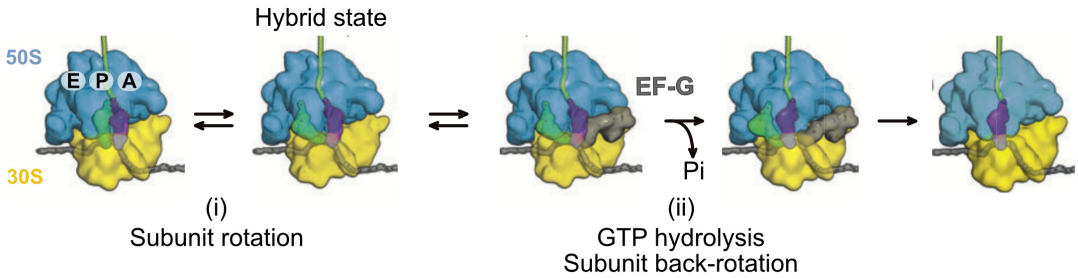

Figure 1.13 Translocation occurs in two steps. (i) Ribosome rotation forms the hybrid state, with tRNAs tilted toward their ultimate destination, followed by (ii) EF-G catalyzed motion of the tRNAs and mRNA relative to the ribosome during subunit back-rotation. Adapted from figure 6 of Voorhees and Ramakrishnan 2013 (*84*).

In the first step of translocation, the small and large subunits adopt a rotated conformation, in which the tRNAs take on a 'hybrid state' where they partially occupy two tRNA binding sites (*80*, *81*). The acceptor stem of each tRNA shifts within the 50S toward the site of the ribosome it will ultimately occupy after translocation (*82*,

83). In the hybrid state, the acceptor stem of the P-site tRNA is held by the L1 stalk in the E site of the 50S, a conformation only possible for deacylated tRNA. Likewise, the acceptor stem of peptidyl-tRNA in the A site tilts toward the P site.

EF-G binds the rotated state of the ribosome and catalyzes translocation in a GTP dependent manner. The shape of EF-G mimics delivery of tRNA to the A site, as its GTPase domain is analogous to that of EF-Tu. By hydrolyzing GTP (*85*), EF-G locks the tRNAs in the hybrid state (*86–89*). Biochemical studies suggest that translocation slides the tRNAs bound to mRNA simultaneously within the ribosome (*85*). The rotation of the ribosome back to the canonical state causes a shift by one codon. After translocation, the next codon is available in the A site and the elongation cycle repeats. Eventually, a signal at the end of the protein coding sequence is reached, marking the completion of elongation.

1.2.3 Termination and recycling

Termination requires a stop codon, encoded by the mRNA, to mark the end of translation. Stop codons are not typically decoded by a tRNA but are instead recognized by proteins called release factors (RFs). After termination, recycling factors are responsible for disassembling the translation complex, allowing the ribosome to initiate another round of translation (Figure 1.14).

Release factors terminate translation by hydrolyzing the peptide from the tRNA and thereby releasing it (*90–92*). The genetic code has three codons (UAG, UAA, and UGA) that typically function as stop signals. In bacteria, these are recognized by two class I release factors, RF1 and RF2. Recognition is redundant for the UAA stop codon, whereas RF1 uniquely recognizes UAG and RF2 recognizes UGA (*92*). Both release factors have a loop with a recognition motif consisting of three amino acids: Pro-Ala-Thr in RF1 and Ser-Pro-Phe in RF2 (*93*). The first and third amino acids of the recognition motif recognize, the second and third nucleotides of the stop codon, respectively. Upon initial binding to the ribosome, the RF extends from its compact conformation (*94–97*) to point its catalytic motif into the PTC (*98–100*). Class I release factors contain a catalytic GGQ motif that fits into the PTC and hydrolyzes the ester bond joining the peptide to P-site tRNA (*101*).

After termination, the release factor dissociates, allowing the ribosome to be recycled. In some species, the GTPase RF3, a class 2 release factor, removes the class I release factor from the A site. RF3 binds the ribosome with RF1 or 2 in the A site,

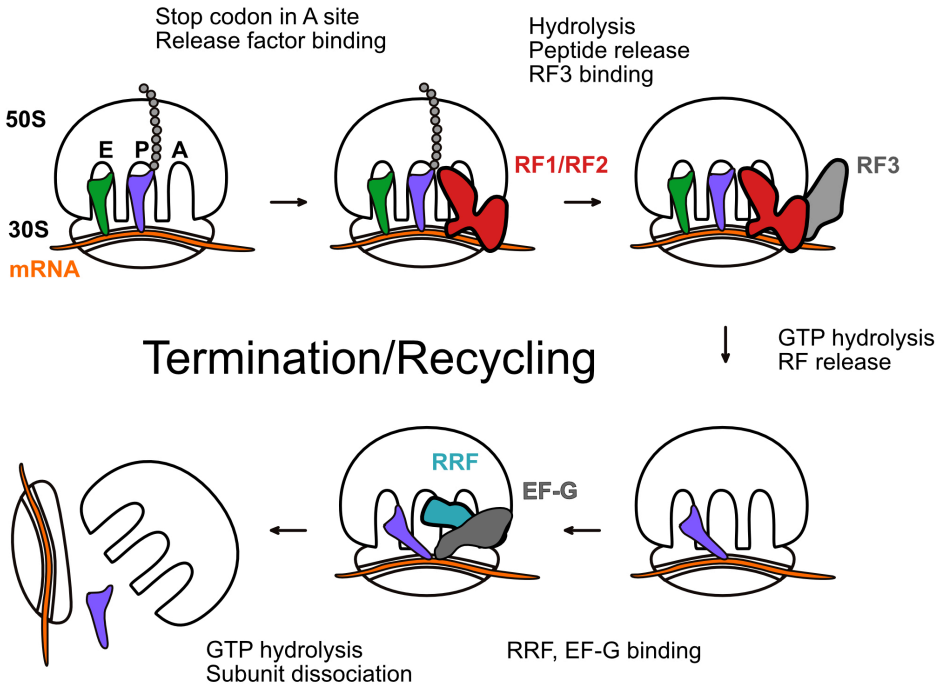

Figure 1.14 Translation termination and ribosome recycling in bacteria. A class I release factor (RF1 or 2, red) recognizes a stop codon and hydrolyzed the completed protein from tRNA in the P site. A class II release factor (RF3, gray) dislodges the class I release factor followed disassembly of the 70S involving ribosome release factor (RRF, teal) and EF-G (dark gray).

inducing ribosome rotation (*102*, *103*) and hydrolyzing GTP to stimulate dissociation of the release factors. Ribosome recycling proceeds as ribosome release factor (RRF) and EF-G bind and split the ribosomal subunits (*104*). RRF binds the ribosome in the A and P sites and destabilizes inter-subunit bridges via the GTP dependent action of EF-G (*105*). The exact mechanism of ribosome splitting is unclear, as sufficient structures of RRF and EF-G bound to the 70S ribosome remain outstanding.

Many species may recycle ribosomes without the help of additional factors. For instance, RF3 is not essential for survival (*106*, *107*) and is absent entirely in many species. Though not essential, *in vitro* studies suggest that RF3 and RRF increase the rate of ribosome turnover (*108*). The efficiency of recycling factors may therefore provide an advantage as the ribosome spends less time in an unproductive state.

Translation is an essential and complicated process, with the propensity for problems to arise at multiple steps. Organisms have evolved numerous pathways to deal with such issues. The specifics of translational stalling and the corresponding fail-safe mechanisms in bacteria are the subject of the subsequent sections.

1.3 Translational stalling and rescue

In bacterial cells, ribosomes begin translating mRNA prior to the completion of transcription. In some cases, incomplete mRNA synthesis or damage may result in the absence of a stop codon. The lack of a signal denoting the end of translation leads to a ribosomal stall upon reaching the end of such a message. Since bacterial cells have minimal mRNA quality control pathways prior to translation, stalling on faulty mRNA is a constant problem. Alleviating this problem is then essential for maintaining cellular function and so, bacterial cells have evolved multiple pathways to rescue stalled ribosomes.

1.3.1 Formation of a nonstop translation complex

When ribosomes reach the 3' end of an mRNA without encountering a stop codon, they get trapped as a 'nonstop' translation complex (Figure 1.15). Ribosomes in this state lack a codon in the A site but contain an mRNA and a P-site tRNA bound to the nascent peptide. Here, neither tRNAs nor release factors alone are sufficient to recognize the empty A site, leaving the ribosome in an assembled, but inactive state.

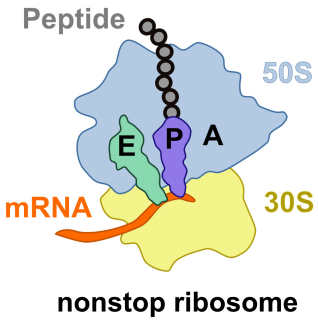

Figure 1.15 Anatomy of a nonstop ribosome. A nonstop ribosome is one that has reached the 3' end of an mRNA. The A site is therefore empty and peptidyl-tRNA occupies the P site.

The formation of a nonstop ribosome often occurs due to mRNA truncation from premature transcription termination, mRNA damage or inappropriate RNase activity. Alternatively, ribosomes can stall at the end of full-length transcripts if they accidentally frame-shift or read though the in-frame stop codon (Figure 1.16). For instance, miscoding antibiotics, like kanamycin and streptomycin, cause conformational changes in the 30S subunit which permit non-cognate tRNAs to decode stop codons (*109*), potentially causing the ribosome to reach the end of an mRNA. Likewise,

biochemical evidence shows that cells overexpressing suppressor tRNAs, which decode stop codons, consequently experience increased levels of nonstop stalling (*110*).

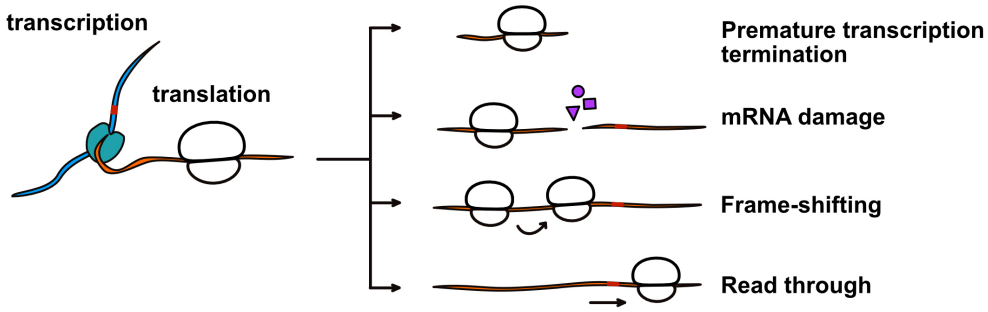

Figure 1.16 Formation of a nonstop translation complex. A variety of causes result in a ribosome translating an mRNA without detecting a stop codon.

Ribosomes that pause in the middle of a transcript may also become nonstop complexes if endonucleolytic cleavage of mRNA occurs in the A site. Pausing is usually a result of stochastic delays in translation due either to nutrient starvation, large mRNA secondary structure, restricted movement of the nascent peptide, or inefficient stop codons (*111–116*). Irrespective of cause, if the stall is not resolved these paused ribosomes become substrates for ribosome dependent endonucleases. One such nuclease is RelE, a subunit of the RelBE toxin-antitoxin heterodimer. A crystal structure of RelE bound to the ribosome shows that RelE interacts with 16S rRNA to position the mRNA into its catalytic center in the A site, inducing a conformational change that initiates mRNA cleavage (*117*). Stress conditions can also stimulate mRNA cleavage within the ribosome, acting as a form of translational regulation. For example, thermal stress activates YoeB, which cleaves mRNA in a ribosome dependent manner and creates a nonstop complex that is targeted by ribosome rescue pathways (*118*).

1.3.2 Rescue pathways

Trapped nonstop ribosomes must be rescued and released from the 3’ end of an mRNA. Ribosomes may detach from the tRNA and mRNA by way of drop-off (*119*, *120*) if stalled shortly after initiation, while the nascent polypeptide is only two or three amino acids long. Drop off is not possible once the peptide extends through the exit tunnel and out of the ribosome. As neither tRNAs nor canonical release factors recognize the empty A site of nonstop ribosomes, dedicated pathways with specific rescue factors are required to resolve these ribosomal stalls.

Trans-translation is the primary rescue mechanism for nonstop ribosomes, existing in >99% of all sequenced bacteria (*121*). *Trans*-translation functions to (i) target the aberrant mRNA for degradation (ii) tag the nascent polypeptide for

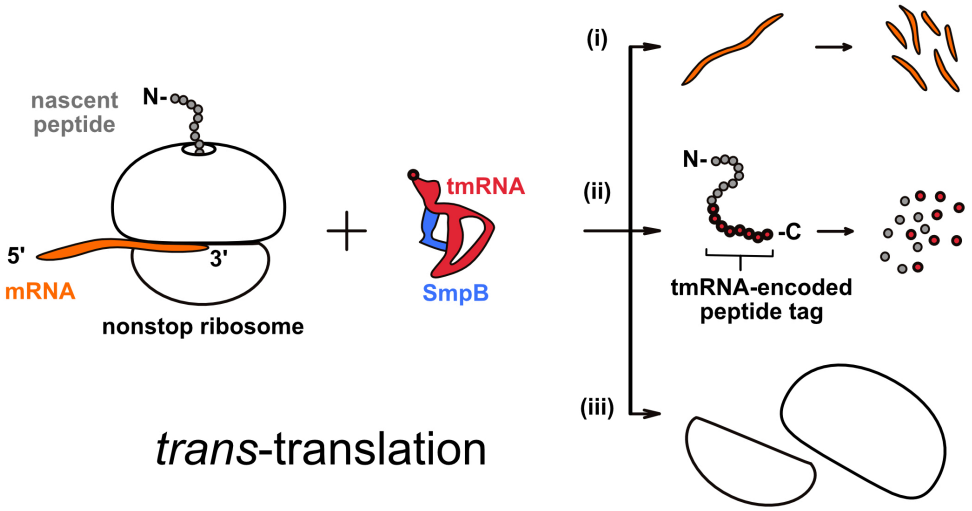

Figure 1.17 *Trans*-translation rescues nonstop ribosomes. Two key factors, tmRNA and SmpB enter the ribosome resulting in three useful outcomes for the cell. (i) The original mRNA, which is often damaged, is degraded in a tmRNA dependent manner. (ii) Translation of an RNA sequence in tmRNA adds a polypeptide tag to the nascent peptide, which not only releases the polypeptide but also targets it for degradation by cellular proteases. (iii) Because translation could terminate on the message within tmRNA, the ribosome is released and recycled.

degradation by cellular proteases, and (iii) terminate translation and release the ribosome (Figure 1.17). The pathway is constantly active in dividing bacterial cells, with 2-4% of translational events resulting in stalls (*122*) and 0.5–1.0% of ribosomes undergoing *trans*-translation at any one time (*123*, *124*).

Trans-translation involves two factors that hijack the stalled ribosome: transfer-messenger RNA (tmRNA, from the gene *ssrA*) and small protein B (SmpB). tmRNA functions as both a tRNA and an mRNA at different steps during the rescue process, whereas SmpB binds to tmRNA and anchors the complex on the ribosome. tmRNA-SmpB enters the ribosome by first mimicking a tRNA and then functions as an mRNA, tricking the ribosome into translating an encoded message for a short peptide. When this peptide is appended to the end of the incomplete protein it acts to target the protein for degradation. Translation then terminates at a stop codon within tmRNA, allowing the ribosome to be released.

Cell survival requires at least one rescue mechanism to promote ribosome recycling and maintain sufficient translation capacity within the cell (*125*). Many

species contain backup mechanisms that release nonstop ribosomes in the absence of *trans*-translation. These include alternative ribosome release factor A (ArfA) or ArfB. ArfA is a short peptide that enhances peptidyl-tRNA hydrolysis by binding to nonstop ribosomes. Screens for synthetic lethality identified *arfA* as essential in the absence of *ssrA* (*126*). However, it can be shown that the antibiotic puromycin promotes the growth of *arfA ssrA* double mutants. Puromycin dissociates nonstop ribosomes by stimulating peptide release in a codon independent manner (*127–129*), and therefore ArfA too was expected to play a role in peptide release. This was verified directly when overexpression of ArfA from a plasmid was shown to complement *arfA ssrA* double mutants.

ArfA's peptide release activity is integral to its role on the ribosome. ArfA not only fractionates with ribosomes in pelleting assays, but also co-purifies with ribosomal proteins when isolated by affinity purification (*126*). *In vitro* experiments with crude *E. coli* extracts initially confirmed the rescue activity of ArfA (*126*). Purified ArfA was seen to hydrolyze peptidyl-tRNA *in vitro* on ribosomes stalled when translating a model mRNA lacking a stop codon. This assay suggests that there is a competition between ArfA's peptide release activity and the tagging and degradation activity of tmRNA. Cumulatively, these results show that ArfA participates in peptide release and promotes rescue of nonstop ribosomes in the absence of *trans*-translation (*130*).

However, ArfA does not contain the catalytic GGQ motif typically found in release factors (*131–133*). This suggests that like tmRNA, ArfA cooperates with a release factor to stimulate peptide release and ribosome recycling. Indeed, RF2 was found to bind nonstop ribosomes only in the presence of ArfA (*134*). Hydroxyl radical probing experiments suggested that ArfA binds in the decoding center and mRNA channel (*135*) possibly replacing a stop codon. The molecular mechanism of ArfA-dependent peptide release was determined when a surprising series of five back-to-back papers showed the structure of ArfA bound to the ribosome with RF2 (*136–140*). ArfA was shown to recruit RF2 to the empty A site of a nonstop ribosome where RF2 can then release the stalled nascent chain (Figure 1.18). ArfA substitutes for a stop codon in the A site as its unstructured C-terminal tail anchors it in the mRNA channel (*136*). The N-terminal region of ArfA forms a β-strand that interacts with RF2, stabilizing a switch loop in RF2 that controls the catalytic GGQ motif, positioning it into the peptidyl-transferase reaction center.

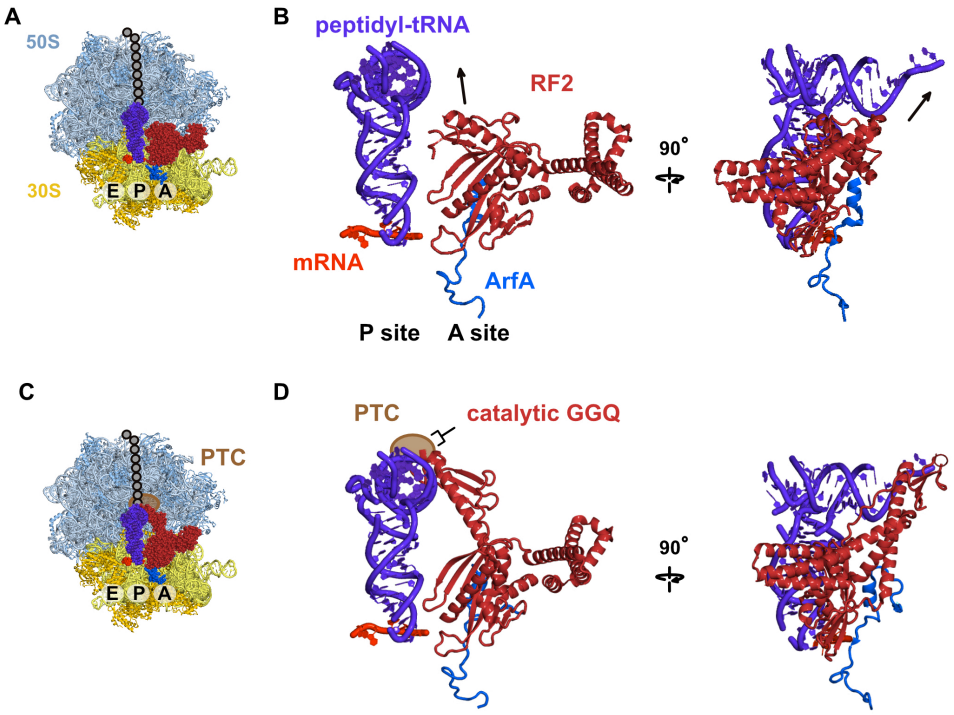

Figure 1.18 Mechanism of nonstop ribosome rescue by ArfA. ArfA mediated ribosome rescue uses RF2 to release the nascent chain. (A) Overview of the first stage of ArfA mediated rescue [PDB 5MDW; (*136*)]. (B) ArfA occupies the A site and mRNA channel, providing a surrogate stop codon that is recognized by RF2. The release factor takes on a pre-catalytic state. (C) overview of the second stage of ArfA mediated rescue [PDB 5MDV; (*136*)]. (D) The catalytic domain of ArfA swings upward into the PTC to release the polypeptide.

Interestingly, ArfA expression is regulated by tmRNA. An RNaseII cleavage site in the *arfA* coding sequence produces a transcript that mandates ribosomal stalling by cleavage prior to the stop codon. Release of these nonstop ribosomes produces truncated, but active, ArfA that supports the growth of cells lacking tmRNA. When tmRNA activity is depleted, ArfA is not tagged for degradation and cellular levels of ArfA increase. Basal levels of ArfA or the presence of additional alternative release factors, like ArfB, may permit the initial release of ArfA in the absence of tmRNA.

An additional nonstop ribosome rescue factor, ArfB, supports the growth of *ssrA arfA* double mutants and rescues stalled ribosomes (*141*). ArfB is a 140 amino acid long release factor homolog containing a GGQ catalytic motif. However, unlike RF1 or 2, it lacks a stop codon recognition motif and therefore functions independently from stop codons. ArfB plays only a minor role in normal cellular function, as it is dispensable for *E. coli* growth (*142*), however it is required in the absence of both *ssrA* and *arfA*. Neither *ssrA arfB* nor *arfA arfB* double mutants are lethal, but growth of *ssrA arfA arfB* triple mutants with an arabinose inducible plasmid containing *ssrA,* stop

growing in arabinose deficient media. To verify whether ArfB acts as a release factor, the catalytic GGQ was mutated to a GAQ sequence. This rendered ArfB incapable of supporting life in an *ssrA arfA* double mutant, suggesting that peptide release by ArfB may support viability in cases of tmRNA or ArfA inactivation.

Apart from the catalytic GGQ motif, ArfB has an unstructured C-terminal tail that is also required for ribosome rescue. C-terminal tail mutants of ArfB could not suppress lethality of *ssrA arfA* double mutants and fractionated less with the ribosome in pelleting assays compared to full length ArfB. The mechanism of ArfB interaction was revealed by a crystal structure of ArfB bound in the otherwise vacant A site of the ribosome (Figure 1.19). The structure shows that the C-terminal tail of ArfB forms an alpha helix in the empty mRNA channel, explaining how it specifically recognizes a stalled ribosome. Furthermore, the N-terminal domain of ArfB occupies the A site, positioning the catalytic GGQ motif into the PTC to promote hydrolysis of peptidyl-tRNA (*143*). This agrees with *in vitro* experiments suggesting ArfB rescues ribosomes stalled at the 3' end of mRNA (*144*).

Although ArfA and ArfB are essential for the survival of bacteria in the absence of tmRNA-SmpB, *trans*-translation is the primary mechanism used to release stalled ribosomes. *Trans*-translation is the preferred rescue mechanism as it not only releases the polypeptide, but also targets the incomplete protein for degradation and facilitates decay of the faulty mRNA.

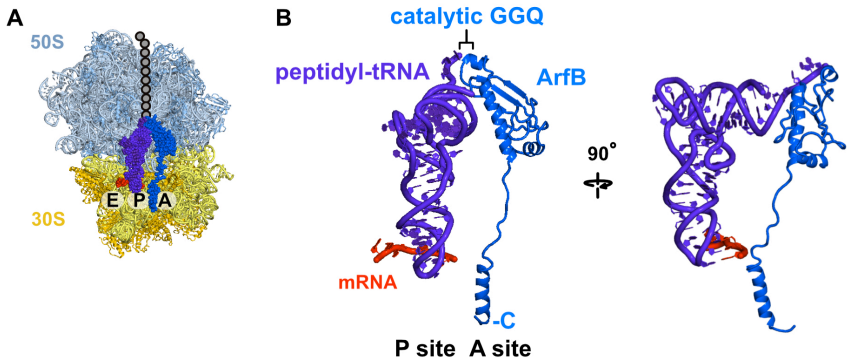

Figure 1.19 Mechanism of nonstop ribosome rescue by ArfB. (A) Overview of ArfB binding a nonstop ribosome [PDB 4V95; (*143*)]. (B) ArfB binds in the A site of a nonstop ribosome. Its C-terminal tail forms an alpha helix in the mRNA channel anchoring the N-terminal catalytic domain in position to hydrolyze peptidyl tRNA and release the nascent chain.

1.4 *Trans*-translation

1.4.1 A brief history and general overview of *trans*-translation

tmRNA, formerly known as 10S or 10Sa RNA, was initially observed as an unidentified band of radiolabelled cellular RNA on a polyacrylamide gel (*145*). This RNA species was small, stable and estimated to be present at about 1000 molecules per haploid genome. Purification of 10S RNA showed that it was composed of two dissimilar sequences, named 10Sa and 10Sb (*146*). 10Sb was later identified as RNaseP, while 10Sa was identified as a new gene and named *ssrA* (small stable RNA), later found to encode tmRNA (*147*). Early on, *ssrA* was also observed in *M. tuberculosis* (*148*), *M. capricolum* and B. *subtilis* (*149*) and then later characterized in nearly all sequenced bacterial genomes (*150*).

Initial observations gave some hints as to the importance and function of 10Sa RNA. Genetic experiments showed that *ssrA* knockout mutants in *E. coli* grow more slowly than parental strains (*151*) and had increased temperature sensitivity (*152*). A folded pre-tRNA^{Ala}-like structure in the termini of *E. coli* 10Sa RNA was noticed after sequence comparison to other tRNAs (Figure 1.20) (*153*). Further experiments showed that alanyl-tRNA synthetase (AlaRS) charges the tRNA-like structure of 10Sa RNA with alanine and that a G-U base pair in the acceptor stem region was critical for this alanylation event, similarly for tRNA^{Ala}.

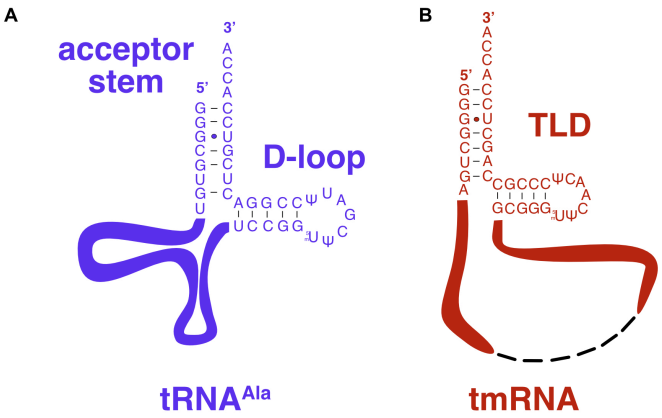

Figure 1.20 Secondary structure comparison of tRNA^{Ala} to tmRNA. (A) The acceptor stem and D-loop of tRNA^{Ala} resemble the secondary structure of the joined 3' and 5' ends of tmRNA, called the tRNA-like domain (TLD).

The connection between 10Sa RNA and a role in peptide tagging was first observed when mouse derived interleuken-6 (mIL6) expressed in *E. coli* showed a series of peptides with the same C-terminal modification. The modification, or 'tag',

was identical to a peptide sequence encoded within 10Sa RNA and was not observed in cells devoid of *ssrA*. At this time, the tagging function of 10Sa RNA was not yet associated with defective translation. There were contradicting reports on 10Sa RNA binding ribosomes in vivo (*149*, *151*, *154*, *155*) and therfore it was unclear how the chimeric mIL6-tag peptides were formed.

These observations were connected in a landmark paper in 1996 (*156*) which proposed the first mechanism of *trans*-translation. 10Sa RNA was renamed to transfer-messenger RNA (tmRNA) after it was discovered to act as both tRNA and mRNA when interacting with the ribosome. Sauer and colleagues described how tmRNA tags nascent peptides from transcripts lacking stop codons, which then allows proteases to recognize the nascent peptide and degrade it. Alanine-charged tmRNA first enters the A site of a ribosome stalled on the 3' end of an mRNA. After peptidyl transfer of the nascent chain to alanine on the 3'CCA of tmRNA, the ribosome switches from translating the original mRNA to a reading frame within tmRNA encoding a polypeptide tag. This study showed the first definitive link between the ribosome and tmRNA-dependent polypeptide tagging activity, and that specific proteases degrade the tagged proteins initially translated from faulty mRNAs. Message swapping was thought to be a process like frame-shifting, but would instead involve two different molecules in trans, giving the mechanism its name.

A critical co-factor, small protein B (SmpB), was later discovered to be essential for *trans*-translation. The *smpB* gene was first identified as one of two open reading frames neighboring *ssrA* (*157*). Although the function of *smpB* was still unknown at the time, proximity to *ssrA* suggested an interaction with tmRNA. It would take another eight years before SmpB was shown to be essential for the peptide-tagging activity of tmRNA (*158*). *In vivo*, nonstop transcripts are only tagged by tmRNA when SmpB is co-expressed. Also, strains lacking *smpB* have identical phenotypes to those lacking *ssrA*. Gel shift assays confirm that SmpB binds tightly to tmRNA and binding studies showed that SmpB is required for tmRNA binding to the ribosome.

Over the subsequent twenty years, there were a number of studies that furthered our understanding of *trans*-translation. tmRNA was found to undergo extensive processing prior to its binding with SmpB and interaction with the ribosome. Additionally, structural studies described the conformation of tmRNA-SmpB on the ribosome, while mutational analysis determined essential components of the complex required for *trans*-translation.

1.4.2 tmRNA-SmpB before the ribosome

The *ssrA* gene encodes a primary transcript that is processed to yield a mature tmRNA molecule (*159*). A pre-tmRNA precursor approximately 100 nucleotides longer than the mature RNA is first produced (*147*, *160*). RNaseP trims the 5' terminus of tmRNA (*153*), while RNaseIII or RNaseE cleaves the 3' terminus which is then trimmed by exonucleases RNaseT or RNasePH (*161*, *162*). In *E. coli*, RNA processing results in a 363 nucleotide-long mature tmRNA. Individual nucleotides of tmRNA are also post-transcriptionally modified. Three uridine residues in the T-loop are altered, one catalyzed by TrmA into 5-methyl uridine (5-MU) (*163*) and two catalyzed by TruB into pseudouridine 5-monophosphate (PSU) (*163*, *164*). These modifications are the same as those in the acceptor branch of *E. coli* $tRNA^{Ala}$ and may be important for the downstream function of tmRNA (Figure 1.20).

tmRNA was suggested to have a $tRNA^{Ala}$-like structure (*149*, *153*), which was supported by secondary structure predictions (Figure 1.21) by chemical probing (*165*),

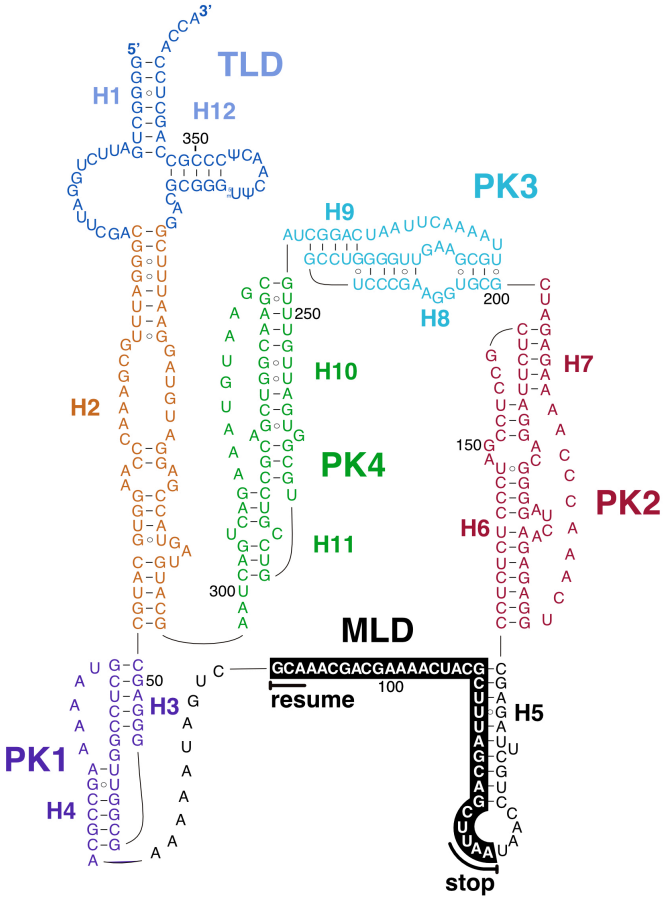

Figure 1.21 Secondary structure of *E. coli* tmRNA. The two ends of tmRNA join to form the tRNA-like domain (TLD; dark blue), which connects to a loop of pseudoknots (PKs) 1-4. Between PK1

and PK2 is the mRNA-like domain (MLD) with is part of helix 5 (H5). The first codon decoded by the ribosome (the resume codon) and the stop codon, is underlined.

phylogenetic analysis (*166*) and comparative sequence analysis (*150*). Indeed, tmRNA has three domains, a tRNA-like domain (TLD) formed by the acceptor-stem region from $tRNA^{Ala}$, a single stranded mRNA-like domain (MLD) that encodes the peptide tag, and a ring of four pseudoknots (PKs) that complete the loop.

The TLD has a characteristic acceptor arm conformation resembling that of tRNA, but lacks the traditional anticodon stem loop (*167*). Instead, the corresponding stem extends to join the ring of pseudoknots harboring the MLD. During *trans*-translation, the ribosome restarts translation on the MLD which is often described as containing an 'open reading frame'. However, this peptide coding sequence lacks a start codon and an upstream SD and therefore is technically not an open reading frame but more accurately called the 'tag-reading frame'.

In *E. coli*, four pseudoknots flank the MLD, forming a loop joined by short single stranded RNA segments. The pseudoknot (PK) loop stabilizes tmRNA but was not known to have a direct role in interacting with the ribosome, neither contacting the ribosome or other elongation factors (*168*). The number of pseudoknots varies in tmRNA depending on species (*169*, *170*). For instance, plastid tmRNA lacks pseudoknot structures altogether (*121*). In *E. coli*, three of the four pseudoknots are dispensable for *trans*-translation *in vitro* and can be replaced with single stranded RNA (*169*). Indeed, the existence of two piece tmRNAs that lack all but one pseudoknot supports the minimal functional importance of the PK loop (*159*, *171*, *172*).

As described, small protein B (SmpB) is also required for *trans*-translation (*173–175*). SmpB is an approximately 18 kDa protein that is highly conserved in most bacterial species (*159*). SmpB binds to tmRNA (*176–179*), occupying the space normally taken by the anticodon stem loop of a tRNA. Initial structural studies showed that SmpB consists of an oligo-nucleotide binding fold with a β-barrel core surrounded by three α-helices (*180*, *181*). The binding fold was later found to interact with the TLD of tmRNA (Figure 1.22), binding the elbow region and stabilizing the acceptor stem in an extended conformation (*167*, *182*). SmpB binds with high affinity (*183*) which is important for tRNA mimicry and its function within the ribosome.

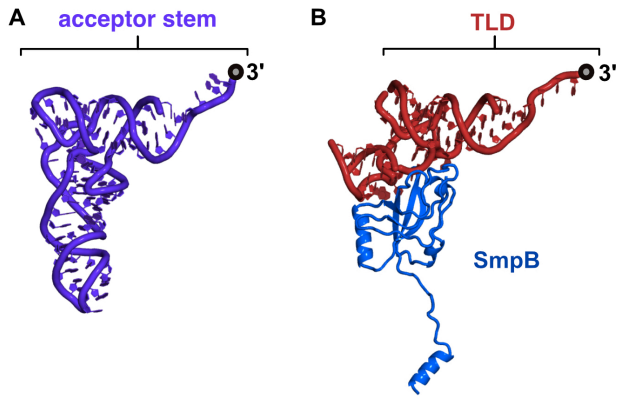

Figure 1.22 TLD-SmpB has the same shape as tRNA. (A) A tRNA has a similar overall shape to (B) the TLD of tmRNA bound to SmpB (PDB 6Q95).

Prior to ribosome binding, SmpB stabilizes the acceptor stem of tmRNA and enhances its interactions with alanyl-tRNA synthetase (AlaRS) (*184*). AlaRS is a class II synthetase that catalyzes the esterification of alanine onto $tRNA^{Ala}$. The enzyme also charges tmRNA with alanine on its 3' CCA (*153*). A highly conserved G-U wobble base pair at the discriminator position in the acceptor stem of tmRNA is key to recognition of tmRNA by AlaRS (*185*). Interestingly, SmpB binding enhances aminoacylation, possibly because it stabilizes the shape of tRNA when bound in place of the anticodon stem loop (*173*, *176*, *177*, *186*).

After alanylation of tmRNA, GTP-bound EF-Tu forms a complex with Ala-tmRNA-SmpB (*176*, *187–189*). EF-Tu typically forms a complex with aminoacyl-tRNA and brings the tRNA to the ribosome. Analogously, EF-Tu binds the acceptor stem of tmRNA while SmpB binds in place of the anticodon stem loop (*176*, *189*, *190*) and the entire complex mimics a tRNA prepared for delivery to the ribosome.

1.4.3 Mechanism of *trans*-translation

Trans-translation rescues nonstop ribosomes using tmRNA and SmpB. tmRNA binds SmpB and with the guidance of EF-Tu, they enter the empty A site of a nonstop ribosome. SmpB distinguishes between stalled and actively translating ribosomes by probing whether there is mRNA in the A site and downstream mRNA channel. Translation then switches from the original mRNA to a reading frame within tmRNA that encodes a short polypeptide, which when added to the end of the nascent chain, targets the incomplete peptide for degradation by proteases. tmRNA-SmpB binding on the ribosome also recruits RNaseR, which degrades the original mRNA as it is released

during *trans*-translation. The reading frame within tmRNA ends in a stop codon, resulting in the release and recycling of the ribosome.

During recognition of nonstop ribosomes, Ala-tmRNA-SmpB is delivered to an empty A site as a complex with EF-Tu-GTP and binds analogously to canonical tRNA (*191*). The first steps towards understanding the structural details of this process came from a 14 Å cryo-EM map of the complex in a pre-accommodated state, with tmRNA-SmpB bound partially in the A site and the antibiotic kirromycin blocking the dissociation of EF-Tu. This showed how the tmRNA-SmpB-EF-Tu complex mimics a tRNA being delivered to the ribosomes, but with a ring of pseudoknots forming a loop around the small subunit. Much later, a seminal paper in 2012 by Neubauer et al. showed a 3.2 Å crystal structure of the ribosome in the pre-accommodated state with a fragment of tmRNA bound to SmpB and EF-Tu blocked by kirromycin (Figure 1.23) (*190*). As anticipated by previous crystal structures of SmpB (*167*), the structure of the pre-accommodated complex shows that the core of SmpB occupies the position normally bound by the anticodon stem loop of tRNA.

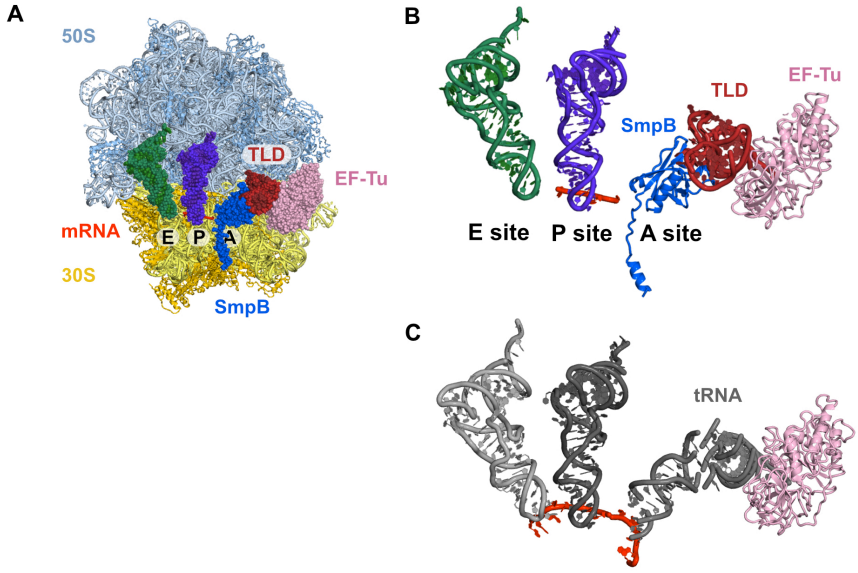

Figure 1.23 A high-resolution structure of the first stage of *trans*-translation. (a) Overview of the ribosomal pre-accommodated complex [PDB 4V8Q; (*190*)]. (b) The C-terminal tail forms an alpha helix in the mRNA channel, detecting a nonstop ribosome. EF-Tu is bound to TLD-SmpB (c) like it would to tRNA [PDB 4V5L; (*71*)].

Although the globular core of SmpB was known to bind to the TLD of tmRNA, the role of the C-terminal tail was unclear until the Neubauer et al crystal structure (*190*). Sensitivity to trypsin suggested that the tail of SmpB is exposed and flexible. Therefore, previous isolated crystal structures had the C-terminal tail either

cleaved off or unstructured in solution. tmRNA tagging activity however, requires the C-terminal tail of SmpB (*180*, *181*, *192–194*). The most highly conserved residues are at the start of the tail, one of which was a glycine. It was suggested that these residues are necessary for the flexibility of the tail and to ensure its positioning within the ribosome (*195*). The crystal structure from Neubauer et al. confirmed the role of the tail of SmpB as critical for anchoring tmRNA-SmpB on the ribosome (*190*).

The C-terminal tail of SmpB forms an alpha helix in the empty mRNA channel, which is essential for recognition of nonstop ribosomes. Binding of the tail in the channel requires highly conserved, positively charged residues (*190*, *196*). Additionally, conserved residues at the base of SmpB's tail interact with decoding center nucleotides A1493 and G530. Interestingly, mutations of decoding center nucleotides that normally affect peptidyl transfer and GTP hydrolysis rates in canonical decoding are less detrimental for *trans*-translation. This suggests a decrease in specificity for these nucleotides by SmpB compared to the precise conformational requirements for detecting cognate codon:anticodon geometry (*197*). Nevertheless, the decoding-like interactions ultimately result in a closed 30S conformation that triggers GTP hydrolysis in EF-Tu (*71*).

EF-Tu departs after hydrolysis of GTP, leaving tmRNA-SmpB to accommodate into the A site of the ribosome. Accommodation requires SmpB and results in peptidyl transfer of the nascent peptide to the alanine on tmRNA (*156*, *193*, *196*, *197*). SmpB crystal structures fit into low resolution EM maps suggest that SmpB interacts with the decoding center similarly to the anticodon stem loop (ASL) in canonical tRNA (Figure 1.24A) (*198*). During accommodation, SmpB is suspected to move deeper into the decoding center (*199*), and the TLD swings by 30 degrees to point into the peptidyl transferase center where it accepts the nascent polypeptide. After accommodation, tmRNA-SmpB must vacate the A site for translation to continue.

As for canonical elongation, EF-G translocates tmRNA-SmpB from the A site into the P site. A low resolution cryo-EM structure of tmRNA-SmpB bound to the ribosome at an intermediate state of translocation suggests analogous activity of EF-G for tmRNA-SmpB (Figure 1.24B), contacting the base of SmpB as it would the anticodon stem loop of tRNA (*200*). Additionally, a large 30S head movement seen in this structure suggests that translocation opens a latch in the A site of the ribosome (A-site latch) which permits the loading of the MLD into the A site. Low-resolution structures of tmRNA-SmpB bound in the P site suggest that SmpB continues to mimic a

tRNA (Figure 1.24C), with SmpB remaining bound to tmRNA. Biochemical evidence lend support to the interpretations of these low resolution structures, suggesting SmpB functions at various stages of *trans*-translation and not just during accommodation (*158*, *178*, *186*).

EF-G catalyzed translocation stimulates the dissociation of deacylated tRNA and mRNA (*201*). The original mRNA is thought to be degraded by RNaseR, a sequence-independent 3' to 5' exonuclease that is recruited to stalled ribosomes in a tmRNA-dependent manner (*202–205*). Although there is limited evidence for how tmRNA may recruit RNaseR to nonstop ribosomes, *trans*-translation is correlated with RNaseR activity in many species. For instance, in *Caulobacter crescentus*, SmpB regulates the action of RNaseR important for cell cycle degradation of tmRNA. In *Streptococcus pneumonia*, SmpB and RNaseR are co-transcribed and cross regulated (*206*). Additionally, tmRNA-dependent degradation of mRNA has also been shown to facilitate mRNA quality control in *E. coli* (*207*).

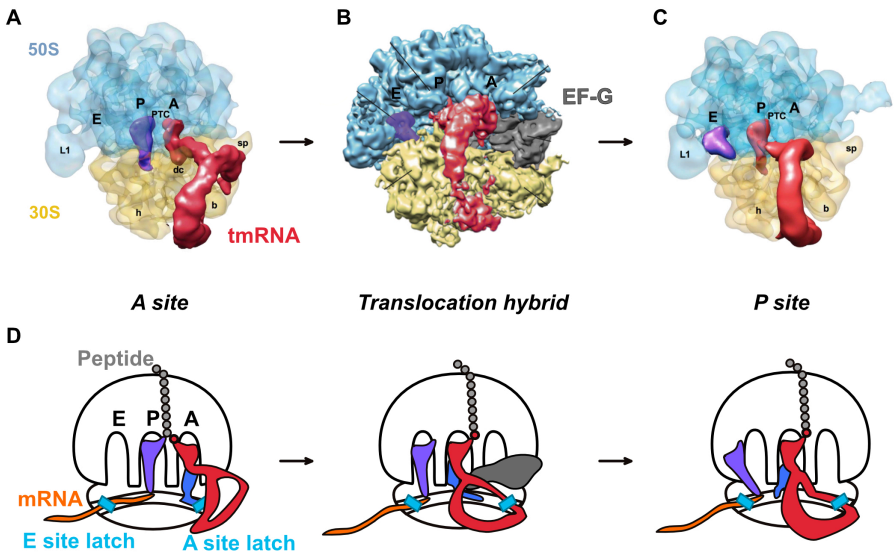

Figure 1.24 Low-resolution EM reconstructions show the general architecture of tmRNA-SmpB in and between the A and P sites. (A) tmRNA-SmpB accommodated into the A site at 13 Å resolution (*168*). (B) Post translocational hybrid state of tmRNA-SmpB in the P site with EF-G bound at 8 Å resolution. (C) tmRNA-SmpB occupying the P site after translocation at 13 Å resolution. Panels A and C are adapted from Weis et al. 2010 (*168*) and panel B adapted from Ramrath et al. 2012 (*200*). (D) Cartoon representation of tmRNA-SmpB translocation and MLD loading into the mRNA channel at the A site.

The ribosome, no longer bound to the original mRNA, switches to the MLD of tmRNA as EF-G catalyzes translocation into the P site (Figure 1.24D). Message

swapping in this way requires the connection of the TLD-SmpB (upon which EF-G is acting) to the MLD. Pseudoknot 1 (PK1) makes this connection, transmitting the movement of translocation to shift the MLD. Studies show that deletion of PK1, or replacement with a structured but shorter RNA sequence, shuts down tagging activity (*169*). However, other studies suggest the opposite, showing that the substitution of PK1 with an RNA hairpin, or even lacking PK1 altogether, permits *trans*-translation (*208*, *209*). Although the structured element of PK1 may not be important, a unifying theory could be that the distance connecting the TLD to the MLD is the critical factor for successful message swapping.

Message swapping results in translation of the tag-reading frame within the MLD of tmRNA. The five nucleotides upstream of the resume codon of the tag-reading frame are critical for positioning it correctly in the A site (*210–212*). *In vitro trans*-translation experiments confirm the specific starting point of the tag-reading frame (*174*, *211*, *213*), placing the first codon (GCA, encoding alanine in *E. coli*) in the decoding center (*201*). To complete *trans*-translation, the ribosome terminates at a stop codon at the end of the tag-reading frame (*156*), and is released and recycled. Without correct positioning of the MLD, the ribosome may translate tmRNA out of frame and therefore stall again after failing to reach another stop codon.

Successful translation of tmRNA adds a peptide tag to the nascent chain, which targets the aberrant protein for degradation by ATP-dependent proteases. These proteases recognize the last few hydrophobic amino acids (AA in *E. coli*) encoded by tmRNA (Figure 1.25A) (*214–217*). The ClpXP protease is the primary protease that degrades tmRNA-tagged peptides (*184*, *214*, *218*). For this, stringent starvation protein B (SspB) initially binds the tagged peptide (Figure 1.25B), increasing the peptide's affinity to the ClpX ATPase (*219*). ClpX then binds the C-terminal AA residues and unfolds the tagged protein in an ATP-dependent manner (*216*). Finally, the ClpP peptidase subunit binds and degrades the aberrant peptide (Figure 1.25C). Tsp protease performs this task in the periplasm, while, cytosolic but membrane associated tmRNA tagged products are degraded by FtsH protease (*215*).

Interestingly, tmRNA mutants engineered to encode a polypeptide tag that does not target nascent chains for proteolysis still complements *ssrA* knockout mutants. When not lethal, removal of ssrA usually causes adverse effects including temperature sensitivity and enhanced repressor activity (*153*, *220*). Since tmRNA-dependent peptide

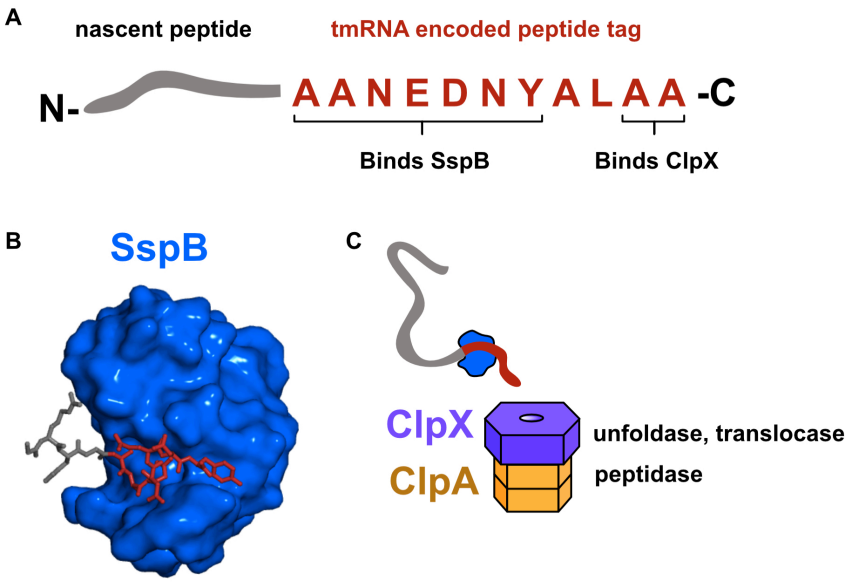

Figure 1.25 Proteases degrade tmRNA-tagged nascent peptides. (A) The polypeptide tag encoded within the MLD of tmRNA has two key binding positions used for targeted degradation. (B) Stringent starvation protein B (SspB) binds the first seven residues of the tag (PDB 1OU8), delivering the peptide to (C) ClpX which recognizes the last two hydrophobic residues. ClpX unfolds the peptide and transfers it directly to the ClpP protease.

release maintains cell survival, these defects are attributed primarily to the build up of stalled ribosomes and the consequently decreased translation capacity of the cell (*221*, *222*).

1.5 Project aims

Although *trans*-translation is generally well understood, there is limited understanding of the process at atomic detail. Apart from the single high-resolution structure of a fragment of tmRNA bound to SmpB during delivery to the ribosome by EF-Tu (*190*), high-resolution structures of intermediates of *trans*-translation downstream from initial binding are yet to be determined. The current high-resolution crystal structure truncated the large flexible tmRNA so as to be compatible with crystallization. Full-length tmRNA has been visualized by a handful of low-resolution reconstructions that provide only general information about the conformation of tmRNA-SmpB on the ribosome.

The recent revolution in cryo-EM technology, including detector design and image processing software, now make determining high-resolution structures of large,

flexible macromolecular complexes potentially feasible. We therefore set out to trap intermediates of *trans*-translation using full-length tmRNA-SmpB. A structure of tmRNA-SmpB bound in the A site was needed to understand how tmRNA-SmpB accommodates into the ribosome during the first stage of *trans*-translation. To understand the subsequent movement of tmRNA-SmpB through the ribosome and how message swapping occurs, we also sought to solve structures of downstream *trans*-translation intermediates. In particular, we wanted to understand the role of SmpB in binding tmRNA on the ribosome during the later stages of *trans*-translation, to see how SmpB and such a large circularized tmRNA navigates through the ribosome, and how this movement loads the MLD into the mRNA channel. Finally, we were interested in determining the previously unattempted structure of tmRNA-SmpB after translocation past the P site.

2 tmRNA-SmpB recognizes nonstop ribosomes

2.1 Introduction

Trans-translation begins when elongation factor-Tu (EF-Tu) delivers tmRNA-SmpB to a ribosome (*191*). A decoding-like event triggers the dissociation of EF-Tu, after which tmRNA-SmpB is accommodated into the A site. The resulting peptidyl-transferase reaction transfers the nascent peptide to the alanine-bound tRNA-like domain (TLD) of tmRNA (*156*) (Figure 2.1).

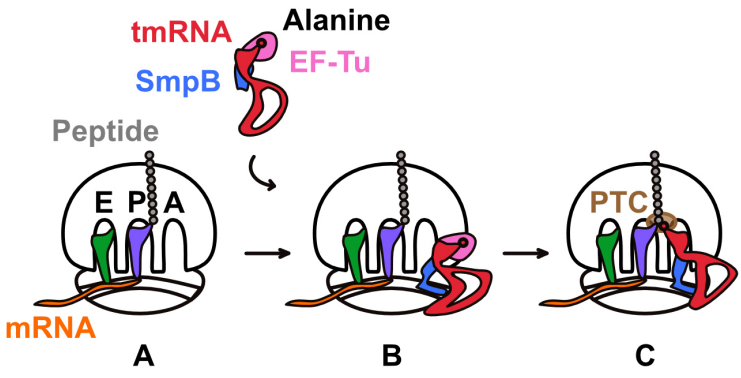

Figure 2.1 Cartoon schematic of tmRNA-SmpB accommodation into a nonstop ribosome. (A) A nonstop ribosome lacks mRNA in the A site. (B) EF-Tu delivers tmRNA-SmpB to the nonstop ribosome in a state called pre-accommodation. (C) EF-Tu hydrolyzes GTP and dissociates. tmRNA-SmpB then accommodate into the A site and the nascent peptide is transferred to alanine on tmRNA.

In order for *trans*-translation to initiate successfully, tmRNA must therefore be charged with alanine. Alanyl-tRNA synthetase (AlaRS), an enzyme that normally charges $tRNA^{Ala}$, catalyzes the covalent attachment of alanine to tmRNA (*223*). A G-U base-pair in the acceptor arm of tmRNA is critical for enzyme specificity, similar to the determinant G3-U70 pair in $tRNA^{Ala}$ (*185*, *223–226*). Importantly, the anticodon of $tRNA^{Ala}$ is not required for recognition by AlaRS (*227*) as tmRNA lacks an anticodon stem loop, which is instead replaced by SmpB. After aminoacylation, EF-Tu binds the acceptor stem of tmRNA and stabilizes the charged state (*187*, *228*).

EF-Tu delivers tmRNA-SmpB to the ribosome in a manner analogous to the delivery of tRNA. The interactions of EF-Tu with the acceptor stem of tmRNA and the factor binding site on the ribosome, including the sarcin-ricin loop, are nearly identical to canonical tRNA (*229*, *230*). As further evidence of this similarity, a previous structural study shows that the antibiotic kirromycin, which prevents EF-Tu from leaving the ribosome after GTP hydrolysis, can be used to trap a fragment of tmRNA bound to SmpB and EF-Tu on the ribosome (*230*, *231*). Given these parallels, it is difficult to explain other studies claiming that delivery and accommodation of tmRNA-SmpB is not coupled to GTP hydrolysis by EF-Tu (Miller 2014; Kurita 2014). Either the interaction of tmRNA secondary structure elements with the head of the ribosome, or the lack of canonical decoding center interactions in the A site could play a role in this discrepancy.

Although delivery of tmRNA occurs regardless of the translation state of the ribosome (*66*), initiation of *trans*-translation only occurs on stalled ribosomes (*232*) and is more efficient on ribosomes that have reached the 3’ end of an mRNA. tmRNA-SmpB must therefore distinguish these stalled, or ‘nonstop’, ribosomes from actively translating ones. The primary difference between nonstop and translating ribosomes is that nonstop ribosomes lack mRNA in the A site and downstream mRNA channel. A mechanism for discriminating between stalled and translating ribosomes was first visualized by Neubauer and colleagues (*229*). Their structure of a fragment of tmRNA bound to SmpB and EF-Tu on the ribosome shows how the unstructured C-terminal tail of SmpB detects a nonstop ribosome by forming an alpha helix in the mRNA channel. This alpha helix fills the space otherwise occupied by mRNA in actively translating ribosomes. Ribosomes with mRNA extending past the A site are therefore poor substrates for *trans*-translation. Specifically, long mRNA extending past the A site has been shown to block peptidyl-transfer to tmRNA, however, it does not block the

activation of EF-Tu (*233*). This suggest that tmRNA-SmpB samples the A site in a way that permits the release of EF-Tu, while ultimately rejecting tmRNA-SmpB from the ribosome due to the presence of mRNA in the channel.

Prior to the study presented here, the work of Neubauer et. al. represented the first and only high-resolution structure of tmRNA-SmpB bound to the ribosome. However, this structure includes only a fragment of tmRNA. A structure of full-length tmRNA-SmpB bound in the A site was needed to understand how tmRNA-SmpB accommodates into the ribosome during the first stage of *trans*-translation. Here, cryo-electron microscopy was used to determine the structure of *T. thermophilus* 70S ribosomes assembled with tmRNA-SmpB in the A site. We show that during accommodation, the conformational change of tmRNA-SmpB is analogous to canonical tRNA. Additionally, the alpha helix in the C-terminal tail of SmpB remains bound while tmRNA makes important contacts on the solvent side of the ribosome, through a loop of RNA from pseudoknot 2 (PK2).

2.2 Results and discussion

2.2.1 Preparation of *T. thermophilus* tmRNA-SmpB bound to the ribosome

Thermus thermophilus ribosomes, tmRNA and SmpB were purified in an attempt to assemble a complex representing the accommodation of tmRNA-SmpB into the A site of the ribosome. tmRNA was transcribed *in vitro* with T7 RNA polymerase and purified on a denaturing polyacrylamide gel. Because tmRNA was not purified from an *in vivo* sample, it is not charged with alanine. To remedy this, AlaRS was used *in vitro* to attach an alanine residue to the 3' CCA of the acceptor stem of tmRNA (*223*). tmRNA must be charged with alanine for *trans*-translation to initiate and therefore a method of detecting successful aminoacylation was a necessary precedent for complex assembly.

A filter-binding assay was developed to quantify ^{14}C-radiolabeled alanyl-tmRNA. This was done using an automated scintillation counting system permitting high-throughput testing and optimization. Initially, using a previously described method, reactions yielded only 10% of tmRNA which was aminoacylated (*229*). This is less than the expected 28% reported to be achievable *in vitro* for the aminoacylation of

T. thermophilus tmRNA with *E. coli* AlaRS (*234*). To help us understand why the reactions were inefficient, *E. coli* $tRNA^{Ala}$ was prepared and aminoacylated as a control. A variety of conditions were systematically tested including buffer composition, order of addition of components, and tmRNA folding methods. Ultimately, increasing the concentration of AlaRS led to an improved aminoacylation of 24%, or 31% as efficient as charging of *E. coli* $tRNA^{Ala}$ (Figure 2.2). Interestingly, aminoacylation of *E. coli* tmRNA by AlaRS showed similar results with a total of 23% of tmRNA being aminoacylated, 33% as efficient as for *E. coli* $tRNA^{Ala}$. These results suggest that tmRNA-SmpB is not an ideal substrate for AlaRS. Determining the efficiency of aminoacylation of tmRNA was important for the preparation of ribosome-bound complexes, as only charged Ala-tmRNA is functional for *trans*-translation.

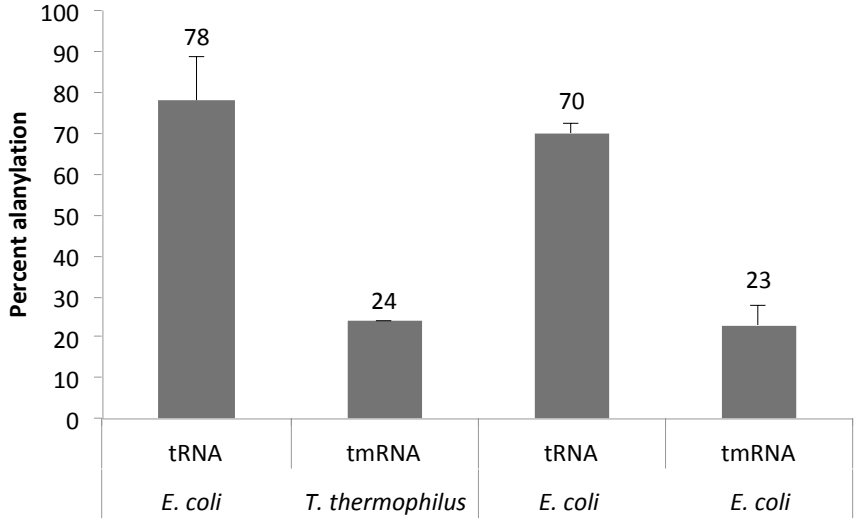

Figure 2.2 Optimization of tmRNA amioacylation. Alanyl-tRNA synthetase (AlaRS) was used to aminoacylate $tRNA^{Ala}$ and tmRNA with ^{14}C-alanine. $tRNA^{Ala}$ control reactions were conducted simultaneously for both tmRNA species. Reactions were precipitated onto glass microfiber filters, washed, dried, and disintegrations per minute (DPM) counted by liquid scintillation. Values were corrected for background and compared to a hypothetical maximum defined by calculating the expected DPM were aminoacylation 100% efficient for the total amount of RNA added. Error bars represent the standard deviation of triplicates.

Initial attempts to purify charged Ala-tmRNA by polyacrylamide gel electrophoresis or reverse phase HPLC failed (data not shown), though these approaches were previously used successfully for the purification of aminoacyl-tRNA (*235–237*). It's possible that these purification methods lacked the resolution required to discriminate between charged and uncharged tmRNA species, as tmRNA is much larger, containing nearly five times as many nucleotides as tRNA. Purification of Ala-

tmRNA from tmRNA was ultimately abandoned and aminoacylation reactions were used directly for the initiation of *trans*-translation on nonstop ribosomes.

Nonstop translation complexes were assembled by mixing aminoacyl-tRNA, a short mRNA and *T. thermophilus* 70S ribosomes. *Trans*-translation was initiated by adding Ala-tmRNA-SmpB with EF-Tu-GTP to promote its delivery to the ribosome. The formation of stalled ribosomes as substrates for *trans*-translation was tested using both P-site fMet-tRNA^{fMet} or Phe-tRNA^{Phe}, with short mRNAs containing a ribosome binding site and the corresponding P-site codon.

Aminoacylated tmRNA-SmpB was delivered to stalled ribosomes and binding was verified by sucrose gradient centrifugation. Both tRNA-mRNA pairs used to assemble nonstop ribosomes showed a peak shift relative to empty 70S ribosomes, as well as an additional peak corresponding to excess factors (Figure 2.3A).

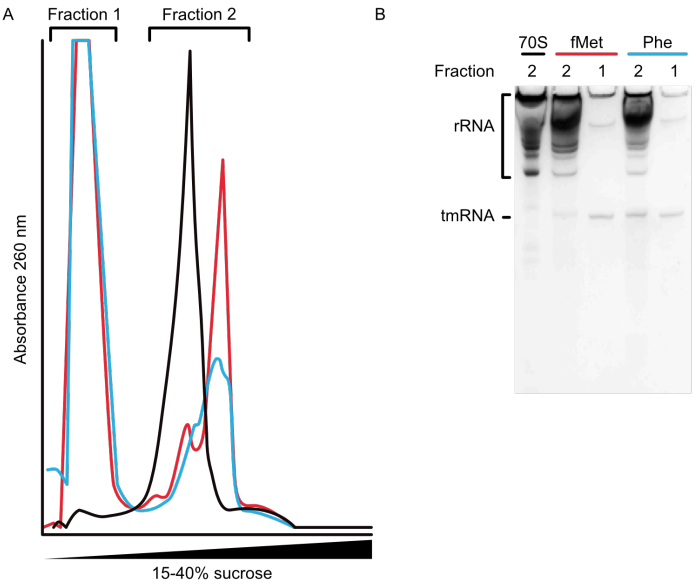

Figure 2.3 Verification of tmRNA-SmpB occupancy on the ribosome. (A) Reactions assembling nonstop ribosomes with tmRNA-SmpB bound in the A site were fractionated by sucrose gradient centrifugation. *T. thermophilus* 70S ribosomes were tested alone (black) or in complex with tmRNA-SmpB, mRNA lacking a codon in the A site, and fMet-tRNA^{fMet} (red) or Phe-tRNA^{Phe} (blue). (B) Pooled sucrose gradient fractions were analyzed for the presence of tmRNA on denaturing polyacrylamide-urea gels.

These interpretations are based on the fact that shifting of the 70S ribosome peak into heavier sucrose fractions is indicative of a change in ribosome mass, density, or shape, likely due to factor binding. Additionally, tmRNA co-migrated with the ribosome-containing fractions, suggesting that it was bound to the ribosome (Figure

2.3B). More tmRNA co-migrated with stalled ribosomes when assembled with Phe-tRNA^{Phe}, and so these complexes were chosen for preparation of cryo-EM grids.

Cryo-EM samples were prepared on copper quantifoil grids coated with a ~50 Å thick layer of amorphous carbon as a support. Grid conditions and alternate supports including graphene oxide or thin ice alone were tested using empty *T. thermophilus* 70S ribosomes. Copper carbon coated grids gave a reproducible distribution of ribosomal particles and consistent ice thickness suitable for cryo-EM data collection (Figure 2.4A). After optimization of ribosome concentration and ice thickness, a dataset was collected on a 300 kV Polara microscope. Initial two-dimensional class averages, processed in RELION, show the presence of a variety of views of the ribosome, suggesting a good distribution of particle orientations and the potential for high-resolution structure determination (Figure 2.4B).

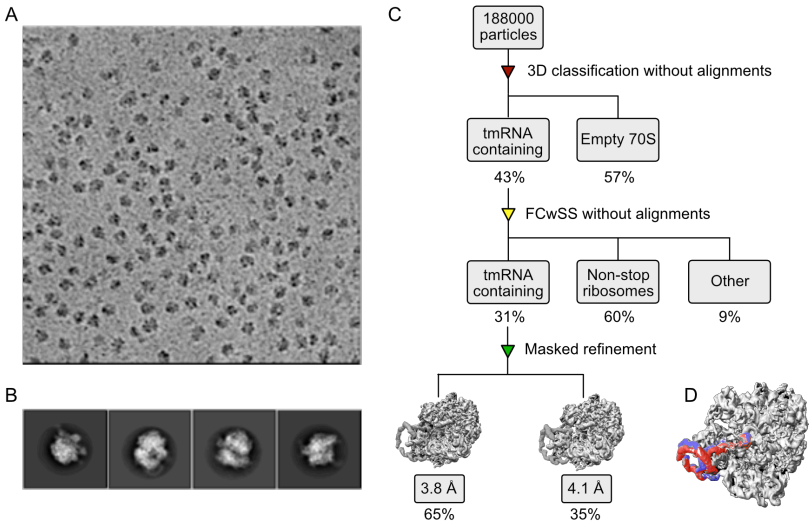

Figure 2.4 Cryo-EM data collection and processing of *T. thermophilus* ribosomes with tmRNA-SmpB bound in the A site. (A) Representative micrograph taken at 75k magnification on a 300 kV Polara cryo-TEM (FEI). (B) Representative two-dimensional classes. (C) Three-dimensional classification workflow in RELION and resulting electron density maps. (D) Superimposition of maps showing different tmRNA pseudoknot loop conformations (blue, red).

Our dataset contained 188,000 particles after initial 2D classification. After 3D classification, 81,000 particles appeared to contain tmRNA-SmpB bound in the A site of the ribosome. However, the map showed density for tmRNA at lower occupancy than the ribosome. To remove empty ribosomes and select for particles containing tmRNA, focused classification with signal subtraction (FCwSS) was performed with a mask over tmRNA-SmpB in the A site. This resulted in 24,000 particles containing tmRNA-SmpB. Three-dimensional classification indicates that in this sample only about half of

all ribosomes formed a nonstop complex and only a third of those were loaded with tmRNA (Figure 2.4C). This clearly shows that the *in vitro* assembly of this *trans*-translation intermediate is inefficient. Despite this, particle numbers were sufficient for near-atomic resolution structure determination.

Two maps were obtained at resolutions of 3.8 Å and 4.1 Å from approximately 16,000 and 9,000 particles, respectively. Three-dimensional classification reveals that the pseudoknot loop of tmRNA occupies a continuum of conformations, which were averaged into two main classes (Figure 2.4D). The range of motion was confirmed by joining particles in the final maps and re-classifying with either three or four available classes. The classes obtained from this test contained tmRNA-bound ribosomes with conformations of the pseudoknot loop intermediate to those previously observed (data not shown).

With the exception of the movement seen for the pseudoknot loop, the two maps were otherwise identical. To maximize the quality of the density, the maps were joined and the first high-resolution structure of full-length tmRNA bound to the ribosome was built (Figure 2.5). Although the overall map quality was adequate for building an atomic model, the tmRNA was especially flexible and of lower local resolution. Secondary structural elements of tmRNA, primarily the highly flexible pseudoknot loop, were unable to be unambiguously built and were instead homology modelled based on secondary structure predictions (*165*, *166*) and initial 3D predictions of the structure of tmRNA (*200*).

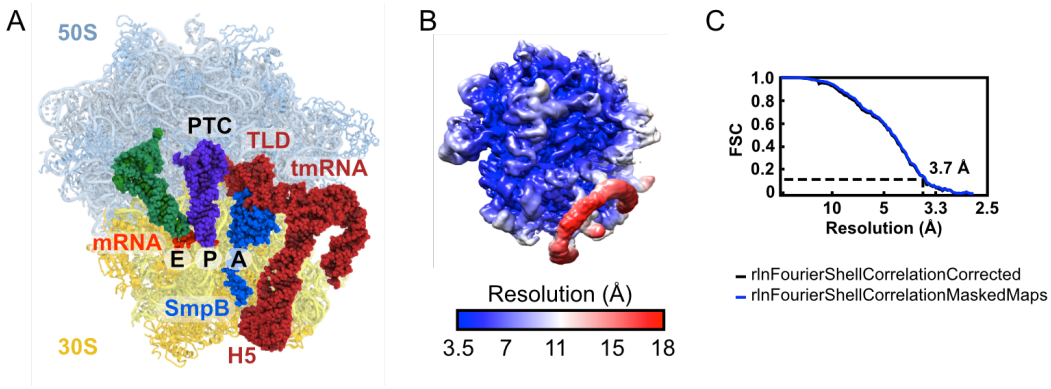

Figure 2.5 Structure of *T. thermophilus* tmRNA-SmpB bound in the A site of the ribosome. (A) Overview of the structure of tmRNA-SmpB occupying the A site of a nonstop ribosome. (B) Electron density map colored by local resolution ranging from 3.5 Å to 18 Å. (C) Fourier shell correlation (FSC) curve showing map resolution of 3.7 Å with dashed line at FSC=0.143.

The structure shows that the TLD of tmRNA points into the A site, below which SmpB binds the decoding center and downstream mRNA channel. Nearby, mRNA and tRNA are bound in the P site and E site, respectively. The pseudoknot loop of tmRNA wraps around the beak of the 30S subunit where it is anchored on the solvent side of the ribosome.

2.2.2 The structure of tmRNA-SmpB bound in the A site

tmRNA-SmpB contacts the ribosome in two places when occupying the A site of a nonstop ribosome. In the first position, SmpB binds in the decoding center, mimicking a codon:anticodon interaction and filling the downstream mRNA channel. At a second position, pseudoknot 2 (PK2) of tmRNA binds to the solvent side of the ribosome while helix 5 (H5) crowds the entrance of the mRNA channel near the tail of SmpB.

SmpB is 'decoded' by the ribosome in a manner analogous, but not identical to, the usual codon:anticodon interaction in the A site. Trp126 of SmpB stacks with G530 as in the pre-accommodated state (*229*), which is consistent with previous studies showing that tmRNA-SmpB binds poorly when Trp126 is mutated to alanine (*238*). Additionally, the conserved aromatic residue His12 of SmpB is seen to stack with A1493 (Figure 2.6A). Although A1493 plays a critical role in canonical decoding, the mutation of His12 to cysteine has been shown to have little effect on the overall activity of *trans*-translation (*233*). The binding of SmpB agrees with biochemical experiments showing that decoding center nucleotides are protected upon SmpB binding in the A site (*239*). However, unlike canonical decoding of tRNA, A1492 does not participate in decoding SmpB and remains only partially flipped out as seen in Neubauer et al. 2012. Nevertheless, the head and body of the 30S subunit are in a closed conformation, resembling that of canonical decoding.

SmpB also mimics an mRNA in the downstream mRNA channel (Figure 2.6A). Conserved positively- and negatively-charged residues in the tail of SmpB (Figure 2.6B) interact with the mRNA channel to stabilize the TLD-SmpB in the A site. Previous studies have shown that at least one positively charged residue in the tail is required for *trans*-translation (*195*). Comparing the position of the tail of SmpB to that in the pre-accommodated state crystal structure shows that it remains in a nearly identical position after accommodation (Figure 2.6C).

Trans-translation activity is shown to be reduced on ribosomes that contain mRNAs with ≥9 nucleotide extensions downstream from the P-site codon (*232*). An extension of this length corresponds to the distance at which the mRNA would clash with H5 at the entrance of the mRNA channel (Figure 2.6D).

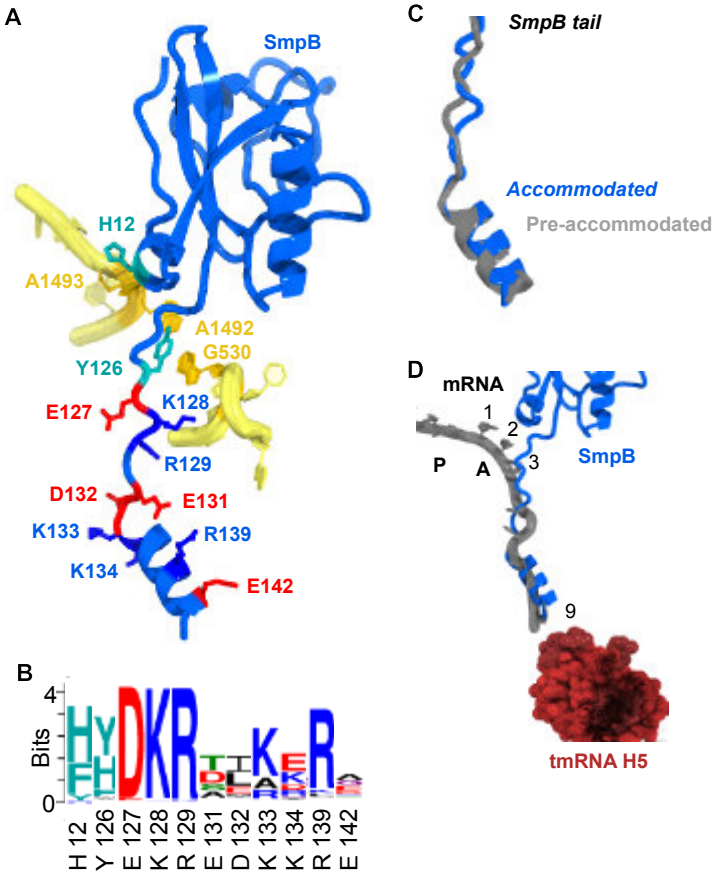

Figure 2.6 SmpB initially binds in the A-site decoding center and downstream mRNA channel. (A) Conserved aromatic residues (teal) interact with decoding center nucleotides (gold) while conserved positively (blue) and negatively charged (red) residues mimic an mRNA in the channel. (B) Sequence logo from multiple sequence alignment of SmpB showing conserved residues. (C) Global superimposition of *T. thermophilus* ribosome complexes showing the tail of SmpB when it is bound in the A site (blue) compared to when it is bound in a pre-accommodated state (gray, PDB 4V8Q, Neubauer et. al. 2012). (D) Superimposition of the A-site structure with a structure containing mRNA (gray, PDB 4V6F, Jenner et. al. 2010).

H5 of tmRNA, a highly conserved segment of secondary structure, crowds the entrance of the mRNA channel as it is in close proximity with the tail of SmpB. Arginine 132, 136 and 143 of protein uS3 make electrostatic interactions that stabilize the phosphate backbone of H5 (Figure 2.7). Other structures containing mRNA hairpins at the entrance of the mRNA channel interact with arginine residues of uS3 in a way that may stabilize their positions as well, however, the conformation of these hairpins is

entirely different to that of H5 of tmRNA (*240*, *241*). Additionally, protein uS3 can similarly stabilize mRNA on the solvent side of the ribosome (*242*).

H5 is ultimately positioned by the neighboring secondary structural element PK2, binding to the solvent side of the ribosome. tmRNA is anchored to the small subunit by an interaction between PK2 and ribosomal protein uS3 (Figure 2.7). A single stranded RNA loop of PK2 is sandwiched in a pocket of uS3 formed by a loop joining two alpha helices and a beta strand. Binding of PK2 may explain why tmRNA-SmpB can be delivered to a nonstop ribosome in the absence of the C-terminal tail of SmpB (*193*). Binding of PK2 and H5 may therefore play a role in initial recognition of a nonstop translation complex.

Additionally, the binding of PK2 to the solvent side of the ribosome during the early stages of *trans*-translation may explain why the tail of SmpB is dispensable for the activation of GTP hydrolysis by EF-Tu. The decoding-like interactions with SmpB would still be possible if the position of tmRNA were maintained by interactions between PK2 and uS3. However, without the alpha helix of the C-terminal tail of SmpB in the mRNA channel, entrance of tmRNA-SmpB into the A site is prevented. Indeed, removal of the tail has been shown to prevent peptidyl transfer *in vitro* (*195*).

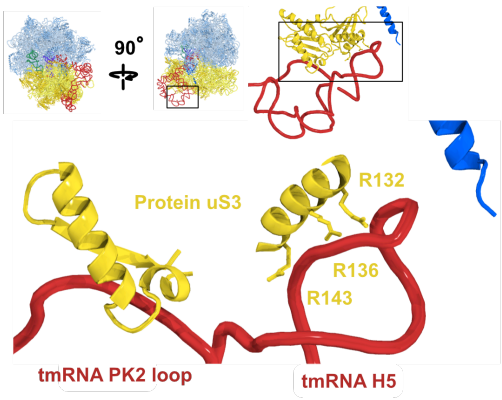

Figure 2.7 Pseudoknot 2 of tmRNA binds protein uS3 on the solvent side of the ribosome. A single stranded RNA loop from PK2 of tmRNA binds protein uS3 while arginine residues of protein uS3 interact with the phosphate backbone tmRNA's H5.

As tmRNA-SmpB enters the A site of the ribosome, it undergoes a conformational change analogous to tRNA. This change includes two similarly flexible regions: (i) the conserved Gly122 (Gly132 in *E. coli*) at the beginning of the tail of SmpB bends to allow the body of SmpB to fully rotate into the A site, and (ii) the elbow of the TLD acts as a hinge around which the acceptor arm swings into the

peptidyltransferase reaction center (PTC) (Figure 2.8). These movements are similar to those of the anticodon stem loop (ASL) and elbow of tRNA, respectively (*84*).

The alanine-bound 3'CCA of tmRNA is positioned into the PTC and the nascent peptide is transferred to tmRNA through a peptidyltransferase reaction. Consistent with this, density for the nascent di-peptide is observed in the peptide exit tunnel (data not shown). In this conformation tmRNA-SmpB mimics a tRNA ready to be translocated into the P site by elongation factor G (EF-G).

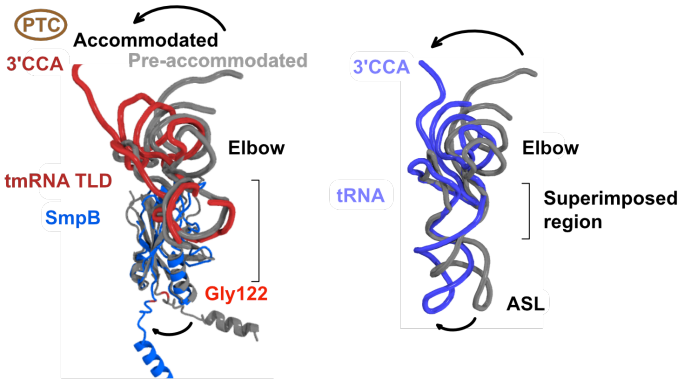

Figure 2.8 TLD-SmpB mimics the flexibility of a tRNA as it accommodates into the A site of the ribosome. Local superimposition of the tRNA-like domain (TLD) of tmRNA bound to SmpB (left) in the A site (red, blue) or pre-accommodated (gray) compared to canonical tRNA (right) in the A site (purple) or pre-accommodated (gray).

2.3 Conclusions

The structure of full-length tmRNA-SmpB bound in the A site of the ribosome shows important binding interactions between tmRNA-SmpB and the ribosome. By comparing this structure with the crystal structure of the pre-accommodated state (*229*), we can now describes the initial stages of *trans*-translation in atomic detail.

Analogous to a tRNA, the initial delivery of tmRNA-SmpB to the ribosome is coordinated by EF-Tu. EF-Tu simultaneously binds tmRNA and the ribosome to position SmpB near the A site. If the ribosome detects correct codon:anticodon interactions in the A site, EF-Tu hydrolyzes GTP and subsequently dissociates. However, since the substrate for *trans*-translation is a ribosome specifically lacking mRNA in the decoding center, correct codon:anticodon interactions are inherently impossible for nonstop ribosomes. Instead, tmRNA-SmpB mimics a codon:anticodon

interaction in the A site and stimulates decoding-like interactions in a non-canonical way. SmpB is a protein and therefore has no structural similarity to the cognate mRNA-tRNA normally decoded in the A site, nevertheless, it takes the place of both mRNA and tRNA in the decoding center. This is possible due to aromatic residues, which interact with the decoding center nucleotides, and thereby trick the ribosome into 'decoding' what is actually a protein. This decoding event causes the ribosome to take on a closed conformation and results in the dissociation of EF-Tu.

Although delivery of tmRNA-SmpB to the ribosome involves interactions between EF-Tu and the ribosome analogous to canonical translation, the structure of full-length tmRNA-SmpB bound in the A site shows additional interactions that are not possible for tRNA. Along with indirect binding to the ribosome through EF-Tu, tmRNA binds directly to the solvent side of the ribosome. Specifically, pseudoknot 2 and helix 5 of tmRNA interact with protein uS3 to anchor tmRNA to the ribosome. This direct binding may represent an initial function of tmRNA-SmpB in identifying nonstop ribosomes and explain why there are specific mRNA length dependencies for *trans*-translation. Indeed, binding of PK2 to uS3 on the solvent side of the ribosome positions H5 of tmRNA at the entrance of the mRNA channel. This position is incompatible with actively translating ribosomes that typically contain mRNAs extending out of the mRNA channel. Therefore, even before the C-terminal tail of SmpB binds in the A site, direct binding of tmRNA may be limited to nonstop ribosomes.

Although we suspect binding of PK2 to the ribosome occurs prior to tmRNA-SmpB accommodation, without a structure of the full-length tmRNA-SmpB trapped with EF-Tu we cannot claim precisely when discrimination of nonstop ribosomes by H5 occurs. However, tmRNA binding as the first step in the discrimination of nonstop ribosomes would explain why the C-terminal tail of SmpB is dispensable during the early stages of *trans*-translation (*193*). Additionally, without direct interactions between tmRNA and the ribosome, the large pseudoknot loop would be even more mobile and could interfere with accommodation of tmRNA-SmpB into the A site. Instead, when tmRNA is anchored to the ribosome, SmpB can probe the A site during what could be considered a second, although potentially simultaneous, step in discriminating nonstop ribosomes. If SmpB occupies an A site with an empty mRNA channel, the C-terminal tail of SmpB forms an alpha helix in place of mRNA and therefore confirms that the channel lacks mRNA.

In this way, a two-step discrimination process begins with initial positioning of tmRNA-SmpB on the ribosome by EF-Tu, permitting tmRNA-SmpB to probe the ribosome at two positions; (i) H5 at the entrance of the mRNA channel and, (ii) SmpB inside the mRNA channel. Ultimately, alpha helix formation by the tail of SmpB stabilizes it in a position favorable for decoding-like interactions. The ribosome is tricked into decoding SmpB, acting as a switch that causes dissociation of EF-Tu, licensing entry of tmRNA-SmpB into the ribosome.

It is not surprising that the decoding-like interactions seen in the pre-accommodated state are maintained after tmRNA-SmpB is accommodated. The same overall pattern is seen during canonical translation elongation, as cognate codon:anticodon base-pairing interactions are maintained after EF-Tu dissociates. Overall, tmRNA-SmpB accommodates into the A site in a manner remarkably analogous to tRNA. It is striking that a large RNA-protein complex can so effectively mimic a tRNA and trick the ribosome into decoding in the absence of an A-site mRNA or tRNA.

The methodology used to assemble the ribosomal complex and determine its structure gives us confidence in our overall conclusions. Importantly, using *T. thermophilus*, the same species as the previously determined crystal structure of the pre-accommodated state, guarantees that differences between the two structures were not species specific, but instead represent mechanistic function. Additionally, new image processing techniques in RELION allow for the unambiguous separation of particles to guarantee a homogeneous complex *in silico*. In particular, a systematic classification approach using FCwSS gives us confidence that our structure contains only ribosomes with tmRNA bound, and that of those tmRNA-bound ribosomes, only those containing tRNA and mRNA were selected.

Although state-of-the-art techniques in cryo-EM were used to determine this structure, the inherent mobility of tmRNA resulted in only moderate resolution of the factor, and especially poor resolution in regions of the pseudoknot loop. We therefore cannot confirm the complete secondary structure of tmRNA using our current data set. However, tmRNA as homology modelled (*200*) in accordance with secondary structure predictions, fits remarkably well into the overall shape of the density. Additionally, the nature of our claims regarding tmRNA avoid requirements for nucleotide level resolution apart from the well defined regions such as the loop of PK2 and H5, and the acceptor stem of tmRNA. Additional datasets were collected attempting to improve this

resolution (Table 5.2, #3-5), however, considerable resolution gains were never achieved. Indeed, the native structure of the *trans*-translation intermediate may be unlikely to reach high-resolution using current techniques due to the flexibility of tmRNA.

Determining the structure of full-length tmRNA-SmpB bound in the A site of the *T. thermophilus* 70S ribosome represents a critical advancement in our understanding of the initial stages of *trans*-translation. Ultimately, binding of tmRNA-SmpB in the A site results in domain closure between the head and body of the small subunit, and peptidyl transfer to tmRNA. After this handover event, tmRNA is bound to the nascent peptide and is poised to become the new template for translation. To understand the subsequent movement of tmRNA-SmpB through the ribosome and how message swapping from the original mRNA to tmRNA occurs, structures of downstream *trans*-translation intermediates were also required.

The next chapter will discuss an exciting series of three structures of *trans*-translation intermediates, assembled for the first time using a physiologically relevant nonstop ribosome containing a full-length nascent polypeptide chain. An *E. coli in vitro* transcription and translation system was adapted for *in vitro trans*-translation. Selectively removing required translation factors from this system made it possible to capture downstream intermediates in the absence of any antibiotic or stalling factor.

2.4 Materials and methods

Protein and RNA purification

Thermus thermophilus HB8 70S ribosome (*49*), tmRNA (*191*), SmpB (*229*), and *E. coli* alanyl tRNA synthetase (*243*) were purified as previously described. The mRNA sequences used GGCAAGGAGGUAAAA**AUG**UA and AGGAGGUGAGG**UUU**U, with the Shine-Dalgarno sequence underlined and the P-site codon in bold, were synthesized by Integrated DNA Technologies. fMet-tRNA^{fMet} (*237*) and Phe-tRNA^{Phe} (*236*) were prepared as described.

tmRNA Aminoacylation

tmRNA was refolded by heating at 90°C for 1 min in folding buffer (5 mM $MgCl_2$, 20 mM NH_4Cl, 10 mM Hepes-KOH pH 7.5) and cooled at room temperature for 30 min before placing on ice. Aminoacylation reactions (50 mM K-HEPES pH 7.5, 60 mM NH_4Cl, 7 mM $MgCl_2$, 1 μM tmRNA, 1.5 μM SmpB, 30 μM Alanine, 4 mM ATP, 0.2 μM Alanine-tRNA ligase, 2 U/ml inorganic pyrophosphatase) were incubated at 37°C for 30 min. For filter binding assays, ^{14}C-alanine was used. The reaction was spotted in triplicate on glass microfiber filters. The filters were washed once with ice-cold 10% trichloroacetic acid/50% ethanol to precipitate the tmRNA and then washed three times with ice-cold 70% ethanol to remove unbound ^{14}C-Alanine. Filters were dried at 60°C for 1 h and disintegrations per minute counted by liquid scintillation.

Ribosome Complex Formation

Nonstop ribosome reactions [Buffer G (50 mM KCl, 10 mM NH_4Cl, 10 mM Mg-acetate, 5 mM HEPES, pH 7.5) 400 nM *Thermus thermphilus* 70S, 1.6 μM mRNA, 1.6 μM tRNA] were incubated at 55°C for 15 min. Accommodated state complexes were then formed by adding aminoacylated tmRNA-SmpB (400 nM final) followed by an additional incubation at 55°C for 15 min.

Ribosome complexes were analyzed by sucrose gradient fractionation (15-40% sucrose, Buffer G) with an ultracentrifuge (Beckman SW40-Ti rotor, 22000 rpm, 16 h, 4°C). Fractions were collected from bottom to top with absorbance at 260 nm monitored and used to indicate the presence of ribosomes. Peaks were pooled, concentrated, acidic phenol:chloroform extracted and ethanol precipitated. Isolated RNA from the peaks was analyzed on a 6% polyacrylamide gel with 8M urea.

Electron Microscopy

Ribosome complex reactions were diluted to 70 nM ribosome concentration in Buffer G and 3 μl was incubated for 30 s on glow-discharged R2/2 carbon Quantifoil grids, coated with an ~50 Å-thick amorphous carbon film. The grids were blotted for 4.5 s in 100% humidity at 4 °C and then flash-frozen in liquid ethane using a Vitrobot MKII (FEI).

A Polara microscope (FEI) operated at 300 kV was used with a 1.5 s exposure and total dose of 35 $e^{-}Å^{-2}$ and a defocus range of −2.0 to −3.5 μm in 0.3 μm increments.

Images were recorded using EPU automated data acquisition software with a Falcon III direct electron detector (FEI) at a pixel size of 1.34 Å.

Image Processing

All image processing was completed using Relion 2.0 software (*244*). The frames of the micrographs were aligned using motion correction (*245*) and then contrast transfer function parameters were calculated using Gctf (*246*). Relion manual picking mode was used to define a subset of particles. After two-dimensional (2D) classification, class averages were then used as a template for automatically picking the entire set of micrographs (*247*). After particle extraction, an initial 2D classification was used to remove all non-ribosomal particles. Ribosomal particles underwent an initial three-dimensional (3D) refinement using a template map (EMD-3493) low pass filtered to 40 Å. An initial 3D classification was used to select only tmRNA-containing particles. This subset of particles went through another round of 3D refinement along with movie-refinement, post processing, particle polishing and then a third round of 3D refinement. Focused classification with signal subtraction (FCwSS) was conducted with a mask over tmRNA-SmpB followed by another round of 3D refinement and post processing to produce the final maps.

Model Building, Refinement and Validation

A starting model of a *T. thermophilus* 70S ribosome (PDB 4V51) was docked into the post-processed maps using Chimera (*248*). Protein and RNA chains were fitted to the density using rigid-body fit in Coot (*249*). SmpB from *T. thermophilus* [(*190*); PBD 4V8Q] and homology-modelled *E. coli* tmRNA [(*200*); PDB 4V6T] were used as starting models. tmRNA was broken into major helical or pseudoknot domains, rigid-body fit to the density using Chimera and reattached in Coot. To adjust the structure of tmRNA to more closely fit the shape of the density while maintaining the base-pairing as predicted, morph chain and real space refinement in coot were repeated iteratively with libg generated restraints (*165*, *166*, *250*). Figures were created using Pymol (*251*) or Chimera (*248*).

Models were refined in real space with Phenix (*252*). $FSC_{average}$ was monitored during refinement and the final models were assessed with MolProbity (*253*). Cross validation to prevent overfitting was performed as previously described (*250*).

3 The movement of tmRNA-SmpB through the ribosome

3.1 Introduction

Ribosomes translate mRNA through a repeating cycle of codon recognition and protein chain extension events cumulatively called elongation. Both canonical translation elongation and *trans*-translation share key aspects of this process. First, an elongation factor, EF-Tu, delivers tRNA to the ribosome where it pairs with the mRNA. During decoding, the ribosome verifies that the correct tRNA anticodon is bound to the mRNA codon, after which the protein chain is transferred to the tRNA via a peptidyl transfer reaction. Lastly, during translocation, the peptide-bound tRNA shifts by one codon relative to the ribosome, allowing decoding and peptidyl transfer to repeat. During translocation, the peptidyl-tRNA bound in the A site slides into the P site and consequently causes the deacylated tRNA in the P site to move into the E site. Like decoding, translocation requires a protein elongation factor to proceed, which in bacteria is EF-G. Translocation proceeds in two steps, involving both the rotation of the ribosome and an EF-G catalyzed reaction dependent on GTP hydrolysis (Figure 3.1).

Translocation starts with the intrinsic oscillation of the ribosome between either a canonical or rotated state (*86*, *254*). In the rotated state, the small and large subunits twist relative to one another, and the tRNAs take on a so called ‘hybrid state’. In general, ribosomal subunit rotation causes the tRNAs to tilt within the 50S subunit toward the position they will ultimately occupy after translocation. In the hybrid state

conformation, the acceptor stem of deacylated tRNA in the P site tilts toward the E site while the anticodon stem loop remains bound in the P site. The acceptor stem is trapped by the L1 stalk, a binding interaction possible only for deacylated tRNA (*255*). Likewise, peptidyl-tRNA bound in the A site, tilts toward the P site.

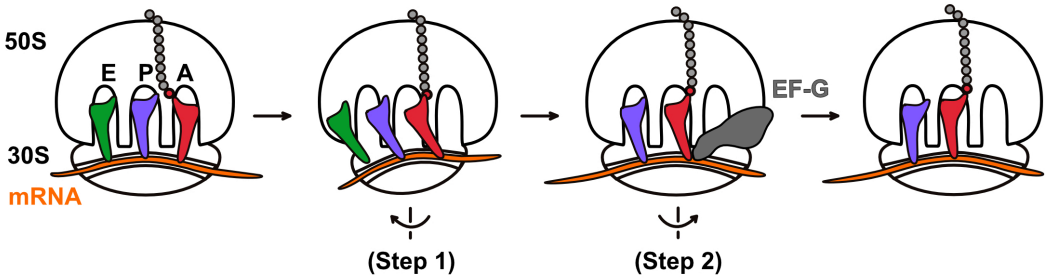

Figure 3.1 The mechanism of canonical translocation. A ribosome with a tRNA bound in the A site undergoes peptidyl transfer. The 30S subunit rotates, and the tRNAs take on hybrid state conformations. EF-G catalyzes the shifting of mRNA-tRNAs relative to the 30S subunit during rotation back to the canonical state. The A site is now occupied by a new codon.

During the second step of translocation, EF-G binds the ribosome, contacting tRNA in the A site and hydrolyzing GTP to catalyze the movement of the mRNA and tRNAs by one codon. The GTP bound form of EF-G stabilizes the rotated state (*86–89*) and subsequent GTP hydrolysis leads to a rate-limiting step which permits ribosome rotation back to the canonical conformation (*256*). This 'back-rotation' in the presence of EF-G causes the tRNAs and mRNA to slide relative to the ribosome. mRNA and tRNA are shown to move at the same rates relative to the ribosome, suggesting that they move as a unit during translocation, with codon:anticodon base pairing maintained (*256–258*).

For elongation to continue during canonical translation, peptidyl-tRNA must move from the A site into the P site, shifting the ribosome by exactly three nucleotides to reveal the next codon. Likewise, successful *trans*-translation is dependent on EF-G-catalyzed translocation. Peptidyl-tmRNA-SmpB bound in the A site of the ribosome is translocated into the P site, vacating the A site and consequently permitting the mRNA-like domain (MLD) of tmRNA to load into the A site. The ribosome begins translation on tmRNA by decoding the first codon of the tag-reading frame harbored within the MLD. The tag-reading frame encodes a polypeptide that is recognized by proteases and terminates with a stop codon, allowing the ribosome to be released and the aberrant protein to be degraded.

EF-G translocates tmRNA-SmpB in a manner analogous to that of tRNA. Although a rotated state has not yet been observed for ribosomes bound by tmRNA-SmpB, the antibiotic fusidic acid has been used to trap EF-G on the ribosome after translocation of tmRNA-SmpB into the P site. A low-resolution cryo-electron microscopy (cryo-EM) structure of this complex suggests that the body of SmpB replaces the canonical binding surface of EF-G (*259*), which normally contacts the anticodon stem loop of tRNA (*260*). This study also shows how an extreme swivel and tilt of the head of the 30S subunit may create space essential for the movement of tmRNA between the ribosomal subunits. Additionally, this head tilt opens the latch in the A site between the head and the body of the 30S subunit, producing a gap of 20 Å through which the MLD can pass during its loading into the mRNA channel.

Other low-resolution cryo-EM studies show the general conformation of tmRNA-SmpB bound in the P site after translocation (*168*). When tmRNA-SmpB occupies the P site the MLD is only loaded into about half of the entire mRNA channel. The channel upstream of the A site is blocked by an additional latch in the E site which must be opened if the MLD is to be fully loaded into the channel. tmRNA-SmpB, however, has not been observed in a state translocated past the P site, therefore it is unclear how or when the MLD reaches this conformation.

To understand the movement of tmRNA-SmpB through the ribosome and how swapping between the original mRNA and tmRNA occurs, structures of *trans*-translation intermediates are needed. After determining the structure of *T. thermophilus* tmRNA-SmpB bound in the A site of the ribosome, solving a structure of tmRNA-SmpB translocated into the P site was the next obvious step. In particular, we wanted to understand the role of SmpB binding tmRNA to the ribosome, how SmpB and such a large circularized RNA can navigate through the ribosome, and how tmRNA-SmpB movement loads the MLD into the mRNA channel. Additionally, we were interested in observing the never-before-seen conformation of tmRNA after translocation out of the P site.

3.2 Results and discussion

3.2.1 Development of an *in vitro trans*-translation system

In an attempt to trap tmRNA-SmpB bound in the P site, Ala-tmRNA-SmpB-EF-Tu-GTP was added to nonstop ribosomes as previously described (Chapter 2.2.1),

with elongation factor G (EF-G) included to promote translocation. A cryo-EM dataset was collected of this *T. thermophilus* complex and the reconstruction showed that instead of a ribosome with tmRNA-SmpB bound in the P site, another A-site complex was formed (Table 5.2, #2). In this case, there were no biochemical methods we could use to assay for the formation of a relevant complex and using cryo-EM for this purpose is time consuming and low throughput. Therefore, a rapid and high-throughput method was necessary to verify successful translocation of tmRNA-SmpB from the A site into the P site. A useful assay would need to distinguish between purely structural differences of the A site and P site complex. Previous low-resolution structures of tmRNA-SmpB bound in the A site show that for *in vitro* nonstop ribosomes, mRNA and tRNA can dissociate spontaneously after accommodation of tmRNA-SmpB (*261*). Consequently, apart from the location of tmRNA-SmpB, there may be no chemical difference between ribosomes with tmRNA-SmpB bound in either site.

To solve this problem, an *in vitro* transcription and translation system in *E. coli* was adapted for *trans*-translation, allowing us to assemble physiologically relevant nonstop ribosomes. The system contains all necessary components for transcription and translation from a DNA template (*262*), making it possible to control each step of *trans*-translation and verify the assembly of intermediates. By translating an mRNA without a stop codon, we assembled nonstop ribosomes with full-length nascent chains. Our DNA template also contained an N-terminal FLAG tag which we could use to affinity purify the nonstop ribosomes, enriching for only those that would be effective substrates for *trans*-translation and removing all contaminating transcription and translation factors. *Trans*-translation was initiated as before by adding Ala-tmRNA-SmpB-EF-Tu-GTP. By adding back only the factors required for the next step of *trans*-translation, we could assemble complexes at each step of the process.

Affinity purification of these nonstop ribosomes requires the nascent peptide to remain bound to tRNA in the P site. While this complex rarely disassembles spontaneously *in vivo*, dissociation has been observed *in vitro.* We wanted to minimize spontaneous release in our system so as to have sufficient sample for cryo-EM grid preparation. To do this, both background *trans*-translation activity and spontaneous peptide release had to be controlled in our system.

We hypothesized that *in vitro* release of the nascent chain could occur due to either (i) the presence of tmRNA-SmpB, (ii) the presence of alternate release factors ArfA or ArfB or, (iii) the spontaneous hydrolysis of the tRNA-peptide ester bond under

neutral reaction conditions. In an attempt to alleviate this problem, total tRNA was purified from an *E. coli* strain lacking *ssrA*. As tmRNA is known to co-purify in total tRNA preparations, this removed the largest known source of background tmRNA. Additionally, to minimize the spontaneous release of the nascent peptide, valine was encoded as the C-terminal amino acid, as this residue is shown to have the least labile ester bond with tRNA (*263*). Definitively removing background *trans*-translation and alternate release factors requires a strain lacking *ssrA*, *arfA* and *arfB*, which is not viable. Instead, we proceeded cognizant that these contaminants could be present, causing a decrease in the yield of nonstop ribosomes.

Because *E. coli* was used in both the *in vitro* system (*262*) and in many previous biochemical studies of *trans*-translation, it was adopted in favor of *T. thermophilus* (see Chapter 2). *E. coli* translation factors, ribosomes and tmRNA-SmpB were purified and used in conjunction with purified components generously donated by the Hegde lab. With the components of the system in hand, we began assembling *trans*-translation complexes. To assay for different intermediates, ^{35}S-methionine was used to specifically track newly synthesized nascent polypeptide. By following the change in molecular weight of the nascent peptide we could understand whether it was bound to tRNA, tmRNA or nothing (Figure 3.2).

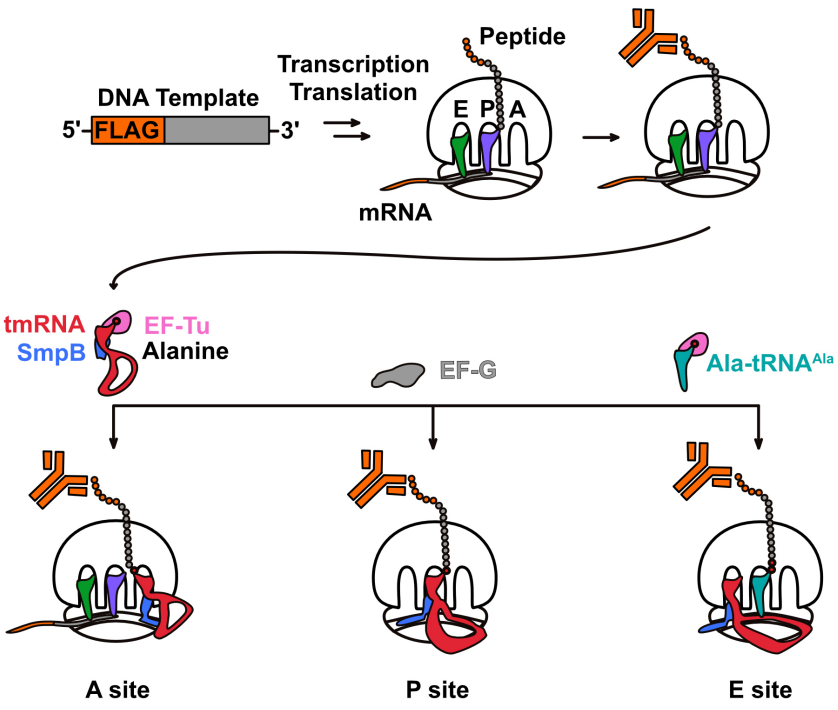

Figure 3.2 Schematic cartoon of *in vitro trans*-translation assay. The selective addition of factors required for subsequent steps of *trans*-translation permits the accumulation of intermediates that can be easily purified.

As no methionine is encoded in the tag-reading frame of tmRNA, the signal detected should therefore be proportional to the amount of nascent chain.

Transcription and translation of the engineered DNA template lacking a stop codon produced the starting material for the assay. Affinity purification using anti-FLAG resin yielded nonstop ribosomes, verified by detecting peptidyl-tRNA with full-length nascent chains (Figure 3.3A, lane1). RNaseA digestion confirmed that higher molecular weight peptides are bound to RNA (Figure 3.3A, lane 2). The presence of the RNA bound species suggests the successful assembly of nonstop ribosomes.

While the isolated nonstop ribosomes remain bound to the affinity resin, addition of Ala-tmRNA-SmpB-EF-Tu-GTP initiates *trans*-translation. A complex with tmRNA-SmpB occupying the A site and bound to the nascent peptide was confirmed by the disappearance of peptidyl-tRNA and the appearance of a higher molecular weight peptidyl-RNA species (Figure 3.3A, lane 3). The shifting molecular weight of the nascent chain is consistent with peptidyl-transfer to tmRNA.

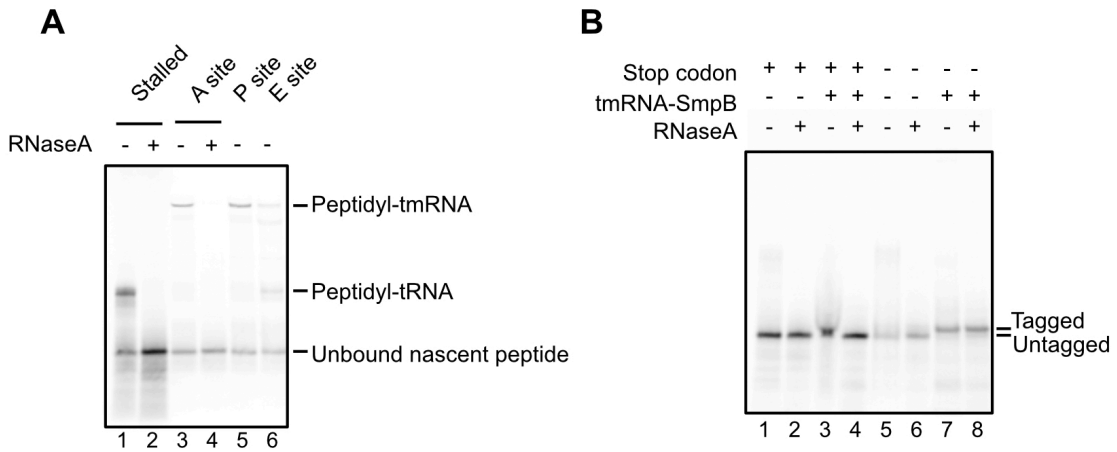

Figure 3.3 Verification of *trans*-translation intermediate assembly. (A) Nonstop ribosomal complexes were assembled *in vitro* by translating an mRNA template with an N-terminal FLAG tag and no in frame stop codon. Reactions contained ^{35}S-methionine to track the nascent chain. Nonstop complexes were captured with anti-FLAG affinity resin and washed to remove translation factors (stalled). RNase A digestion was used to detect the presence of RNA-bound nascent chains. Ala-tmRNA-SmpB-EF-Tu-GTP was added to initiate *trans*-translation (A site). Addition of EF-G translocates tmRNA-SmpB into the P site, with no change to the binding state of the nascent chain (P site). Subsequent addition of Ala-tRNA^{Ala}-EF-Tu-GTP with EF-G restarts translation on tmRNA, transferring the nascent chain to tRNA^{Ala} (E site). (B) Control reactions show that complete tagging of the nascent polypeptide was possible when all required *trans*-translation factors were included.

The step-wise addition of factors required for *trans*-translation permits any position of tmRNA within the ribosome to be trapped and purified. Therefore, towards our original goal, elongation factor G (EF-G) was added to the A-site complex to translocate tmRNA-SmpB into the P site. As expected, no change in molecular weight of the peptidyl-tmRNA species was observed (Figure 3.3A, lane 4).

This assay suffers from similar limitations as those described for the mixing of *T. thermophilus* components (see Chapter 2), namely, it was not directly possible to distinguish between ribosomes containing tmRNA-SmpB bound in the A site versus the P site. However, the P site complex was verified indirectly by proceeding with the next step of *trans*-translation, attempting to trap tmRNA-SmpB bound in the E site. After addition of Ala-tRNA^{Ala}, the peptidyl-tmRNA species disappeared and peptidyl-tRNA re-appeared (Figure 3.3A, lane 5). This is consistent with translation beginning on the tag-reading frame within tmRNA, the first codon of which codes for tRNA^{Ala}. This intermediate was obtained in the presence of EF-G, leading us to assume that we had formed a complex with tmRNA-SmpB mimicking a tRNA bound in the E site.

The three intermediates (A-site, P-site or E-site bound tmRNA-SmpB) were then purified from excess *trans*-translation factors by washing the resin and eluting with FLAG peptide.

3.2.2 Cryo-EM data collection and processing of *E. coli trans*-translation intermediates

The structure of tmRNA-SmpB bound in the P site was not yet determined at high-resolution, therefore, this was the first sample prepared for cryo-EM (Figure 3.4A, B). Data collection resulted in two intermediates: ribosomes with tmRNA-SmpB bound in either the A site or P site (Figure 3.4C). The presence of the A site intermediate suggests translocation of tmRNA-SmpB into the P site is inefficient. Similarly, a dataset was collected on a second complex with tmRNA-SmpB thought to occupy the ribosomal E site. This sample yielded a ribosomal complex with tmRNA-SmpB bound in a conformation after translocation past the P site and also contained an earlier A site intermediate (Figure 3.4C).

Particles representing the same conformations in both datasets were joined and reprocessed. This resulted in three near-atomic resolution structures of *E. coli* tmRNA-SmpB bound to the ribosome in the A site, P site and unexpectedly, in a conformation with tmRNA bound on the solvent side of the E site.

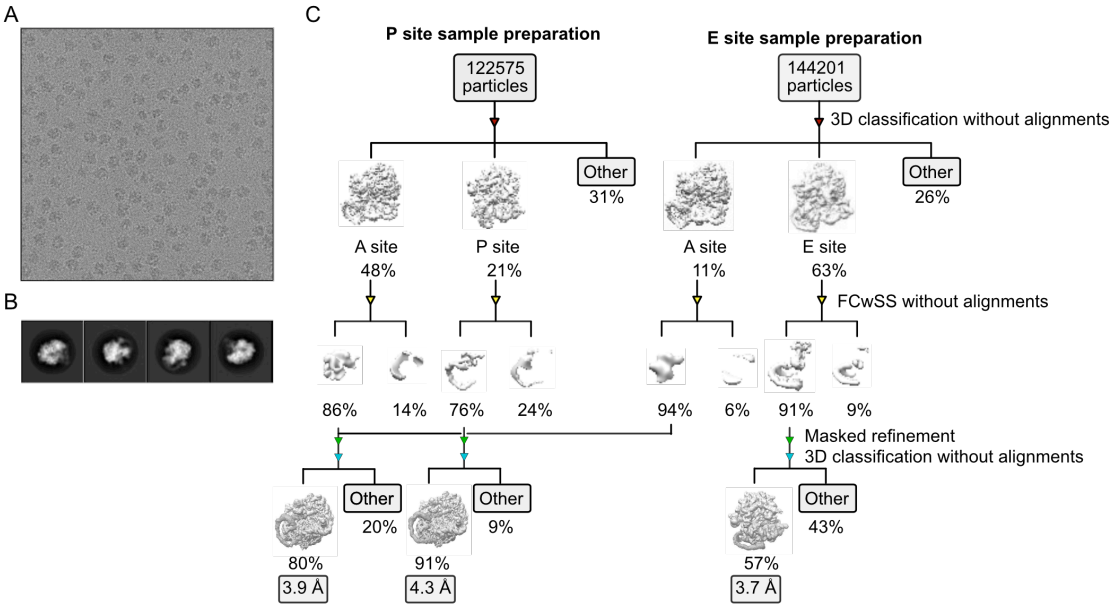

Figure 3.4 Cryo-EM data collection and processing of *E. coli trans*-translation intermediates with tmRNA-SmpB bound in three key states on the ribosome. (A) Representative micrograph taken at 75k magnification on a 300 kV Polara Cryo-TEM (FEI). (B) Representative two-dimensional classes. (C) Processing workflow in RELION and resulting electron density maps.

Processing included three rounds of three-dimensional (3D) classification to separate different states of tmRNA bound to the ribosome. The cryo-EM data processing software, RELION was used for all reconstructions presented here. After an initial refinement containing all particles, 3D classification was used to separate ribosome complexes based on the binding position of tmRNA-SmpB. To ensure a homogeneous set of particles and eliminate any ribosomes not containing tmRNA-SmpB, focused classification with signal subtraction (FCwSS) was used, masking over tmRNA-SmpB. FCwSS is a unique style of classification in which all signal outside of an area of interest is removed prior to classification. This technique is particularly useful when the majority of signal surrounding the area of interest is expected to be identical in all classes. Here, the large subunit of the ribosome, which is relatively rigid, contributes a large amount of signal and therefore mandates the use of FCwSS.

After FCwSS, factor-containing classes were pooled and refined with a mask around the 30S subunit. Masking around the 30S during refinement improves the local resolution within that region, where we anticipated most of the interesting contacts between tmRNA-SmpB and the ribosome would take place. A final 3D classification was used to remove any remaining poorly aligned particles, after which the final reconstruction was refined with a mask around the 30S subunit.

The three high-resolution structures of *E. coli* tmRNA-SmpB bound to the ribosome show the movement of tmRNA-SmpB through the ribosome and explain the importance of the C-terminal tail of SmpB during the later stages of *trans*-translation. Additionally, we observe a novel structure of tmRNA-SmpB bound on the solvent side of the E site of the ribosome, showing the complete loading of the MLD of tmRNA into the mRNA channel. These structures are described in detail in the following sections.

3.2.3 Structures of *trans*-translation intermediates in *E. coli*

The structure of tmRNA-SmpB bound in the A site shows that in the *in vitro* system, washing the complex removes the original tRNA and mRNA from the ribosome. In this state, the P-site tRNA is no longer bound to the nascent peptide but is bound to the mRNA by base pairing interactions. Trapping a physiologically relevant *E. coli* structure of tmRNA-SmpB bound in the A site therefore required a modification to the protocol to maintain tRNAs and mRNA bound in the P and E site. For this, the step in which the A-site complex is washed was eliminated. Instead, nonstop ribosomes were first eluted from the affinity resin after which Ala-tmRNA-SmpB-EF-Tu-GTP was added to initiate *trans*-translation without any further purification. A dataset was collected on a 300kV Titan Krios microscope and showed that the adjusted purification method was able to trap the desired structure which we could resolve at 3.7 Å (Figure 3.5 A, B, C).

Determining the structure of *E. coli* tmRNA-SmpB bound in the A site was important for two reasons. First, it could be compared to the analogous structure in *T. thermophilus*. Global superposition of the two structures shows that the tail of SmpB in *E. coli* is in a very similar position to that in *T. thermophilus* but forms a longer alpha helix (Figure 3.5D). This suggests that *trans*-translation initiates similarly between the two organisms. Second, the movement of tmRNA-SmpB from the A site into the P site is best understood by comparing complexes from the same species. This way any differences between the A and P site complexes represent mechanism rather than species-specific conformational nuances.

After accommodation of tmRNA-SmpB and peptidyl-transfer of the nascent chain to alanine on tmRNA, EF-G translocates tmRNA-SmpB into the P site and the mRNA is released and degraded (*264*). In agreement with this, mRNA and tRNA are absent in the 4.4 Å structure of tmRNA-SmpB bound in the P site (Figure 3.6).

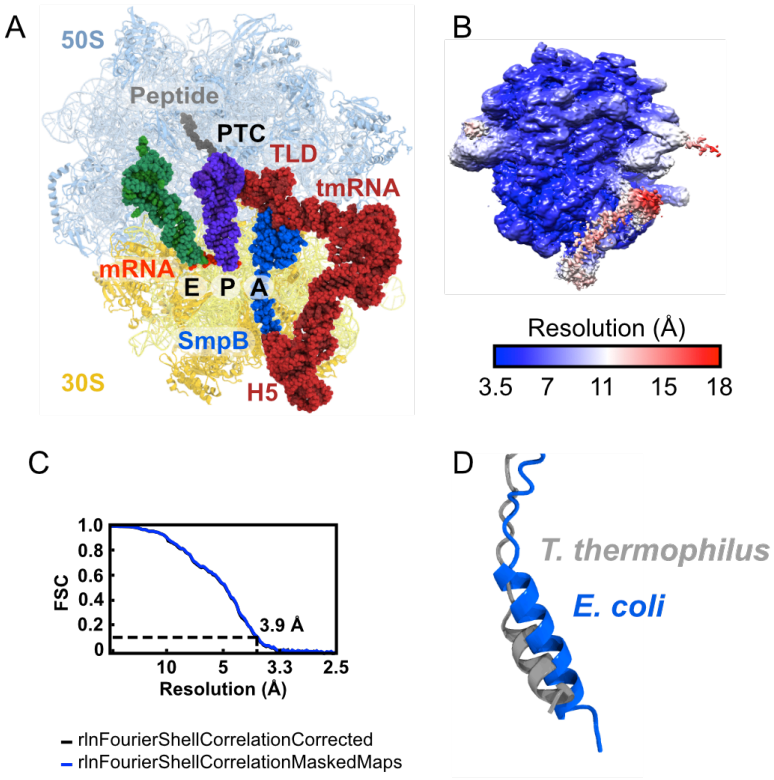

Figure 3.5 Structure of *E. coli* tmRNA-SmpB bound in the A site of the ribosome. (A) Overview of the ribosomal complex with tmRNA-SmpB occupying the A site of a nonstop ribosome. The TLD (red) points into the peptidyl-transferase center (PTC) where it is joined to the nascent peptide (gray). (B) Electron density map colored by local resolution ranging from 3.5 Å to 18 Å. (C) Fourier shell correlation (FSC) curve showing map resolution of 3.9 Å with dashed line at FSC=0.143. (D) Global superposition of tmRNA-SmpB bound in the A site showing the tail of SmpB for *T. thermophilus* (gray) or *E. coli* (blue).

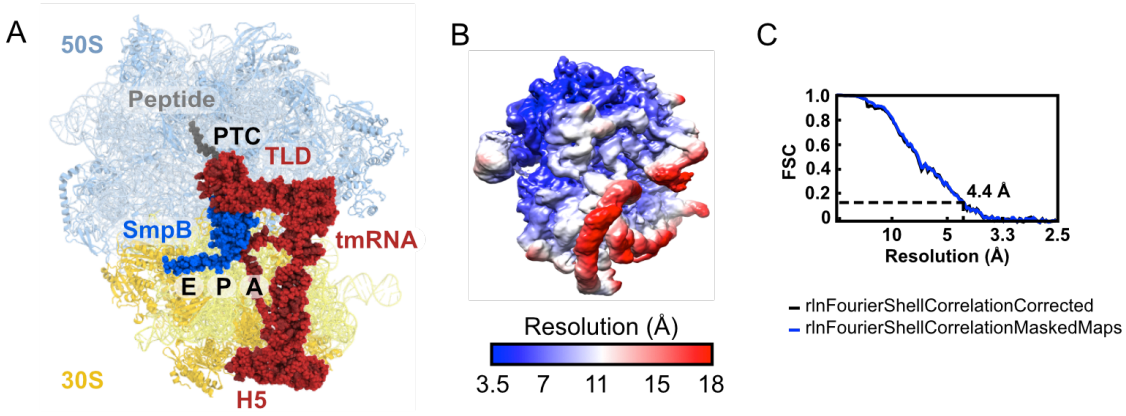

Figure 3.6 Structure of *E. coli* tmRNA-SmpB bound in the P site of the ribosome. (A) Overview of the structure of tmRNA-SmpB bound in the P site of the ribosome with the mRNA-like domain (MLD) occupying the A site. (B) Electron density map colored by local resolution. (C) Fourier shell correlation (FSC) curve showing map resolution of 4.4 Å with dashed line at FSC=0.143.

As EF-G translocates tmRNA-SmpB from the A site into the P site, the ribosome switches messages from the original mRNA to tmRNA (*259*). The tail of SmpB and H5 of tmRNA vacate their previous positions which blocked the A site so that the MLD of tmRNA can pass through the A-site latch and occupy the mRNA channel. For this, the C-terminal tail of SmpB remains alpha-helical but flips, binding the mRNA channel in the E site and therefore anchors tmRNA-SmpB in the P site (Figure 3.7A). The highly conserved Gly132 (Gly122 in *T. thermophilus*) facilitates helix flipping by acting as a flexible joint between the body and tail of SmpB. This is consistent with biochemical analysis describing the role of the C-terminal tail in positioning the tag-reading frame (*265*).

In addition, helix H5 of tmRNA moves to unblock the entrance of the mRNA channel, permitting access for the MLD (Figure 3.7B). This movement supports the previous claim that the initial position of H5 (of the A-site complex) clashes with the space normally occupied by an mRNA. Indeed, we would not expect a change in the position of H5 were adequate space available for the MLD to extend from the mRNA channel.

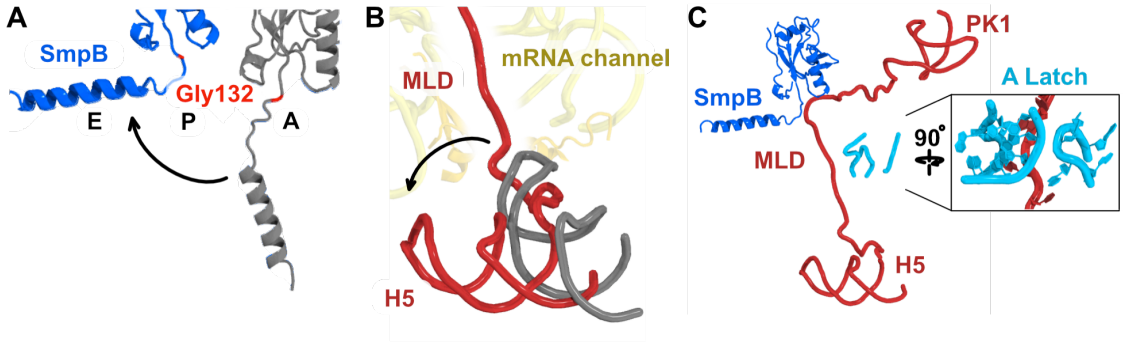

Figure 3.7 Movement of the tail of SmpB and H5 of tmRNA vacates the mRNA channel in the A site. (A) Global superposition of ribosomes with SmpB occupying the A-site (gray) or P-site (blue) with conserved glycine residues highlighted (red). (B) Helix 5 of tmRNA changes position from the A site complex (gray) to the P site complex (red), allowing the MLD to pass through the mRNA channel in the space previously occupied by the tail of SmpB. (C) The MLD bypasses the latch in the A site (inset) and contacts the junction of the body and tail of SmpB to set the tag-reading frame.

Loading the MLD through the A-site latch and into the mRNA channel is necessary but not sufficient for translation to accurately restart on tmRNA. The tag-reading frame within the MLD must also be correctly positioned for translation of the polypeptide tag and termination at an in-frame stop codon. For this, the MLD interacts with the base and tail of SmpB. Indeed, we can trace otherwise unassigned density

leading to the base of SmpB, across the A site and out the mRNA channel, confirming that the MLD interacts with SmpB (Figure 3.7C). This is consistent with biochemical evidence suggesting that the five nucleotides upstream of the tag-reading frame are critical for correctly positioning the first codon in the A site (*211*, *213*).

Physical obstacles imposed by the 50S subunit must be circumvented by tmRNA as it moves through the ribosome. During translocation of tmRNA-SmpB from the A site into the P site, helix 2 (H2) of tmRNA must bypass the A-site finger (Figure 3.8A, B).

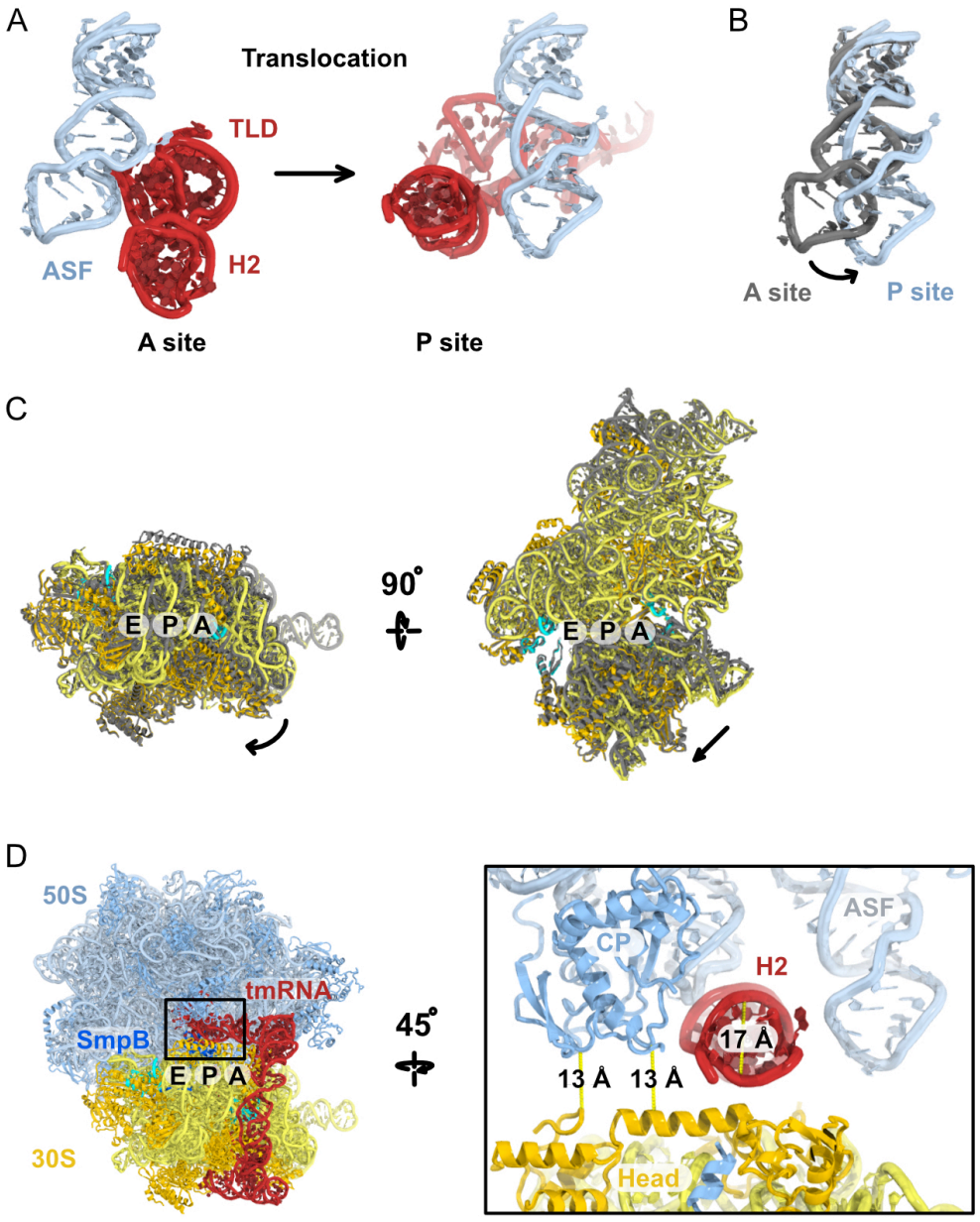

Figure 3.8 Obstacles in the 50S subunit physically separate translocation of tmRNA-SmpB. (A) Comparison of the A site finger when tmRNA-SmpB is bound in the A site versus after translocation into the P site. (B) Superimposition of A-site finger showing the conformational

change observed. (C) Superimposition of 30S from the P-site structure with 30S from the A-site structure. (D) Measured gap between the central protuberance (CP) and the head of the 30S subunit when tmRNA-SmpB binds the P site.

H2 is a conserved element of tmRNA that connects the acceptor stem to the pseudoknot loop and protrudes from the tRNA-binding sites to the outside of the ribosome. It is expected that H2 must travel between the ribosomal subunit interface. The A-site finger is a helix of 23S rRNA that nearly connects this interface, extending from the 50S subunit toward the head of the 30S subunit. In the P-site structure, the A-site finger binds in a bent position on the opposite side of H2 compared to the A-site structure. The flexibility of the A-site finger suggests that it may move, perhaps by force, out of the way during EF-G catalyzed translocation.

Likewise, during translocation of tmRNA-SmpB out of the P site, H2 of tmRNA must circumvent another even larger obstacle, the central protuberance (CP). This RNA-protein feature of the 50S typically contacts the head of the 30S subunit. In the structure of tmRNA-SmpB bound in the P site, the head of the 30S is observed in an extremely tilted conformation, with a ~13 Å gap (Figure 3.8C). The diameter of H2 is larger, spanning ~17 Å at its most narrow point. It is unclear how H2 passes between the head of the 30S and the CP of the 50S. However, binding of tmRNA in the P site begins inducing conformational changes on the ribosome that may be permissive for passage between the subunit interface.

After tmRNA-SmpB is positioned in the P site, Ala-tRNA^{Ala} decodes the first codon, or 'resume codon', of the tag-reading frame in the MLD in the A site. EF-G then translocates peptidyl-tRNA^{Ala} into the P site, consequently forcing tmRNA-SmpB toward the E site. Unexpectedly, tmRNA-SmpB does not mimic a tRNA binding in the E site. Instead, tmRNA-SmpB shifts past the E site to the solvent side of the ribosome as seen here in the 3.7 Å structure (Figure 3.9A, B, C).

To complete loading into the mRNA channel, the MLD must bypass another latch that joins the head and body of the small subunit, this time located in the E site. We see the MLD loaded through the E-site latch and into the mRNA channel after the second translocation step, which is analogous to the first step (Figure 3.9D). PK1 and H5 flank the single-stranded MLD, and continuous density is seen running through the mRNA channel. The position of H5 is approximately the same as that of tmRNA-SmpB occupying the P site, thus continuing to provide room for the MLD to exit the channel.

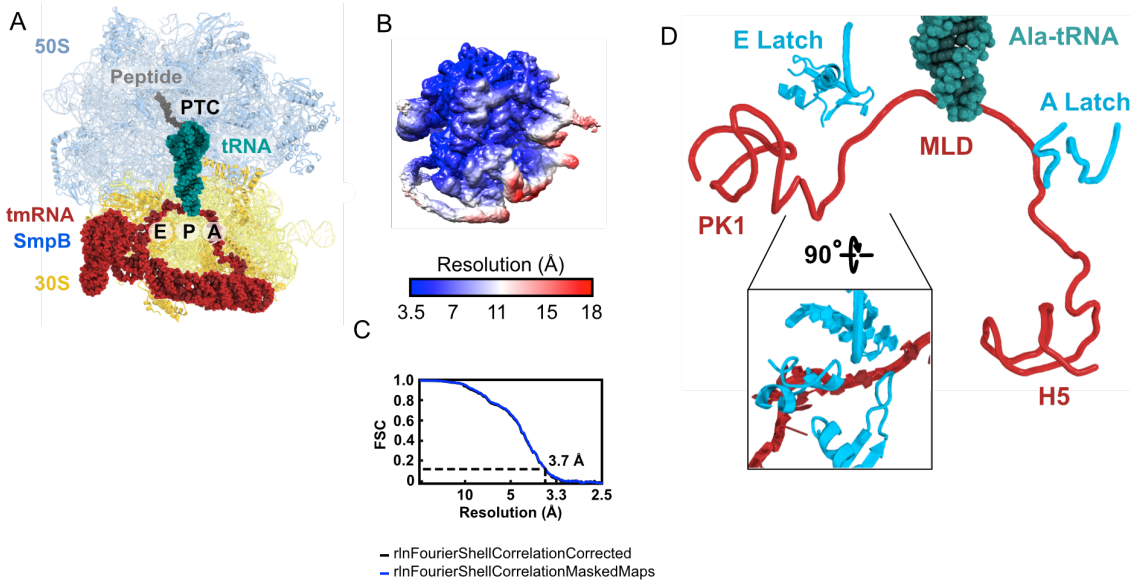

Figure 3.9 Structure of tmRNA-SmpB translocated from the P site past the E site. (A) Overview of the ribosomal complex with tmRNA-SmpB bound on the solvent side of the E site and the MLD fully loaded into the mRNA channel. (B) Electron density map colored by local resolution. (C) Fourier shell correlation (FSC) curve showing map resolution of 3.7 Å with dashed line at FSC=0.143. (D) Both latches blocking the mRNA channel have been bypassed by the MLD.

During movement of tmRNA-SmpB between all three states, the single stranded loop of RNA from PK2 remains bound to protein uS3, anchoring tmRNA to the solvent side of the small subunit. In this way, PK2 acts as a hinge around which tmRNA bends and pivots (Figure 3.10A). Indeed, the anchoring interactions of PK2 coordinate the different positions of H5 seen during *trans*-translation. PK2 is highly conserved (*266*) and its interactions with uS3 may therefore represent a function of tmRNA in most species.

It was surprising we did not find tmRNA-SmpB to occupy the E site and instead observed what could be considered a structure one step further along in *trans*-translation. Although it is technically possible that an intermediate E-site tmRNA-SmpB complex was skipped in the *in vitro trans*-translation system, superimposing tmRNA-SmpB from our structure onto a model of canonical tRNA in the E site induces severe clashes with the ribosome that make a stable E site complex unlikely (Figure 3.11 A, B). If tmRNA-SmpB were to occupy the E site in a manner that mimics a tRNA, three points of contact are expected: (i) the PK2 loop with uS3, (ii) the acceptor arm of the TLD with the L1 stalk, and (iii) the codon:anticodon interaction between the MLD and tRNA in the P site. Without conformational changes to tmRNA, PK1 would clash with the central protuberance if all three binding interactions are satisfied.

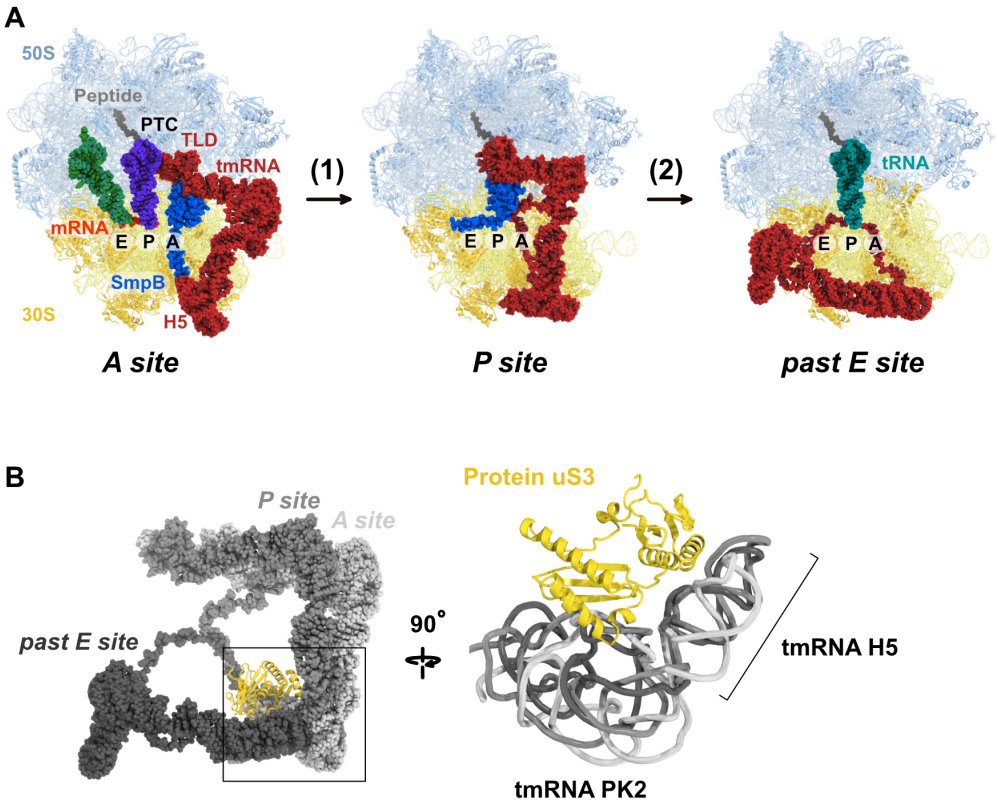

Figure 3.10 Pseudoknot 2 binds protein uS3 during the entire movement of tmRNA-SmpB through the ribosome. (A) Three *E. coli trans*-translation intermediates determined in this study are separated translocation events. tmRNA-SmpB bound in the A site is (1) first translocated into the P site, after which translation restarts as a tRNA decodes tmRNA and a (2) second translocation shifts tmRNA-SmpB past the E site, to the outside of the ribosome. (B) Global superimposition of all three structures, showing only tmRNA (grays) and a consensus protein uS3 (yellow).

Even though conformational changes to tmRNA are possible and even likely, tmRNA bends primarily at junctions between its pseudoknot domains, which are made of single stranded RNA. Indeed, both the observed movements of PK1 and PK2-H5 are pivots around such points. At a third point of flexibility, bending at the elbow region permits the movement of the acceptor arm during accommodation. tmRNA must therefore either bend within helical region H2 or unravel PK1 to occupy the E site and maintain the three expected binding points. Both of these changes would require base pair disruption and are expected to be less favourable than simply vacating the E site. Additionally, tRNA-mimicry by tmRNA-SmpB may in this case not be sufficient for the specific interactions between the L1 stalk and the acceptor stem. For this, we would expect the C-terminal tail of SmpB to maintain its alpha helical form and bind in the place of mRNA upstream of the E site. However, if this interaction were not to occur, a stable E site complex would be even less likely.

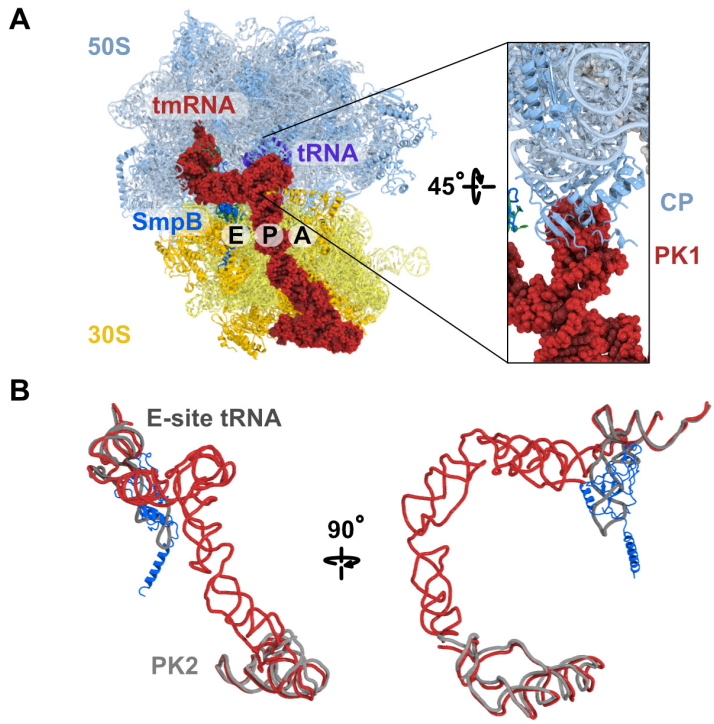

Figure 3.11 Docking tmRNA-SmpB into the E site. (A) tmRNA-SmpB superimposed into a hypothetical E-site conformation with minimal conformational changes required shows a clash (inset) between tmRNA and the central protuberance (CP). (B) Docking tmRNA for the hypothetical E-site conformation. tmRNA-SmpB superimposed onto an E-site tRNA (dark gray, from the A-site structure) and PK2 (light gray, from the P-site structure). tmRNA from the P-site structure determined in this study was used as a starting model. The TLD was superimposed onto the acceptor arm of E-site tRNA while contacts between PK2 and protein S3 were maintained. H2, PK1, PK2 and PK3 were adjusted to connect the domains without any conformational changes within the domains.

Lastly, an extreme head movement is needed to open the E-site latch to load the MLD into the mRNA channel. Such a movement must occur during the second translocation event if tmRNA is to pass along the interface between the 50S and 30S subunits. Translocation of tmRNA into the E site is therefore an ideal time to load the MLD into the E site. However, this is only possible if TLD-SmpB does not bind in the E site. The structures determined here suggest a translocation-mediated two-step mechanism as the simplest explanation for loading of the MLD in to the mRNA channel.

3.3 Conclusions

Both tmRNA and SmpB mimic parts of a tRNA and mRNA during their movement though the ribosome, ultimately tricking the ribosome into continuing an otherwise atypical form of elongation. Initial delivery by EF-Tu depends on tmRNA-SmpB mimicking a tRNA while accommodation into the ribosome requires SmpB to mimic an mRNA to recognize the empty mRNA channel. Simultaneously, during *trans*-translation, SmpB acts as the anticodon stem loop of a tRNA by binding to the acceptor stem of tmRNA. Similarly, as tmRNA-SmpB moves through the ribosome, the C-terminal tail of SmpB continues mimicking an mRNA, binding in the space subsequently occupied by an actual piece of RNA, the MLD, after translocation.

Two translocation events move tmRNA-SmpB through the ribosome, resulting in complete loading of the MLD into the mRNA channel. After EF-G translocates tmRNA-SmpB from the A site into the P site, the tail of SmpB flips and binds in the E site, anchoring the factors in position. SmpB also interacts with the MLD to position it in the now empty A site for translation to restart on tmRNA. Thus, SmpB identifies legitimate nonstop ribosomes by verifying that the mRNA channel is empty, and then vacates that space to make way for the MLD. A second translocation event catalyzed by EF-G forces tmRNA-SmpB past the E site and to the solvent side of the ribosome, loading the MLD fully into the mRNA channel. It is here that tmRNA-SmpB deviates from tRNA-mimicry, as it is not seen to bind in the E site after translocation out of the P site like in canonical translocation.

Loading the MLD into the mRNA channel is necessarily mediated by a looping mechanism that bypasses two latches, one during each translocation event. The MLD bypasses the first latch as tmRNA-SmpB is translocated from the A site into the P site. Likewise, the second latch is bypassed during translocation of tmRNA-SmpB out of the P site, toward the E site. This mechanism is likely applicable for two-piece tmRNAs as well, since large secondary structures flank the MLD in many bacteria (*172*). The secondary structure elements make a threading mechanism unlikely. To thread tmRNA into the mRNA channel requires extensive unwinding of tmRNA, followed by coordinated passage into the mRNA channel and then reformation of secondary structure. These rearrangements seem unfavorable and as of yet, there is no evidence for how threading would be coordinated. Alternatively, the looping mechanism does not

requireunwinding of tmRNA and takes advantage of translocation, an already energy dependent process, to circumvent the latches otherwise blocking entrance into the mRNA channel.

Although the structures of these intermediates reveal a great deal of atomic detail about the mechanism of *trans*-translation, two important structural questions remain to be answered. First, what are the specific interactions between the MLD and SmpB in the P site that coordinate the correct reading frame on the MLD in the A site? And second, what does tmRNA-SmpB translocation from the P site to the E site look like? We attempted to trap structures that could help address questions. However, in both cases, cryo-EM data collection revealed only the previously determined intermediates. We collected data for a complex of tmRNA-SmpB bound in the P site with $tRNA^{Ala}$ decoding the MLD in the A site complex (Table 5.2, #11). However, again obtained a reconstruction with tmRNA-SmpB bound past the E site, possibly due to contaminating EF-G in the system.

Trapping an EF-G-bound intermediate during translocation of tmRNA-SmpB from the P site toward the E site could provide insight into why tmRNA-SmpB was not observed to mimic a tRNA binding in the E site as anticipated. Using the antibiotic fusidic acid, we attempted to trap EF-G after it has catalyzed translocation, but prior to dissociation from the ribosome. However again data collection revealed a strangely inseparable mixture of more of the previously determined complexes (Table 5.2, #9). This dataset must be processed further to understand the strange classification phenomenon. Additionally, as no EF-G was detected on the ribosome, the complex must be optimized and crosslinking agents may be required to further prevent EF-G dissociation. We suspect the three structures determined in this study might be the lowest energy states, making transition state intermediates more challenging to trap.

Although these gaps in our understanding of *trans*-translation remain open, determining the structures of *E. coli* tmRNA-SmpB bound in three different states on the ribosome describes for the first time the movement of tmRNA-SmpB at near-atomic resolution. The structures reveal new details about tmRNA-SmpB binding to the ribosome and represent a critical advancement in our understanding of the mechanism of *trans*-translation.

3.4 Materials and methods

Purification of components for the *in vitro trans*-translation system

The *ssrA* gene from *E. coli* MG1655 was cloned into pUC19 under the control of a T7 promoter followed immediately after the 3'CCA by a BsmBI cleavage site. The plasmid was linearized using BsmBI (NEB) as per the manufacturer's instructions, extracted using phenol-chloroform, ethanol-precipitated and resuspended in water. tmRNA was produced by run-off transcription (40 mM Tris-HCl pH 8, 1 mM spermidine, 0.01 % Triton X100, 5 mM DTT, 5 mM NTPs, 30 mM $MgCl_2$, 0.0025 U/ml inorganic pyrophosphatase, 40 U/ml RNAsin Plus RNase Inhibitor (Promega), 0.01 mg/ml T7 RNA polymerase), and purified by gel filtration (10 mM ammonium acetate pH 5.0, 150 mM KCl, 5mM $MgCl_2$) on a HiLoad 16/600 Superdex 200 column. The purified sample was concentrated by ethanol precipitation in the presence of 1 M ammonium acetate pH 5.0 and resuspended in 10 mM HEPES.KOH pH 7.5, 20 mM NH_4Cl, 5 mM $MgCl_2$.

The *smpB* gene from *E. coli* MG1655 was cloned into pET28a (Novagen), generating a plasmid for a construct with an N-terminal 6xHis-tag followed by a SSG flexible peptide linker, a PreScission Protease cleavage site and finally wild-type *E. coli smpB*. Transformed *E. coli* Rosetta DE3 cells (Novagen) were induced with 1 mM IPTG and grown for 4 h at 37°C with 34 µg/ml Chloramphenicol and 30 µg/ml Kanamycin. The protein was purified in batch with Ni-NTA beads (Roche) following lysis in 50 mM Tris-HCl pH 7.4, 1 M KCl, 5 mM imidazole and 2 mM DTT. SmpB was eluted in lysis buffer containing 750 mM imidiazole and dialyzed overnight with Prescission Protease (1.4 mg/L) in dialysis buffer (50 mM Tris-HCl pH 7.4, 500 mM KCl, and 2 mM DTT) at 4°C to cleave the tag. The sample was concentrated to 20 mg/ml, aliquoted and stored at -80°C.

Nonstop template DNA was created by PCR from plasmid pNAT21 containing *dnaX* with an N-terminal FLAG tag in pIDT vector under control of a T7 promoter. Forward primer 5' ATAGCGATTCATCGATGAGCTGACCCG 3' and reverse primer 5' GACCATCAACTGCTGGCGCGCCG 3' were used, flanking the promoter region and the first 91 amino acids encoded by *dnaX*. This template DNA codes for a nascent peptide with an N-terminal FLAG tag and no in-frame stop codons.

Total tRNA was isolated from *E. coli* W3110ΔssrA (*153*) by acidic phenol-chloroform extraction with 25:24:1 phenol:chloroform:IAA, purified using HiTrap DEAE Sepharose FF (in 20 mM Tris 7.4, 100 mM KCl, 1 mM DTT) and eluted with 1 M NaCl. Total tRNA was concentrated by ethanol precipitation and resuspended in water. All remaining PURE system components were purified as described (*262*).

Sample preparation for *E. coli* complexes

The PURE system was used to *in vitro*-transcribe and translate the nonstop DNA template to produce stalled ribosome complexes. Reactions were prepared as described (*262*) but with 4.75 mg/ml ribosomes, 7.5 ng/µl nonstop DNA template and using the total tRNA prepared from *E. coli* W3110ΔssrA. Reactions were incubated at 37°C for 1 h with shaking.

tmRNA was aminoacylated (50 mM K-HEPES pH 7.5, 60 mM NH_4Cl, 7 mM $MgCl_2$, 4 mM ATP, 0.002 U/ml inorganic pyrophosphatase, 20 µM AlaRS, 15 µM EF-Tu, 15 µM SmpB, 10 µM tmRNA, 30 µM alanine) by incubating for a minimum of 1 h at 37°C with shaking, then mixed with 1 mM GTP at room temperature prior to incubation with nonstop ribosomes. Alanyl-$tRNA^{Ala}$ was prepared similarly (50 mM K-HEPES pH 7.5, 60 mM NH_4Cl, 7 mM $MgCl_2$, 4 mM ATP, 0.002 U/ml inorganic pyrophosphatase, 20 µM AlaRS, 15 µM EF-Tu, 10 µM Ala-tRNA, 30 µM Alanine).

While incubating the tmRNA aminoacylation reactions, completed nonstop ribosome reactions were incubated with anti-FLAG resin for 1 h at 4°C. Resin was then washed twice each with Buffer A (50 mM HEPES pH 7.4, 100 mM KOAc, 5 mM $Mg(OAc)_2$, 0.1% Triton X-100), Buffer B (50 mM HEPES pH 7.4, 250 mM KAc, 5 mM $Mg(OAc)_2$, 0.5% Triton X-100, 1 mM DTT) and Buffer C (50 mM HEPES pH 7.4, 100 mM KOAc, 5 mM $Mg(OAc)_2$). This produced a complex of nonstop ribosomes bound to anti-FLAG resin via the nascent chain.

The complex of tmRNA-SmpB bound in the A-site was obtained by adding Ala-tmRNA aminoacylation reactions to the washed, nonstop ribosome bound beads and further incubation at 37°C shaking for 30 minutes to initiate *trans*-translation. Beads were washed three times with Buffer C and the ribosomes eluted with Elution Buffer (50 mM HEPES pH 7.4, 100 mM KOAc, 5 mM $Mg(OAc)_2$, 0.2 mg/ml FLAG peptide) twice for five minutes each at room temperature. This preparation produced a complex with tmRNA-SmpB occupying the A-site. However, the wash steps after Ala-tmRNA incubation caused the complex to lose the original mRNA and tRNA. To trap

an A-site complex containing both mRNA and tRNA, nonstop ribosomes were prepared as above but were instead eluted from beads prior to mixing with Ala-tmRNA aminoacylation reactions at 37°C shaking for 30 minutes, after which no further purification was performed.

The complex of tmRNA-SmpB bound in the P-site was produced by adding 5 μM elongation factor G (EF-G) to the completed tmRNA aminoacylation reaction above and then incubating with nonstop ribosome bound beads, washing and eluting as already described.

To trap the complex of tmRNA-SmpB bound in the E-site, P-site complexes were produced as above and washed three times with Buffer C after which an Ala-$tRNA^{Ala}$ aminoacylation reaction mixed with 1 mM GTP and 5 μM EF-G was added and incubated at 37°C for 30 min before final elution.

Electron microscopy

Quantifoil Cu R2/2 400 mesh grids were coated with a thin sheet (~60 Å) of amorphous carbon and glow discharged for 15 s at 7 V. Eluted *trans*-translation intermediates were diluted to a ribosome concentration of 100 nM in Buffer C and 3 ul aliquots were applied to grids, incubated for 30 s at 4°C and 100% humidity, blotted for 4.5 s and frozen in liquid ethane using a Vitrobot Mark III (FEI).

Micrographs of the *E. coli* A-site complex were collected on a Titan Krios microscope whereas P- and E-site complexes were collected on a Polara, all at 300 keV with a Falcon II detector and automated data collection with EPU (FEI). Movies were collected on the Krios at 75 k magnification, a pixel size of 1.07 Å, a dose of 26.5 $eÅ^{-2}s^{-1}$, 1.67 s exposures, and totalling 67 frames. Movies were collected on the Polara at 93 k magnification, a pixel size of 1.15 Å, a dose of 60 $eÅ^{-2}s^{-1}$, 1 s exposures, and totalling 43 frames. Micrographs of the *T. thermophilus* A-site complex were collected on a Polara at 300 keV with a Falcon II detector and automated data collection with EPU (FEI). Movies were collected at 75 k magnification, a pixel size of 1.34 Å, a dose of 28 $eÅ^{-2}s^{-1}$, 1.5 s exposures and a total of 60 frames. All collections used defocus values of -3.2, -2.9, -2.6, -2.3, -2.0, -1.7 μm.

Image processing

Micrograph movies were processed using RELION-2.1 (*244*). Frames were aligned with Motioncorr (*245*) and contrast transfer functions calculated using Gctf

(*246*). After movie alignment, ribosome particles were picked semi-autonomously (*247*) and selected using reference-free two-dimensional classification to remove ice and other nonribosomal particles. Initial three-dimensional refinement used an *E. coli* 70S ribosome (EMD-3493) low-pass filtered to 40 Å as a reference. Initial three-dimensional refinement was used as input for a first round of three-dimensional classification without alignments (Fig S6). Further separation was done by focused classification with signal subtraction on the tmRNA-SmpB (*267*). Maps were refined again with a mask over the small subunit. Another round of three-dimensional classification without alignment was then used to remove any remaining poorly aligned particles. Finally, maps were refined once more with a mask around the entire ribosome. Final maps were then post-processed using a mask around the entire complex.

Model building

A starting model of an *E. coli* 70S ribosome (PDB 5MDZ) was docked into the post-processed maps using Chimera (*248*). Protein and RNA chains were then fitted more closely to the density using rigid-body fit in Coot (*249*). SmpB from *T. thermophilus* (*190*) was used as a starting model (PDB 4V51) and mutated to correspond to the purified *E. coli* protein. tmRNA as homology-modelled in Ramrath et. al. 2012 was used as a starting model, broken into major helical or pseudoknot domains, rigid-body fit to the density using Chimera and reattached in Coot. An iterative process of morph chain and real space refinement in coot with libg generated restraints (*250*) was used to adjust the structure of tmRNA to more closely fit the shape of the density while maintaining the base-pairing as predicted (*165*, *166*). Figures were created using Pymol (*251*) or Chimera (*248*).

Model refinement and validation

Models were refined in reciprocal space using REFMAC v5.8 optimized for cryo-EM maps using restraints generated by ProSMART and LibG (*250*). $FSC_{average}$ was monitored during refinement and the final models were assessed with MolProbity (*253*) with data shown in Table 5.1. Cross validation to prevent overfitting was performed as described (*250*).

4 Summary and future direction

4.1 The mechanism of *trans*-translation

This work has revealed new atomic details about tmRNA-SmpB that allows us to form a more complete picture of *trans*-translation. Here I summarize our current understanding of the mechanism (Figure 4.1).

A 70S ribosome forms a nonstop translation complex when translation stalls at the 3′ end of a messenger RNA (Figure 4.1A). Nonstop ribosomes do not contain a codon in the A site and therefore neither tRNAs nor release factors can recognize this conformation.

Elongation factor Tu (EF-Tu) delivers Ala-tmRNA-SmpB to the ribosome (Figure 4.1B). When trapped in this conformation the state of the ribosome is termed ‘pre-accommodated’. Contacts between EF-Tu, tmRNA and the ribosome, as well as contacts between pseudoknot 2 (PK2) of tmRNA and ribosomal protein uS3, likely coordinate the position of SmpB in the A site. The binding of PK2 coordinates helix 5 (H5) in a position incompatible with mRNA extending out of the channel. The C-terminal tail of SmpB forms an alpha helix in the empty A site and downstream mRNA channel, further verifying a nonstop ribosome complex and triggering a decoding-like event.

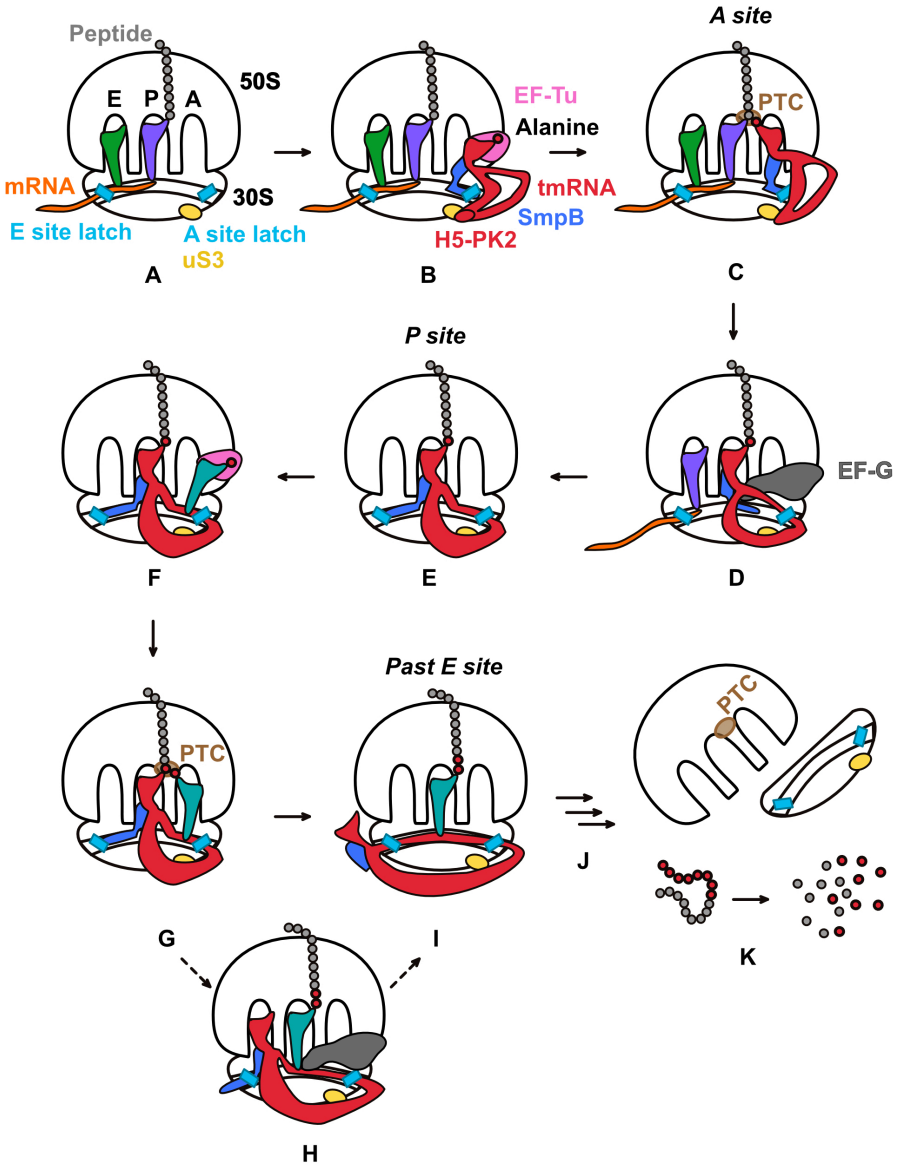

Figure 4.1 The mechanism of *trans*-translation. Cartoon representation of the mechanism of tmRNA-SmpB binding and movement through the ribosomes during *trans*-translation.

Decoding stimulates EF-Tu to hydrolyze GTP and dissociate from the ribosome, permitting tmRNA-SmpB to accommodate into the A site (Figure 4.1C). The tail of SmpB remains in the same alpha-helical conformation as in the pre-accommodated state. Analogous to canonical tRNA, the TLD-SmpB points the alanine on its 3′CCA into the peptidyl transferase reaction center (PTC) where it accepts the nascent peptide.

Elongation factor G (EF-G) translocates tmRNA-SmpB from the A site into the P site and expels the original mRNA and tRNA (Figure 4.1D). Translocation causes 30S subunit head movements to open a latch in the A site (A-site latch), through which the MLD is passed. Large, stable secondary structures flank either side of the single

stranded MLD and therefore the MLD must laterally enter the mRNA channel between the head and body of the 30S.

After tmRNA-SmpB are translocated into the P site, the MLD occupies the space in the A site and mRNA channel previously occupied by the tail of SmpB (Figure 4.1E). To avoid clashing while maintaining its role in anchoring tmRNA within the ribosome, the tail of SmpB flips to the opposite side of the mRNA channel, binding in the E site. SmpB also interacts with the MLD to position the tag-reading frame in the now empty A site for translation to restart on tmRNA.

Canonical translation resumes on the MLD as Ala-tRNA^{Ala} decodes the first codon of the tag-reading frame (Figure 4.1F) and a peptidyl transferase reaction transfers the peptide from tmRNA to tRNA^{Ala} (Figure 4.1G). EF-G then translocates peptidyl-tRNA^{Ala} into the P site and consequently shifts tmRNA-SmpB toward the E site (Figure 4.1H).

Translocation appears to move tmRNA-SmpB through the E site to the solvent side of the ribosome (Figure 4.1I). During this second translocation event, the MLD is again loaded into the mRNA channel, passing through a latch this time in the E site (E-site latch). tmRNA-SmpB deviate from tRNA-mimicry as they do not bind in the E site like a canonical tRNA. However, tmRNA-SmpB must cross the E site and therefore, likely passes through a transition state resembling canonical E site tRNA (Figure 4.1H). After this second translocation event, the MLD is fully loaded into the mRNA channel.

During the entire process of MLD loading, PK2 interacts with protein uS3, binding tmRNA to the outside of the ribosome and coordinating the position of tmRNA as it moves through the ribosome. Translation continues on the MLD until terminating at a stop codon at the end of the tag-reading frame where the peptide and the ribosome are released (Figure 4.1J). The incomplete protein is targeted for degradation by proteases that recognize the polypeptide tag appended by tmRNA-SmpB during *trans*-translation (Figure 4.1K).

4.2 Future direction

Although the work presented here advances our atomic-level understanding of the mechanism of *trans*-translation, important questions remain unanswered. Four

structures, if trapped, would answer many of the remaining structural questions regarding the mechanism of *trans*-translation in *E. coli.*

Understanding the timing of PK2 binding to the ribosome is still unclear. Although we suspect binding of PK2 to the ribosome occurs prior to tmRNA-SmpB accommodation, without a structure of the full-length tmRNA-SmpB trapped with EF-Tu we cannot claim precisely when helix 5 (H5) of tmRNA discriminates nonstop ribosomes. To trap this complex, kirromycin could be used as in a previous structure of a fragment of tmRNA (lacking H5) with SmpB bound in the pre-accommodated state (*190*).

After accommodation and translocation, SmpB bound in the P site coordinates the position of the MLD in the A site. A structure of tmRNA-SmpB bound in the P site with improved resolution around the SmpB-MLD interactions, would be required for understanding exactly how SmpB establishes the correct reading frame on tmRNA. One possible approach for improving the resolution may be to include $tRNA^{Ala}$ to decode the MLD in the A site. Bound A-site $tRNA^{Ala}$ could decrease the range of motion of the MLD near SmpB and therefore improve the electron density in this region. Additionally, to avoid capturing an already determined structural intermediate, the antibiotic kirromycin could be used to trap EF-Tu delivering Ala-$tRNA^{Ala}$ to the MLD.

After translation restarts on the MLD, peptidyl-$tRNA^{Ala}$ is translocated into the P site, forcing tmRNA-SmpB out of the P site to the solvent side of the ribosome. How tmRNA moves between the subunits during this step is still unclear, as the central protuberance appears to physically block translocation. Additionally, deviation from tRNA mimicry after this second translocation event must be investigated further to understand why tmRNA-SmpB does not occupy the E site. Trapping an EF-G-bound intermediate during translocation of tmRNA-SmpB from the P site toward the E site could show how tmRNA moves through the gap between the small and large subunit and provide insight into why tmRNA-SmpB was not observed to mimic a tRNA binding in the E site. Using the antibiotic fusidic acid could trap EF-G after it has catalyzed translocation, but prior to dissociation from the ribosome [as in (*259*)]. Alternatively, using a GTP analogue, like GDPCP, to prevent GTP hydrolysis by EF-G is another possible means of trapping a translocation intermediate.

After complete loading of the MLD into the mRNA channel, translation continues canonically until the end of the tag-reading frame. An aspect of *trans*-

translation not addressed in this study is the termination of translation on tmRNA. After several rounds of translocation on the MLD, H5 must completely unravel for the ribosome to access the stop codon at the end of the tag-reading frame. The interaction between the single stranded RNA loop of PK2 and uS3 may also begin destabilizing once the stop codon reaches the A site. The destabilization of PK2 during termination would certainly be timely and could be important for subsequent ejection of tmRNA from the ribosome. Without a structure of the ribosome bound with tmRNA during termination, we cannot know whether the PK2-uS3 interaction is destabilized and whether or not this is part of the mechanism of *trans*-translation. To trap such a complex would be possible using the *in vitro trans*-translation system described here. All required tRNAs could be included for *trans*-translation along with a mutant release factor that recognizes the stop codon but cannot hydrolyze peptidyl-tRNA. Under these conditions, the ribosome could translate the entire peptide tag encoded by tmRNA but then be trapped during termination.

Determining these structures will almost inevitably use cryo-EM. Indeed, the revolution of cryo-EM technology along with the outstanding support of the scientists and staff at the LMB are the reason the work presented here was possible. This being said, cryo-EM of course does have limitations. Indeed, we were unable to verify the exact secondary structure of tmRNA by cryo-EM. Flexible regions of a reconstruction are difficult to resolve using the existing software and even in cases where this is possible, extremely large datasets are often required. Fortunately, these limitations are more often being overcome as data collection becomes streamlined. Cryo-EM has the advantage of determining high-resolution structures of complicated, often flexible macromolecules in a near-solution state. The tmRNA bound ribosomes represent just that sort of assembly, which previously would have been difficult to solve by crystallography. Only a small amount of sample is required for cryo-EM, making it possible to run complicated reactions at a scale that is financially feasible. In this study the use of a precious *in vitro* system was possible due to the minimal scale of reactions required. Lastly, cryo-EM sample preparation does not require a perfectly homogeneous solution. Indeed, we took advantage of sample heterogeneity and fortuitously obtained a conformational state we had not expected.

In summary, this work has advanced our atomic-level understanding of *trans*-translation but interesting structures remain to be determined to complete a full picture of the mechanism.

5 Appendices

5.1 Stapled ribosomes

5.1.1 Introduction

Bioengineering ribosomes for the incorporation of multiple non-natural amino acids could lead to more advanced probing systems or even synthetic polypeptide production in cells. Such ribosomes would require specificity for a single mRNA and potentially mutated catalytic centers such as the peptidyl transferase center (PTC), as well as connectivity between the modified functions of the large and small subunits. Mutations in the ribosome are often lethal (*268*) and therefore evolution of these functions requires orthogonal ribosomes. Thus the ribosomes would function parallel to, but separate from, endogenous ribosomes within the cell. Gene duplication allows for the independent evolution of progeny from a parent. The progeny, or orthogonal, molecule can take on unique functions simultaneously, but separately, from the parent. In this way, duplication of ribosomal rRNA allows the orthogonal copy to be mutated and evolved (*269*) while the endogenous ribosomes maintain cell viability by synthesizing the proteome.

Directing the incorporation of non-natural amino acids into proteins requires orthogonal ribosome-mRNA pairs. A selection approach was previously used to design ribosomes that uniquely recognize orthogonal mRNA (O-mRNA) (*270*). The Shine-Dalgarno (SD) sequence and its proximity to the start codon in an mRNA transcript are important determinants of the efficiency of translation initiation (*271*, *272*). Orthogonal ribosomes were engineered to contain a mutated anti-Shine-Dalgarno (ASD) sequence

at the end of 16S rRNA that specifically recognizes the mutated Shine-Dalgarno of O-mRNA. Additionally, the SD of O-mRNAs can't be recognized by endogenous 30S. The mRNA-ribosome pair acts independently from endogenous translation and therefore does not mis-regulate translation in the cell.

Ribosomes that recognize only a single mRNA of interest are a critical starting point for the engineering of non-natural polypeptides, however, the building blocks of those polymers must also function orthogonally. Unique tRNA/synthetase pairs and unique codons recognized by those tRNA's are therefore needed. Inefficiencies in cross-species aminoacylation have been exploited to create orthogonal tRNA/synthetase pairs (*273*). Orthogonal synthetases selectively aminoacylate orthogonal tRNA's, and likewise, O-tRNA is not aminoacylated by natural tRNA synthetases. (*273–276*). Additionally, for the system to be entirely orthogonal, the endogenous tRNA synthetases do not recognize the non-natural amino acid (*273*).

These non-natural amino acid adaptor molecules are only useful if a corresponding but independent genetic code is used for O-mRNA. Therefore, unique codons are also required for efficient site-specific non-natural amino acid incorporation by orthogonal tRNA. All 64 naturally occurring codons are recognized by tRNA or release factors and therefore endogenous factors will inevitably compete with non-natural tRNAs for codon usage. Previous studies exploited stop codons as a useful starting point due to their minimal number of interacting partners.

For instance, amber stop codons are only recognized by RF1 and a unique aa-tRNA counterpart, the amber suppressor tRNA. The CUA anticodon of amber suppressor tRNA recognizes the UAG amber stop codon, however, RF1 also competes, decreasing non-natural amino acid incorporation by catalyzing the formation of truncated products. RF1 knockouts are lethal and therefore not a viable option, however, decreasing RF1 activity could be sufficient for maintaining cell viability while increasing the efficiency of non-natural amino acid incorporation. The unique specificity of O-ribosomes for O-mRNA allows for the mutation of the 30S subunit. O-ribosomes were evolved to have diminished ability to recognize RF1 (*277*). Decreasing the functional interaction with RF1 increases the efficiency of amber decoding from 20% to 60%. Although improved, non-natural amino acid incorporation at stop codons is still limited by competition with release factors (*277*). Furthermore, with this approach only two unique codons can be utilized, the third required for termination.

Exploiting amber codons is useful for incorporation of non-natural amino acids at single sites, however, synthetic protein synthesis would require an entire genetic code independent from that used in the cell. For this purpose, a ribosome was engineered to decode quadruplet codons (*278*), establishing a new set of blank codons for which tRNA/synthetase pairs could be assigned. These extended anticodon tRNAs have a bump corresponding to a hole in the orthogonal ribosome that allows for its accommodation. The quadruplet anticodon tRNAs are incompatible with endogenous ribosomes and therefore minimally interfere with endogenous translation. Pyrrolsyl-tRNA synthetase (PylRS) was exploited for the creation of non-natural aa-tRNA/synthetase pairs for quadruplet codons as it does not recognize the anticodon stem loop of tRNA and the quadruplet anticodons could therefore be tolerated (*279*).

Expanding the functionality of the quadruplet-decoding O-30S to the development of an entirely orthogonal 70S ribosome (O-70S) allows the large subunit to be evolved. In an O-70S, areas of particular functional interest, like the PTC or exit tunnel, can be mutated without affecting endogenous translation. An O-70S requires the 50S to be selectively recruited to the same message as the O-30S. Additionally, an orthogonal 50S ideally binds only to O-30S subunits and likewise, an O-30S should not bind to endogenous 50S. Attempts to control 50S-30S binding through non-covalent interactions have been unsuccessful. Alternatively, covalently linking the 50S to the already orthogonal 30S achieved this specificity.

The 23S rRNA was linked to the 16S through an RNA hinge (Figure 5.1A), physically bridging the subunits. Previous studies show that a circularly permuted 23S rRNA can be inserted into 16S rRNA and stapled together using an RNA hinge (*280*, *281*). To join the rRNA of both subunits, the original termini of 23S rRNA was closed and new 5’ and 3’ ends at the point of hinge attachment were opened. This modification is possible because the 23S rRNA can tolerate circular permutation (*282*), and insertions into the 16S rRNA are also possible (*283*, *284*). The circularly permuted 23S rRNA was inserted into the 16S rRNA and attached with an RNA hinge (Figure 5.1B).

Potential locations for hinge insertion were determined by examining structures of *E. coli* ribosomes for areas between the subunits that are in close proximity and that tolerated mutation based on phylogenetic analysis. Ends of helices H101 and h44 fit these criteria and were additionally chosen because they are distant from the mechanistic centers and translation factor binding sites of the ribosome. The J5/J5a region from the Tetrahymena group I self-splicing intron was used as a hinge to connect

h44 to H101 (Figure 5.1B). This RNA hinge is known to have two distinct conformations, an extended form and a U-shaped form (*285*). The structure of this hinge suggested it might be compatible for joining h44 and H101 (PDB 1GID) (Figure 5.1C).

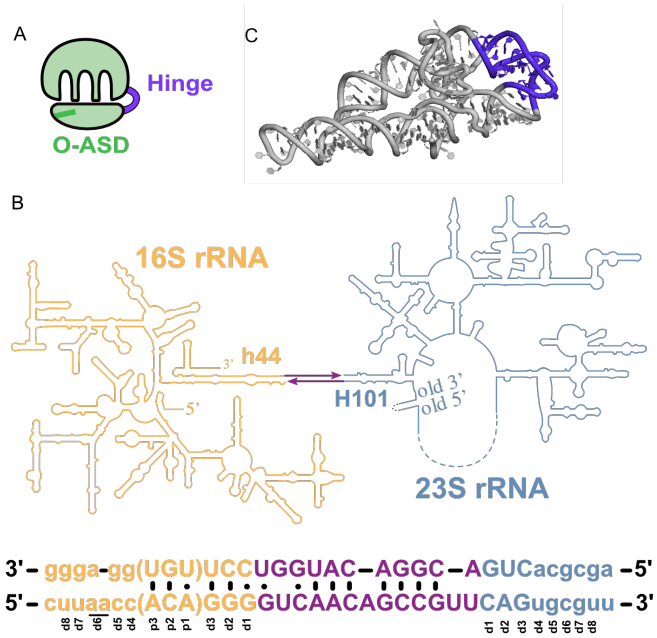

Figure 5.1 Staple design is based on a ribozyme hinge. (A) Cartoon of stapled ribosome with hinge in purple and orthogonal anti-Shine Dalgarno (O-ASD) in green. (B) Overview of *E. coli* rRNA secondary structure showing old 3' and 5' termini of the 23S rRNA connected and h44 connected to H101 by the RNA hinge. Sequence of the hinge is shown with deletion or insertion mutations labeled below each base pair. (C) Original crystal structure (PDB 1GID) of *Tetrahymena* group I self-splicing intron showing the J5/J5a region used as the hinge highlighted in purple.

Unfortunately, the concentration of ribosomes in the cell is such that linking the 30S to the 50S is unlikely to be sufficient for increasing the specificity of these two subunits. Expression of a mutated 23S of the stapled ribosome decreases growth rates, suggesting that endogenous 30S interact with stapled 50S (*286*). Indeed, nothing prevents the stapled 50S from binding endogenous 30S. The pool of large subunits is shared with stapled ribosomes and therefore the stapled ribosome is not entirely orthogonal (Figure 5.2A). Cross assembly was determined by purifying stapled ribosomes via an MS2 hairpin and measuring the co-purification of endogenous subunits (*286*). Cross assembly coefficients near one show that the stapled ribosome interacts extensively with endogenous subunits.

Additionally, stapled ribosomes can interact in trans if two ribosomes are in the open conformation (Figure 5.2B). Until now, no evidence suggests that intra-ribosome interactions (subunits joining in cis) are responsible for translation. Sucrose gradient

centrifugation showed that stapled ribosomes in *trans* dominate and likely support growth of strains containing only stapled ribosomes with an endogenous SD sequence (*286*). The stapled ribosome was further engineered to minimize recognition of endogenous subunits and promote self-assembly in cis over trans.

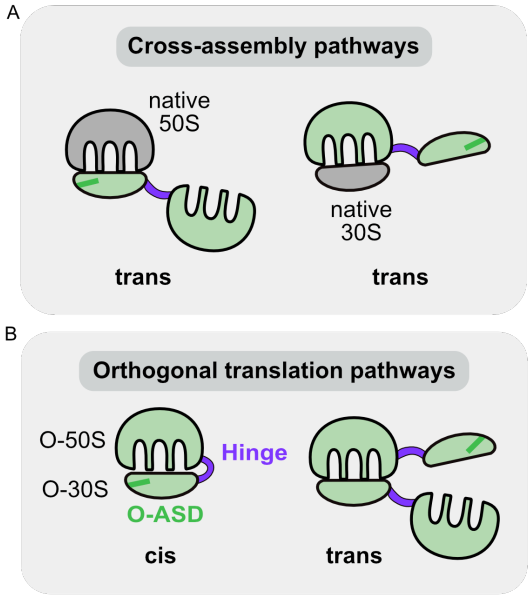

Figure 5.2 Stapled and endogenous ribosome assemblies. (A) Cartoon representation of possible cross assemblies of stapled ribosomes with native ribosomes. (B) Cartoon representation of cis and trans assembly of stapled ribosomes.

To do this, the RNA hinge was optimized in an effort to develop a large subunit that specifically interacts with O-30S and not with endogenous 30S or 50S of other stapled ribosomes. Base pairs on either side of the hinge were systematically inserted or deleted to change the distance and tilt between the subunits (*286*). One variant of stapled ribosome, O-d2d8, having two base pairs deleted from h44 and eight bases pairs deleted from H101, showed substantial reduction in cross assembly with other stapled ribosomes, and maintained activity when endogenous subunits were selectively inhibited with antibiotics for which the stapled ribosome is resistant. Additionally, cross-assembly analysis showed that d2d8 has minimal trans-associated stapled ribosomes. These results suggest that translation is mediated by subunits of a *cis*-70S stapled ribosome.

To validate the orthogonal nature of the optimized stapled ribosome, the 50S subunit was evolved to synthesize long stretches of poly-proline sequences. Proline is a secondary amine and therefore may occupy conformations that are unproductive for peptidyl-transferase. Bacterial ribosomes typically struggle to synthesize poly-proline

sequences in the absence of EF-P, a conserved translation factor that promotes elongation by binding between the P and E site near the PTC (*287–289*). Nucleotide mutations in the PTC and exit tunnel of the stapled ribosome were randomized and ribosomes were selected for successful translation of poly-proline sequences via a chloramphenicol resistance assay. One variant was selected that could translate poly-proline sequences nearly as efficiently as native ribosomes in the presence of EF-P. The variant has fifteen mutations, many of which are purine to pyrimidine mutations, which may alleviate steric clashes otherwise preventing the movement of the poly-proline peptide through the exit tunnel. This study is the first example of the synthetic evolution of a new function for the large subunit (*286*).

The structural study of stapled ribosomes presented below was in collaboration with the Jason Chin lab at the MRC-LMB. Wolfgang Schmied, Zakir Tnimov, and Chayasith Uttamapinant performed the biochemistry and optimized the stapled ribosome (*286*). I joined the project to visualize the nature of stapled ribosome interactions. Cryo-EM was used to observe the conformation of both the 70S stapled ribosome and stapled di-ribosome. In particular we were interested in how the conformation of the staple permits normal ribosome function.

5.1.2 Results and discussion

5.1.2.1 70S stapled ribosome structure

The most efficient stapled ribosome with the least cross-assembly, d2d8, was prepared for observation by cryo-EM. Pelleting and sucrose gradient centrifugation were used to purify d2d8-stapled ribosomes from a strain of *E. coli* containing stapled ribosomes as the sole means of growth. Ribosomes were prepared on copper grids coated with a thin layer of carbon and a dataset was collected on a 300 kV Krios cryo-electron microscope. Three-dimensional classification revealed two main classes. As anticipated, the hinge can form two different conformations, the open and the closed conformation (Figure 5.3).

The hinge occupies an open conformation in approximately half of the ribosomes. Open and closed conformations would be expected to be in natural equilibrium within the cell, however, it is unclear whether under these conditions the exact ratio is due to sample preparation. Under similar purification conditions, ribosomes remain as 70S on the grid and rarely dissociated into subunits. Magnesium is known to stabilize 70S ribosomes and higher concentrations may be needed to stabilize

stapled 70S ribosomes. The hinge may therefore have an adverse effect, actually preventing subunit joining which would also be consistent with the inefficiencies of the stapled ribosome relative to wild type.

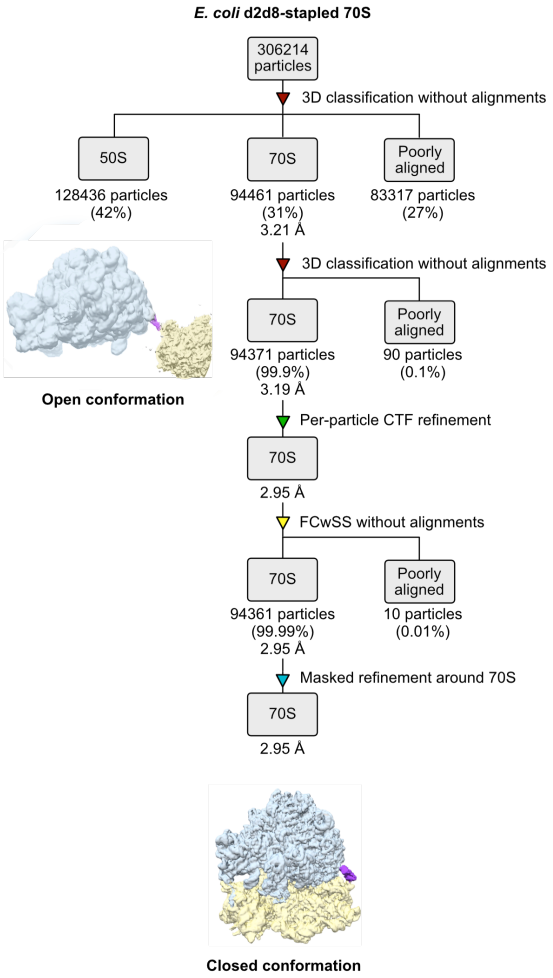

Figure 5.3 *In silico* classification of *E. coli* d2d8-stapled ribosome. Two rounds of three dimensional classification without alignments were followed by per particle contrast transfer function correction and a final focused classification with signal subtraction masking over the hinge (RELION 3.0). Two main classes were observed, representing stapled 70S ribosomes in the opened or closed conformation.

The closed 70S was pursued for further classification and refinement, producing a 3.0 Å resolution reconstruction (Figure 5.4). The map reveals that the subunits are in nearly identical conformations to those in native *E. coli* ribosomes. This suggests d2d8 ribosomes can translate as a 70S assembly in cis, and supports previous findings showing a lack of cross-assembly. It is possible that the other less efficient stapled ribosome mutants with different hinge variants may in fact be preventing subunit joining in cis. The d2d8 mutations may therefore minimize the adverse

conformations generated by the hinge. Indeed, the hinge of stapled ribosomes with high cross-assembly coefficients could be limiting the interaction of the adjoining subunits.

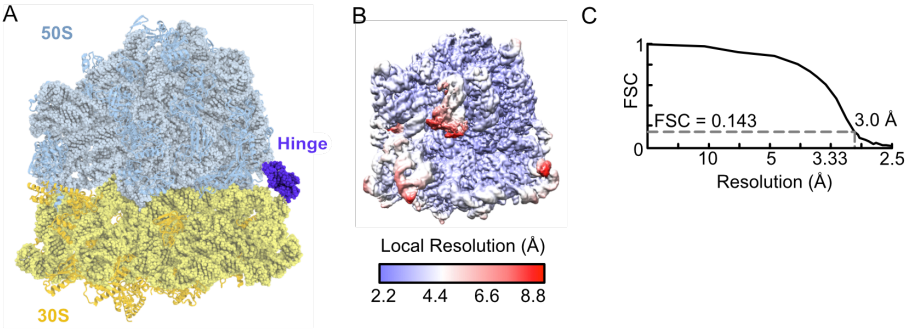

Figure 5.4 Structure of *E. coli* stapled ribosome. (A) Overview of the *E. coli* d2d8-stapled ribosome structure. (B) Electron density map colored by local resolution ranging from 2.2 Å to 8.8 Å. (C) Fourier shell correlation (FSC) curve showing map resolution of 3.0 Å with dashed line at FSC=0.143.

The hinge of the d2d8 stapled ribosome covalently links the large and small subunits. Continuous density can be seen connecting h44 to H101, and the previous crystal structure of the J5/J5a RNA hinge can be docked into the map (Figure 5.5). The hinge adopts the expected U-turn conformation when the ribosome is in the closed state, largely similar to the conformation in the original crystal structure. However, to connect the hinge requires rearrangement of both termini, suggesting inherent flexibility.

This study shows how the structure based design of a stapled ribosome and further optimization of the hinge can produce an engineered ribosome in a near native conformation. Cryo-EM was a useful tool in validating the biochemical evidence as well as understanding the effect of the hinge on the overall conformation of the ribosome.

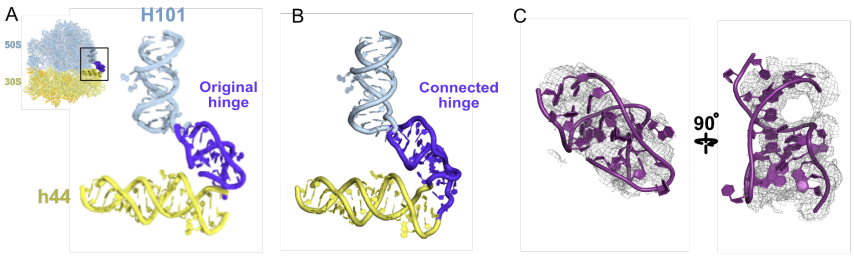

Figure 5.5 The unmodifed hinge fits the density. (A) Closeup of rRNA with unmodified hinge docked in. (B) Adjustment of the ends of the hinge and helix are necessary for attachment. (C) Original unmodified hinge shown fit into density.

5.1.2.2 Towards a di-ribosome structure

Cross-assembly of stapled ribosomes in trans was also investigated by cryo-EM. A different mutant stapled ribosome, d4d7, was more prone to cross-assembly and therefore chosen for purification of the disome species in the cell. Disomes were purified through a sucrose cushion and followed by sucrose gradient centrifugation. Initial maps suggest the disome functions in trans with the attached subunits occupying unique spaces adjacent to a central 70S assembly (Figure 5.6).

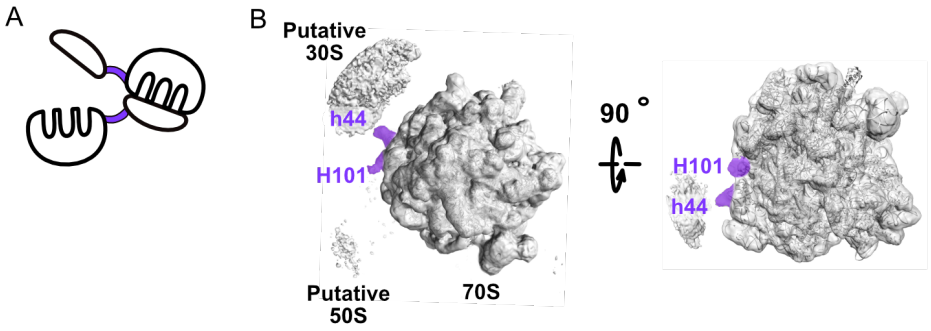

Figure 5.6 Initial maps of the stapled di-ribosome suggests the binding in trans of two 70S ribosomes in open conformations. (A) Cartoon representing possible trans stapled di-ribosome conformation. (B) Initial reconstruction of stapled di-ribosomes. The hinge connecting to h44 or H101 in the small or large subunits, respectively, are highlighted purple.

Superposition of maps of the d2d8 open conformation shows that the position of putative subunits in the disome species are different than those seen in d2d8 stapled ribosomes. This is likely due to the differences in the hinge and could be a reason why cross-assembly is more likely for d4d7 ribosomes. The hinge appears to rotate subunits in a position that is incompatible with binding when the hinge takes on the closed, U-shape, conformation. The formation of a trans 70S ribosome supports the data suggesting cross-assembled stapled ribosomes are capable of translation, and in fact, may be the primary source of activity for variants with high levels of cross-assembly.

5.1.3 Conclusions

Stapled ribosomes with near O-ribosome activity and minimal cross-assembly, take two major forms: opened 70S or closed 70S. A structure of the closed form reveals a ribosome in a conformation identical to native ribosomes, suggesting that the optimized hinge has minimal interference in translation. Similarly, the map of a cross-

assembled disome shows a 70S with subunit appendages, likely the stapled subunits. These stapled ribosomes may be prohibited from binding in *cis* due to the angle at which the hinge orients the subunits.

This structural study highlights the use of cryo-EM as a means of observation and support for biochemical analysis. Although from a structural perspective, the sample under investigation was not particularly different from native ribosomes, the structure validated biochemical data and confirmed the structure-guided approach for choosing the hinge location. The use of cryo-EM as an auxiliary technique in the broader investigation and manipulation of biochemical systems is likely to become more common, particularly for large, globular, and stable macromolecules such as the ribosomes. This structural study gives confidence to the biochemical approach used in the Chin lab and generally informs us that the optimization efforts for O-70S ribosomes are moving in the right direction.

5.1.4 Materials and methods

Electron cryo-microscopy

Quantifoil Cu R2/2 400 mesh grids were coated with a thin sheet (~60 Å) of amorphous carbon and glow discharged for 5 s at 5 mA. Purified *E. coli* 70S d2d8 ribosomes were diluted to 100 nM in 50 mM HEPES pH 7.4, 100 mM KOAc, 5 mM $Mg(OAc)_2$ and applied to grids in 3 µl aliquots. Grids were incubated for 30 s at 4ºC and 100% humidity, blotted for 4.5 s and frozen in liquid ethane using a Vitrobot Mark III (FEI). Micrograph movies of *E. coli* d2d8 70S ribosomes were collected on a Titan Krios microscope at 300 keV with a Falcon III detector using automated data collection with EPU software (all FEI). Movies were collected at a pixel size of 1.06 Å with a dose rate of 15 $e.Å^{-2}.s^{-1}$ over a 1.79 s exposure, consisting of 71 total frames. Defocus values ranging of -3.2, -2.9, -2.6, -2.3, -2.0, -1.7 µm were used.

Image processing

All processing was done using RELION-2.1. Micrograph movie frames were aligned using Motioncorr and contrast transfer functions calculated using Gctf. Aligned movies were removed after manual inspection if micrographs contained ice particles or if contrast transfer functions failed to calculate. Ribosome particles were picked semi-

autonomously and incorrectly picked non-ribosomal particles were identified and discarded by reference-free two-dimensional classification. The resulting 306214 particles were used for initial three-dimensional refinement with an *E. coli* 70S ribosome (EMD-3493) low-pass filtered to 40 Å as a reference. Three-dimensional classification of the initial reconstruction was performed without alignments to discard poorly aligned particles. Two major classes were obtained, one of closed 70S ribosomes (94461 particles) and another containing 'opened' 70S ribosomes (128436 particles). The closed ribosomes were selected and refined. Focused classification with signal subtraction on the RNA hinge gave the final primary class (94371 particles). The quality of the density in the hinge region is lower than in other parts of the structure. However, classification focused on the staple revealed a single class, demonstrating sample homogeneity. This indicated that the lower density in this region is not due to a mixture of particles and it may therefore reflect flexibility in the hinge and/or local variation in the conformation of the hinge.

Model building, refinement and validation

A model (PDB 5MDZ) of the *E. coli* 70S ribosome (*136*) was docked into the reconstruction in Chimera (*248*), and individual RNA and protein chains were rigid body fitted using Coot (*249*). Portions of h44 of 16S rRNA and H101 of 23S rRNA were deleted or added according to the sequence of the d2d8 ribosomal RNA. The RNA hinge, from a group I ribozyme domain (PDB 1GID), was then docked into the remaining, unaccounted for density. An iterative process of morph fit, and real-space-refinement in Coot was used to connect the RNA hinge to the original ribosomal RNA. Real space refinement was carried out in Phenix (*252*) and the model was validated using MolProbity (*253*). Figures were created using Pymol (*251*) or Chimera (*248*).

5.2 Supplemental material for Cryo-EM data collection

Eleven cryo-EM datasets were collected over the course of the tmRNA project. Four datasets (Table 5.1, #1-4) (Table 5.2, tmRNA #1, 6, 7, 10) resulted in models of interesting *trans*-translation intermediates used for publication. The remaining seven datasets were collected in an effort either to reach higher resolution (Table 5.2, tmRNA #3-5), or to trap different *trans*-translation intermediates (Table 5.2, tmRNA #2, 8, 9,

11). These datasets neither improved the resolution nor were successful in trapping new complexes.

Additionally, two datasets were collected for the stapled ribosome project described in Chapter 5.1 (Table 5.2, stapled #1-2) and one was used to build a model for publication (Table 5.1, #5). All datasets were collected at 300 kV with defocus values ranging from -2.0 to -3.5 µm

	#1 *Thermus* A-site EMDB-4475 PDB-6Q95	#2 *E. coli* A-site EMDB-4476 PDB-6Q97	#3 *E. coli* P- site EMDB-4477 PDB-6Q98	#4 *E. coli* Past E- site EMDB-4478 PDB-6Q9A	#5 *E. coli* d2d8 Stapled 70S EMDB-0261 PDB-6HRM
Data collection and processing					
Magnification	75k	75k	93k	93k	75k
Voltage (kV)	300	300	300	300	300
Electron exposure (e–/Å^2)	42	44	60	60	27
Defocus range (µm)	-2.0 to -3.5	-2.0 to -3.5	-2.0 to -3.5	-2.0 to -3.5	-2.0 to -3.5
Pixel size (Å)	1.34	1.07	1.15	1.15	1.06
Symmetry imposed	none	none	none	none	none
Micrographs collected (no.)	1425	2753	1889	1948	
Micrographs used (no.)	1251	2721	1089	1108	
Initial particle images (no.)	187793	79361	122575	144201	306214
Final particle images (no.)	24400	47776	18018	47115	94371
Map resolution (Å) FSC=0.143 CRef=0.5	 3.7 3.67	 3.9 3.91	 4.3 4.39	 3.7 3.70	 3.0 2.95
Map resolution range (Å)	3.5-18	3.5-18	3.5-18	3.5-18	2.2-8.8
Refinement					
Initial model used (PDB code)	4V51	5MDZ	5MDZ	5MDZ	5MDZ
Model resolution (Å) FSC threshold	2.8 0.143	3.1 0.143	3.1 0.143	3.1 0.143	3.1 0.143
Model resolution range (Å)	2.8-50	2.6-7.1	2.6-7.1	2.6-7.1	2.6-7.1
Map sharpening *B* factor (Å^2)	-54.0	-122.6	-84.2	-79.4	-78.8
B factors (Å^2) Protein RNA	 72 129	 120 82	 217 82	 200 82	 86.4 55.1
R.m.s. deviations Bond lengths (Å) Bond angles (°)	 0.01 1.36	 0.01 1.19	 0.01 1.34	 0.01 1.11	 0.01 1.00
Validation MolProbity score Clashscore Poor rotamers (%)	 2.27 8.88 1.36	 1.96 6.76 0.80	 2.12 9.89 0.68	 1.71 4.98 0.78	 1.45 2.96 0.47
Ramachandran plot Favored (%) Allowed (%) Disallowed (%)	 82.75 16.49 0.76	 88.33 11.55 0.12	 87.64 12.26 0.10	 93.01 6.96 0.03	 94.78 5.16 0.05

Table 5.1 Collection, refinement and validation of Cryo-EM data for published models.

Dataset	tmRNA dataset #1		tmRNA dataset #2		tmRNA dataset #3			tmRNA dataset #4		
Complex name	A site		P site		A site			E site		
Species	*T. thermophilus*		*T. thermophilus*		*E. coli*			*E. coli*		
Data collection										
Microscope	Polara		Polara		Polara			Polara		
Pixel size (Å)	1.34		1.17		1.15			1.15		
Electron exposure (e–/Å2)	42		28		40			~55		
Micrographs collected (no.)	1425		3100		1632			1908		
Data Processing										
Micrographs used (no.)	1251		2722		1264			1111		
Initial particle images after 2D (no.)	187793		128719		120882			126313		
Class name	A site	70S	A site	70S	50S	A site	P site	70S	50S	A site	P site	past E site	50S
Final particle images (no.)	24400	75117	37768			81289	6197	31388	16923	35891	4942	32982	17684
Map resolution (Å)	3.7					3.8	10.2			7	18.2	4.8	
PDB/EMDB	6Q95/4475												

Dataset	tmRNA dataset #5			tmRNA dataset #6			tmRNA dataset #7			tmRNA dataset #8			
Complex name	P site			P site			E site			P, E site mix			
Species	*E. coli*			*E. coli*			*E. coli*			*E. coli*			
Data collection													
Microscope	Polara			Polara			Polara			Krios			
Pixel size (Å)	1.15			1.15			1.15			1.07			
Electron exposure (e–/Å2)	60			60			60			61			
Micrographs collected (no.)	2003			1889			1948			2960			
Data Processing													
Micrographs used (no.)	1115			1069			1108			2695			
Initial particle images after 2D (no.)	153632			122575			144201			309195			
Class name	A site	P site	50S	A site	P site	50S	A site	past E site	50S	Asite	Psite	past E site	50S
Final particle images (no.)	83997	25782	36871	52034	18018	34689	15477	47115	34031	115812	43012	107228	43143
Map resolution (Å)	4.9	5.5		3.9	4.4		7.8	3.7		5.2	5.8	5.2	
PDB/EMDB					6Q98/4477			6Q9A/4478					

Dataset	tmRNA dataset #9			tmRNA dataset #10			tmRNA dataset #11			Staple dataset #1			Staple dataset #2	
Complex name	P to E site translocation			A site with P, E tRNA			P site with A-site tRNAAla			Stapled 70S d2d8			Stapled disome d2d7	
Species	*E. coli*			*E. coli*			*E. coli*			*E. coli*			*E. coli*	
Data collection														
Microscope	Krios			Krios			Krios			Krios			Polara	
Pixel size (Å)	1.07			1.07			1.06			1.06			1.34	
Electron exposure (e–/Å2)	80			44			44			27			22	
Micrographs collected (no.)	2783			2753			3291			2044			1103	
Data Processing														
Micrographs used (no.)	2748			2721			3259			2020			922	
Initial particle images after 2D (no.)	238807			79361			316544			306214			74649	
Class name	APE	50S	A site	P site	50S	A site	P site	past E site	Closed 70S	Open 70S	Disome	Other		
Final particle images (no.)	174329	53341	47776	1009	76980	80162	26879	28271	94371	42753	52242	22407		
Map resolution (Å)			3.7			5.2	7	6.4	3	3.8	6.8			
PDB/EMDB			6Q97/4476						6HRM/0261					

Table 5.2 Cryo-EM data collection attempts. Classes from data collections resulting in published structures are highlighted in red.

References

1. G. W. Beadle, E. L. Tatum, Genetic Control of Biochemical Reactions in Neurospora. *Proc Natl Acad Sci U S A*. **27**, 499–506 (1941).

2. O. T. Avery, C. M. MacLeod, M. McCarty, Studies on the Chemical Nature of the Substance Inducing Transformation of Pneumococcal Types: Induction of Transformation by a Desoxyribonucleic Acid Fraction Isolated from Pneumococcus Type Iii. *Journal of Experimental Medicine*. **79**, 137–158 (1944).

3. A. D. Hershey, M. Chase, Independent Functions of Viral Protein and Nucleic Acid in Growth of Bacteriophage. *The Journal of General Physiology*. **36**, 39–56 (1952).

4. A. Gierer, G. Schramm, Infectivity of Ribonucleic Acid from Tobacco Mosaic Virus. *Nature*. **177**, 702 (1956).

5. H. Fraenkel-Conrat, B. Singer, R. C. Williams, Infectivity of viral nucleic acid. *Biochimica et Biophysica Acta*. **25**, 87–96 (1957).

6. J. D. Watson, F. H. Crick, Molecular structure of nucleic acids. *Nature*. **171**, 737–738 (1953).

7. J. D. Watson, F. H. C. Crick, Genetical Implications of the Structure of Deoxyribonucleic Acid. *Nature*. **171**, 964 (1953).

8. S. Zamenhof, G. Brawerman, E. Chargaff, On the desoxypentose nucleic acids from several microorganisms. *Biochimica et Biophysica Acta*. **9**, 402–405 (1952).

9. G. R. Wyatt, The Nucleic Acids of Some Insect Viruses. *The Journal of General Physiology*. **36**, 201–205 (1952).

10. W. B. Wood, P. Berg, The Effect of Enzymatically Synthesized Ribonucleic Acid on Amino Acid Incorporation by a Soluble Protein-Ribosome System from Escherichia Coli*. *Proc Natl Acad Sci U S A*. **48**, 94–104 (1962).

11. G. Gamow, Possible Relation between Deoxyribonucleic Acid and Protein Structures. *Nature*. **173**, 318 (1954).

12. F. Crick, L. Barnett, S. Brenner, R. J. Watts-Tobin, General nature of the genetic code for proteins (1961).

13. S. Brenner, On the Impossibility of All Overlapping Triplet Codes in Information Transfer from Nucleic Acid to Proteins. *PNAS*. **43**, 687–694 (1957).

14. M. W. Nirenberg, J. H. Matthaei, The dependence of cell-free protein synthesis in E. coli upon naturally occurring or synthetic polyribonucleotides. *PNAS*. **47**, 1588–1602 (1961).

15. P. Leder, M. Nirenberg, Rna Codewords and Protein Synthesis, Ii. Nucleotide Sequence of a Valine Rna Codeword. *PNAS*. **52**, 420–427 (1964).

16. H. G. Khorana, Nucleic acid synthesis in the study of the genetic code. *Nobel Lectures: Physiology or Medicine (1963–1970)* (1972).

17. F. H. C. Crick, On Protein Synthesis (1958).

18. M. B. Hoagland, M. L. Stephenson, J. F. Scott, L. I. Hecht, P. C. Zamecnik, A Soluble Ribonucleic Acid Intermediate in Protein Synthesis (1957).

19. W. Holley, G. A. Everett, J. T. Madison, Nucleotide Sequences in the Yeast Alanine Transfer Ribonucleic Acid. **240**, 7 (1965).

20. R. W. Holley, J. Apgar, G. A. Everett, J. T. Madison, M. Marquisee, S. H. Merrill, J. R. Penswick, A. Zamir, Structure of a Ribonucleic Acid. *Science*. **147**, 1462–1465 (1965).

21. A. Claude, The Constitution of Protoplasm. *Science*. **97**, 451–456 (1943).

22. M. L. Petermann, M. G. Hamilton, An Ultracentrifugal Analysis of the Macromolecular Particles of Normal and Leukemic Mouse Spleen. *Cancer Res*. **12**, 373–378 (1952).

23. G. E. Palade, A Small Particulate Component of the Cytoplasm. *J Biophys Biochem Cytol*. **1**, 59–68 (1955).

24. P. O. P. Ts'o, J. Bonner, J. Vinograd, Microsomal Nucleoprotein Particles from Pea Seedlings. *The Journal of Cell Biology*. **2**, 451–466 (1956).

25. F.-C. Chao, H. K. Schachman, The isolation and characterization of a macromolecular ribonucleoprotein from yeast. *Archives of Biochemistry and Biophysics*. **61**, 220–230 (1956).

26. G. E. Palade, P. Siekevitz, Pancreatic Microsomes: An Integrated Morphological and Biochemical Study. *The Journal of Cell Biology*. **2**, 671–690 (1956).

27. P. C. Zamecnik, E. B. Keller, J. W. Littlefield, M. B. Hoagland, R. B. Loftfield, Mechanism of incorporation of labeled amino acids into protein. *Journal of Cellular and Comparative Physiology*. **47**, 81–101 (1956).

28. A. Tissières, J. D. Watson, D. Schlessinger, B. R. Hollingworth, Ribonucleoprotein particles from Escherichia coli. *Journal of Molecular Biology*. **1**, 221–233 (1959).

29. A. Tissieres, D. Schlessinger, F. Gros, Amino Acid Incorporation into Proteins by Escherichia Coli Ribosomes. *Proc Natl Acad Sci U S A*. **46**, 1450–1463 (1960).

30. K. Kruger, P. J. Grabowski, A. J. Zaug, J. Sands, D. E. Gottschling, T. R. Cech, Self-splicing RNA: Autoexcision and autocyclization of the ribosomal RNA intervening sequence of tetrahymena. *Cell*. **31**, 147–157 (1982).

31. C. Guerrier-Takada, K. Gardiner, T. Marsh, N. Pace, S. Altman, The RNA moiety of ribonuclease P is the catalytic subunit of the enzyme. *Cell*. **35**, 849–857 (1983).

32. M. S. Capel, D. M. Engelman, B. R. Freeborn, M. Kjeldgaard, J. A. Langer, V. Ramakrishnan, D. G. Schindler, D. K. Schneider, B. P. Schoenborn, I. Y. Sillers, A. Et, A complete mapping of the proteins in the small ribosomal subunit of Escherichia coli. *Science*. **238**, 1403–1406 (1987).

33. R. P. May, V. Nowotny, P. Nowotny, H. Voss, K. H. Nierhaus, Inter-protein distances within the large subunit from Escherichia coli ribosomes. *The EMBO Journal*. **11**, 373–378 (1992).

34. J. A. Lake, Ribosomal subunit orientations determined in the monomeric ribosome by single and by double-labeling immune electron microscopy. *Journal of Molecular Biology*. **161**, 89–106 (1982).

35. H. Hope, Cryocrystallography of biological macromolecules: a generally applicable method. *Acta Crystallographica Section B*. **44**, 22–26 (1988).

36. H. Hope, F. Frolow, K. V. Böhlen, I. Makowski, C. Kratky, Y. Halfon, H. Danz, P. Webster, K. S. Bartels, H. G. Wittmann, A. Yonath, Cryocrystallography of ribosomal particles. *Acta Crystallographica Section B*. **45**, 190–199 (1989).

37. K. von Böhlen, I. Makowski, H. A. S. Hansen, H. Bartels, Z. Berkovitch-Yellin, A. Zaytzev-Bashan, S. Meyer, C. Paulke, F. Franceschi, A. Yonath, Characterization and preliminary attempts for derivatization of crystals of large ribosomal subunits from Haloarcula marismortui diffracting to 3 Å resolution. *Journal of Molecular Biology*. **222**, 11–15 (1991).

38. J. Frank, J. Zhu, P. Penczek, Y. Li, S. Srivastava, A. Verschoor, M. Radermacher, R. Grassucci, R. K. Lata, R. K. Agrawal, A model of protein synthesis based on cryo-electron microscopy of the E. coli ribosome. *Nature*. **376**, 441–444 (1995).

39. H. Stark, F. Mueller, E. V. Orlova, M. Schatz, P. Dube, T. Erdemir, F. Zemlin, R. Brimacombe, M. van Heel, The 70S Escherichia coli ribosome at 23 å resolution: fitting the ribosomal RNA. *Structure*. **3**, 815–821 (1995).

40. N. Ban, B. Freeborn, P. Nissen, P. Penczek, R. A. Grassucci, R. Sweet, J. Frank, P. B. Moore, T. A. Steitz, A 9 Å Resolution X-Ray Crystallographic Map of the Large Ribosomal Subunit. *Cell*. **93**, 1105–1115 (1998).

41. N. Ban, P. Nissen, J. Hansen, M. Capel, P. B. Moore, T. A. Steitz, Placement of protein and RNA structures into a 5 Å-resolution map of the 50S ribosomal subunit. *Nature*. **400**, 841–847 (1999).

42. W. M. Clemons, J. L. May, B. T. Wimberly, J. P. McCutcheon, M. S. Capel, V. Ramakrishnan, Structure of a bacterial 30S ribosomal subunit at 5.5 A resolution. *Nature*. **400 VN-**, 833–840 (1999).

43. J. H. Cate, M. M. Yusupov, G. Z. Yusupova, T. N. Earnest, H. F. Noller, X-ray crystal structures of 70S ribosome functional complexes. *Science*. **285**, 2095–2104 (1999).

44. N. Ban, P. Nissen, J. Hansen, P. B. Moore, T. A. Steitz, The complete atomic structure of the large ribosomal subunit at 2. *Science*. **289**, 905–920 (2000).

45. F. Schluenzen, A. Tocilj, R. Zarivach, J. Harms, M. Gluehmann, D. Janell, A. Bashan, H. Bartels, I. Agmon, F. Franceschi, A. Yonath, Structure of Functionally Activated Small Ribosomal Subunit at 3.3 \AA Resolution. *Cell*. **102**, 615–623 (2000).

46. B. T. Wimberly, D. E. Brodersen, W. M. Clemons Jr, R. J. Morgan-Warren, A. P. Carter, C. Vonrhein, T. Hartsch, V. Ramakrishnan, Structure of the 30S ribosomal subunit. *Nature*. **407**, 327–339 (2000).

47. B. S. Schuwirth, M. A. Borovinskaya, C. W. Hau, W. Zhang, A. Vila-Sanjurjo, J. M. Holton, J. H. D. Cate, Structures of the Bacterial Ribosome at 3.5 A Resolution. *Science*. **310**, 827–834 (2005).

48. A. Korostelev, S. Trakhanov, M. Laurberg, H. F. Noller, Crystal Structure of a 70S Ribosome-tRNA Complex Reveals Functional Interactions and Rearrangements. *Cell*. **126**, 1065–1077 (2006).

49. M. Selmer, C. M. Dunham, F. V. M. IV, A. Weixlbaumer, S. Petry, A. C. Kelley, J. R. Weir, V. Ramakrishnan, Structure of the 70S Ribosome Complexed with mRNA and tRNA. *Science*. **313**, 1935 – 1941 (2006).

50. R. E. Monro, Catalysis of peptide bond formation by 50 s ribosomal subunits from Escherichia coli. *Journal of Molecular Biology*. **26**, 147–151 (1967).

51. H. J. Rheinberger, H. Sternbach, K. H. Nierhaus, Three tRNA binding sites on Escherichia coli ribosomes. *PNAS*. **78**, 5310–5314 (1981).

52. T. Okamoto, M. Takanami, Interaction of ribosomes and some synthetic polyribonucleotides. *Biochimica et Biophysica Acta (BBA) - Specialized Section on Nucleic Acids and Related Subjects*. **68**, 325–327 (1963).

53. C. G. Kurland, Structure and Function of the Bacterial Ribosome. *Annual Review of Biochemistry*. **41**, 377–408 (1972).

54. H. F. Noller, V. Hoffarth, L. Zimniak, Unusual resistance of peptidyl transferase to protein extraction procedures. *Science*. **256**, 1416–1419 (1992).

55. J. Shine, L. Dalgarno, The 3′-Terminal Sequence of Escherichia coli 16S Ribosomal RNA: Complementarity to Nonsense Triplets and Ribosome Binding Sites. *PNAS*. **71**, 1342–1346 (1974).

56. A. P. Carter, W. M. Clemons, D. E. Brodersen, R. J. Morgan-Warren, T. Hartsch, B. T. Wimberly, V. Ramakrishnan, Crystal Structure of an Initiation Factor Bound to the 30S Ribosomal Subunit. *Science*. **291**, 498–501 (2001).

57. T. Hussain, J. L. Llácer, B. T. Wimberly, J. S. Kieft, V. Ramakrishnan, Large-Scale Movements of IF3 and tRNA during Bacterial Translation Initiation. *Cell*. **167**, 133–144.e13 (2016).

58. A. Simonetti, S. Marzi, A. G. Myasnikov, A. Fabbretti, M. Yusupov, C. O. Gualerzi, B. P. Klaholz, Structure of the 30S translation initiation complex. *Nature*. **455**, 416–420 (2008).

59. P. Milon, M. Carotti, A. L. Konevega, W. Wintermeyer, M. V. Rodnina, C. O. Gualerzi, The ribosome-bound initiation factor 2 recruits initiator tRNA to the 30S initiation complex. *EMBO reports*. **11**, 312–316 (2010).

60. M. A. Canonaco, C. O. Gualerzi, C. L. Pon, Alternative occupancy of a dual ribosomal binding site by mRNA affected by translation initiation factors. *European Journal of Biochemistry*. **182**, 501–506 (1989).

61. A. L. Teana, C. O. Gualerzi, R. Brimacombe, From stand-by to decoding site. Adjustment of the mRNA on the 30S ribosomal subunit under the influence of the initiation factors. *RNA*. **1**, 772–782 (1995).

62. D. Hartz, D. S. McPheeters, L. Gold, Selection of the initiator tRNA by Escherichia coli initiation factors. *Genes Dev.* **3**, 1899–1912 (1989).

63. D. Hartz, J. Binkley, T. Hollingsworth, L. Gold, Domains of initiator tRNA and initiation codon crucial for initiator tRNA selection by Escherichia coli IF3. *Genes Dev.* **4**, 1790–1800 (1990).

64. L. B. Jenner, N. Demeshkina, G. Yusupova, M. Yusupov, Structural aspects of messenger RNA reading frame maintenance by the ribosome. *Nat. Struct. Mol. Biol.* **17**, 555–560 (2010).

65. P. Milón, M. V. Rodnina, Kinetic control of translation initiation in bacteria. *Critical Reviews in Biochemistry and Molecular Biology*. **47**, 334–348 (2012).

66. M. V. Rodnina, T. Pape, R. Fricke, L. Kuhn, W. Wintermeyer, Initial Binding of the Elongation Factor Tu·GTP·Aminoacyl-tRNA Complex Preceding Codon Recognition on the Ribosome. *J. Biol. Chem.* **271**, 646–652 (1996).

67. M. Diaconu, U. Kothe, F. Schlünzen, N. Fischer, J. M. Harms, A. G. Tonevitsky, H. Stark, M. V. Rodnina, M. C. Wahl, Structural Basis for the Function of the Ribosomal L7/12 Stalk in Factor Binding and GTPase Activation. *Cell*. **121**, 991–1004 (2005).

68. J. M. Ogle, J. M. Ogle, D. E. Brodersen, W. M. C. Jr, M. J. Tarry, A. P. Carter, V. Ramakrishnan, Recognition of Cognate Transfer RNA by the 30 S Ribosomal Subunit. *Science (New York, N.Y.)*. **292**, 897–902 (2001).

69. J. M. Ogle, F. V. Murphy, M. J. Tarry, V. Ramakrishnan, Selection of tRNA by the Ribosome Requires a Transition from an Open to a Closed Form. *Cell*. **111**, 721–732 (2002).

70. T. Daviter, H.-J. Wieden, M. V. Rodnina, Essential Role of Histidine 84 in Elongation Factor Tu for the Chemical Step of GTP Hydrolysis on the Ribosome. *Journal of Molecular Biology*. **332**, 689–699 (2003).

71. R. M. Voorhees, T. M. Schmeing, A. C. Kelley, V. Ramakrishnan, The mechanism for activation of GTP hydrolysis on the ribosome. *Science (New York, N.Y.)*. **330**, 835–838 (2010).

72. G. Polekhina, S. Thirup, M. Kjeldgaard, P. Nissen, C. Lippmann, J. Nyborg, Helix unwinding in the effector region of elongation factor EF-Tu–GDP. *Structure*. **4**, 1141–1151 (1996).

73. R. C. Thompson, P. J. Stone, Proofreading of the codon-anticodon interaction on ribosomes. *PNAS*. **74**, 198–202 (1977).

74. T. Ruusala, M. Ehrenberg, C. G. Kurland, Is there proofreading during polypeptide synthesis? *The EMBO Journal*. **1**, 741–745 (1982).

75. A. Sievers, M. Beringer, M. V. Rodnina, R. Wolfenden, The ribosome as an entropy trap. *PNAS*. **101**, 7897–7901 (2004).

76. N. A. of Sciences, Correction for Sievers et al., From the Cover: The ribosome as an entropy trap, PNAS 2004 101:7897-7901. *PNAS*. **101**, 12397–12398 (2004).

77. S. Dorner, C. Panuschka, W. Schmid, A. Barta, Mononucleotide derivatives as ribosomal P-site substrates reveal an important contribution of the 2′-OH to activity. *Nucleic Acids Res*. **31**, 6536–6542 (2003).

78. R. M. Voorhees, A. Weixlbaumer, D. Loakes, A. C. Kelley, V. Ramakrishnan, Insights into substrate stabilization from snapshots of the peptidyl transferase center of the intact 70S ribosome. *Nature Structural & Molecular Biology*. **16**, 528–533 (2009).

79. T. M. Schmeing, V. Ramakrishnan, What recent ribosome structures have revealed about the mechanism of translation. *Nature*. **461**, 1234–1242 (2009).

80. M. S. Bretscher, Translocation in Protein Synthesis: A Hybrid Structure Model. *Nature*. **218**, 675 (1968).

81. D. Moazed, H. F. Noller, Intermediate states in the movement of transfer RNA in the ribosome. *Nature*. **342**, 142 (1989).

82. X. Agirrezabala, J. Lei, J. L. Brunelle, R. F. Ortiz-Meoz, R. Green, J. Frank, Visualization of the Hybrid State of tRNA Binding Promoted by Spontaneous Ratcheting of the Ribosome. *Molecular Cell*. **32**, 190–197 (2008).

83. P. Julián, A. L. Konevega, S. H. W. Scheres, M. Lázaro, D. Gil, W. Wintermeyer, M. V. Rodnina, M. Valle, Structure of ratcheted ribosomes with tRNAs in hybrid states. *PNAS*. **105**, 16924–16927 (2008).

84. R. M. Voorhees, V. Ramakrishnan, Structural Basis of the Translational Elongation Cycle. *Annu. Rev. Biochem.* **82**, 203–236 (2013).

85. M. V. Rodnina, A. Savelsbergh, V. I. Katunin, W. Wintermeyer, Hydrolysis of GTP by elongation factor G drives tRNA movement on the ribosome. *Nature*. **385**, 37 (1997).

86. S. C. Blanchard, H. D. Kim, R. L. Gonzalez, J. D. Puglisi, S. Chu, tRNA dynamics on the ribosome during translation. *PNAS*. **101**, 12893–12898 (2004).

87. S. Dorner, J. L. Brunelle, D. Sharma, R. Green, The hybrid state of tRNA binding is an authentic translation elongation intermediate. *Nature Structural & Molecular Biology*. **13**, 234–241 (2006).

88. P. C. Spiegel, D. N. Ermolenko, H. F. Noller, Elongation factor G stabilizes the hybrid-state conformation of the 70S ribosome. *RNA* (2007), doi:10.1261/rna.601507.

89. J. B. Munro, R. B. Altman, C.-S. Tung, K. Y. Sanbonmatsu, S. C. Blanchard, A fast dynamic mode of the EF-G-bound ribosome. *The EMBO Journal*. **29**, 770–781 (2010).

90. M. R. Capecchi, Polypeptide chain termination in vitro: isolation of a release factor. *Proc Natl Acad Sci U S A*. **58**, 1144–1151 (1967).

91. C. T. Caskey, R. Tompkins, E. Scolnick, T. Caryk, M. Nirenberg, Sequential Translation of Trinucleotide Codons for the Initiation and Termination of Protein Synthesis. *Science*. **162**, 135–138 (1968).

92. E. Scolnick, R. Tompkins, T. Caskey, M. Nirenberg, Release factors differing in specificity for terminator codons. *Proc Natl Acad Sci U S A*. **61**, 768–774 (1968).

93. K. Ito, M. Uno, Y. Nakamura, A tripeptide 'anticodon' deciphers stop codons in messenger RNA. *Nature*. **403**, 680–684 (2000).

94. D. H. Shin, J. Brandsen, J. Jancarik, H. Yokota, R. Kim, S.-H. Kim, Structural Analyses of Peptide Release Factor 1 from Thermotoga maritima Reveal Domain Flexibility Required for Its Interaction with the Ribosome. *Journal of Molecular Biology*. **341**, 227–239 (2004).

95. B. Vestergaard, L. B. Van, G. R. Andersen, J. Nyborg, R. H. Buckingham, M. Kjeldgaard, Bacterial Polypeptide Release Factor RF2 Is Structurally Distinct from Eukaryotic eRF1. *Molecular Cell*. **8**, 1375–1382 (2001).

96. B. Vestergaard, S. Sanyal, M. Roessle, L. Mora, R. H. Buckingham, J. S. Kastrup, M. Gajhede, D. I. Svergun, M. Ehrenberg, The SAXS Solution Structure of RF1 Differs from Its Crystal Structure and Is Similar to Its Ribosome Bound Cryo-EM Structure. *Molecular Cell*. **20**, 929–938 (2005).

97. G. Zoldák, L. Redecke, D. I. Svergun, P. V. Konarev, C. S. Voertler, H. Dobbek, E. Sedlák, M. Sprinzl, Release Factors 2 from Escherichia coli and Thermus thermophilus: structural, spectroscopic and microcalorimetric studies. *Nucleic Acids Res*. **35**, 1343–1353 (2007).

98. B. P. Klaholz, T. Pape, A. V. Zavialov, A. G. Myasnikov, E. V. Orlova, B. Vestergaard, M. Ehrenberg, M. van Heel, Structure of the *Escherichia coli* ribosomal termination complex with release factor 2. *Nature*. **421**, 90–94 (2003).

99. U. B. S. Rawat, A. V. Zavialov, J. Sengupta, M. Valle, R. A. Grassucci, J. Linde, B. Vestergaard, M. Ehrenberg, J. Frank, A cryo-electron microscopic study of ribosome-bound termination factor RF2. *Nature*. **421**, 87–90 (2003).

100. S. Petry, D. E. Brodersen, F. V. Murphy IV, C. M. Dunham, M. Selmer, M. J. Tarry, A. C. Kelley, V. Ramakrishnan, Crystal structures of the ribosome in complex with release factors RF1 and RF2 bound to a cognate stop codon. *Cell*. **123**, 1255–1266 (2005).

101. H. Jin, A. C. Kelley, D. Loakes, V. Ramakrishnan, Structure of the 70S ribosome bound to release factor 2 and a substrate analog provides insights into catalysis of peptide release. *Proceedings of the National Academy of Sciences of the United States of America*. **107**, 8593–8598 (2010).

102. H. Jin, A. C. Kelley, V. Ramakrishnan, Crystal structure of the hybrid state of ribosome in complex with the guanosine triphosphatase release factor 3. *Proceedings of the National Academy of Sciences of the United States of America*. **108**, 15798–803 (2011).

103. J. Zhou, L. Lancaster, S. Trakhanov, H. F. Noller, Crystal structure of release factor RF3 trapped in the GTP state on a rotated conformation of the ribosome. *Rna*. **18**, 230–240 (2012).

104. A. V. Zavialov, V. V. Hauryliuk, M. Ehrenberg, Splitting of the Posttermination Ribosome into Subunits by the Concerted Action of RRF and EF-G. *Molecular Cell*. **18**, 675–686 (2005).

105. N. Gao, A. V. Zavialov, M. Ehrenberg, J. Frank, Specific Interaction between EF-G and RRF and Its Implication for GTP-Dependent Ribosome Splitting into Subunits. *Journal of Molecular Biology*. **374**, 1345–1358 (2007).

106. O. Mikuni, K. Ito, J. Moffat, K. Matsumura, K. McCaughan, T. Nobukuni, W. Tate, Y. Nakamura, Identification of the prfC gene, which encodes peptide-chain-release factor 3 of Escherichia coli. *PNAS*. **91**, 5798–5802 (1994).

107. G. Grentzmann, D. Brechemier-Baey, V. Heurgue, L. Mora, R. H. Buckingham, Localization and characterization of the gene encoding release factor RF3 in Escherichia coli. *PNAS*. **91**, 5848–5852 (1994).

108. M. Y. Pavlov, D. V. Freistroffer, J. MacDougall, R. H. Buckingham, M. Ehrenberg, Fast recycling of Escherichia coli ribosomes requires both ribosome recycling factor (RRF) and release factor RF3. *The EMBO Journal*. **16**, 4134–4141 (1997).

109. T. Aboa, K. Ueda, T. Sunohara, K. Ogawa, H. Aiba, SsrA-mediated protein tagging in the presence of miscoding drugs and its physiological role in Escherichia coli. *Genes to Cells*. **7**, 629–638 (2002).

110. K. Ueda, Y. Yamamoto, K. Ogawa, T. Abo, H. Inokuchi, H. Aiba, Bacterial SsrA system plays a role in coping with unwanted translational readthrough caused by suppressor tRNAs. *Genes to Cells*. **7**, 509–519 (2002).

111. X. Li, M. Yagi, T. Morita, H. Aiba, Cleavage of mRNAs and role of tmRNA system under amino acid starvation in Escherichia coli. *Molecular Microbiology*. **68**, 462–473 (2008).

112. F. Garza-Sánchez, J. G. Gin, C. S. Hayes, Amino Acid Starvation and Colicin D Treatment Induce A-site mRNA Cleavage in Escherichia coli. *Journal of Molecular Biology*. **378**, 505–519 (2008).

113. C. S. Hayes, B. Bose, R. T. Sauer, Stop codons preceded by rare arginine codons are efficient determinants of SsrA tagging in Escherichia coli. *PNAS*. **99**, 3440–3445 (2002).

114. T. Sunohara, T. Abo, T. Inada, H. Aiba, The C-terminal amino acid sequence of nascent peptide is a major determinant of SsrA tagging at all three stop codons. *RNA*. **8**, S1355838202020198 (2002).

115. T. Sunohara, K. Jojima, Y. Yamamoto, T. Inada, H. Aiba, Nascent-peptide-mediated ribosome stalling at a stop codon induces mRNA cleavage resulting in nonstop mRNA that is recognized by tmRNA. *RNA*. **10**, 378–386 (2004).

116. C. S. Hayes, R. T. Sauer, Cleavage of the A Site mRNA Codon during Ribosome Pausing Provides a Mechanism for Translational Quality Control. *Molecular Cell*. **12**, 903–911 (2003).

117. C. Neubauer, Y. Gao, K. R. Andersen, C. M. Dunham, A. C. Kelley, J. Hentschel, K. Gerdes, V. Ramakrishnan, D. E. Brodersen, The Structural Basis for mRNA Recognition and Cleavage by the Ribosome-Dependent Endonuclease RelE. *Cell*. **139**, 1084–1095 (2009).

118. B. D. Janssen, F. Garza-Sánchez, C. S. Hayes, YoeB toxin is activated during thermal stress. *MicrobiologyOpen*. **4**, 682–697 (2015).

119. N. S. Singh, U. Varshney, A physiological connection between tmRNA and peptidyl-tRNA hydrolase functions in Escherichia coli. *Nucleic Acids Research*. **32**, 6028–6037 (2004).

120. G. Das, U. Varshney, Peptidyl-tRNA hydrolase and its critical role in protein biosynthesis. *Microbiology*. **152**, 2191–2195 (2006).

121. P. Gueneau de Novoa, K. P. Williams, The tmRNA website: reductive evolution of tmRNA in plastids and other endosymbionts. *Nucleic Acids Res*. **32**, D104–D108 (2004).

122. K. Ito, Y. Chadani, K. Nakamori, S. Chiba, Y. Akiyama, T. Abo, Nascentome analysis uncovers futile protein synthesis in escherichia coli. *PLoS ONE*. **6**, e28413 (2011).

123. G.-W. Li, E. Oh, J. S. Weissman, The anti-Shine–Dalgarno sequence drives translational pausing and codon choice in bacteria. *Nature*. **484**, 538–541 (2012).

124. J. M. Schrader, B. Zhou, G.-W. Li, K. Lasker, W. S. Childers, B. Williams, T. Long, S. Crosson, H. H. McAdams, J. S. Weissman, L. Shapiro, The Coding and Noncoding Architecture of the Caulobacter crescentus Genome. *PLOS Genetics*. **10**, e1004463 (2014).

125. H. A. Feaga, P. H. Viollier, K. C. Keiler, Release of Nonstop Ribosomes Is Essential. *mBio*. **5**, e01916–14 (2014).

126. Y. Chadani, K. Ono, S. Ozawa, Y. Takahashi, K. Takai, H. Nanamiya, Y. Tozawa, K. Kutsukake, T. Abo, Ribosome rescue by Escherichia coli ArfA (YhdL) in the absence of trans-translation system. *Mol. Microbiol.* **78**, 796–808 (2010).

127. R. R. Traut, R. E. Monro, The puromycin reaction and its relation to protein synthesis. *Journal of Molecular Biology*. **10**, 63–72 (1964).

128. M. E. Azzam, I. D. Algranati, Mechanism of Puromycin Action: Fate of Ribosomes after Release of Nascent Protein Chains from Polysomes. *PNAS*. **70**, 3866–3869 (1973).

129. H. Muto, K. Ito, Peptidyl-prolyl-tRNA at the ribosomal P-site reacts poorly with puromycin. *Biochemical and Biophysical Research Communications*. **366**, 1043–1047 (2008).

130. H. Himeno, Novel factor rescues ribosomes trapped on non-stop mRNAs. *Molecular Microbiology*. **78**, 789–791 (2010).

131. L. Y. Frolova, R. Y. Tsivkovskii, G. F. Sivolobova, N. Y. Oparina, O. I. Serpinsky, V. M. Blinov, S. I. Tatkov, L. L. Kisselev, Mutations in the highly conserved GGQ motif of class 1 polypeptide release factors abolish ability of human eRF1 to trigger peptidyl-tRNA hydrolysis. *RNA*. **5**, 1014–1020 (1999).

132. D.-J. G. Scarlett, K. K. McCaughan, D. N. Wilson, W. P. Tate, Mapping Functionally Important Motifs Spf and Ggq of the Decoding Release Factor Rf2 to the Escherichia Coli Ribosome by Hydroxyl Radical Footprinting Implications for Macromolecular Mimicry and Structural Changes in Rf2. *J. Biol. Chem.* **278**, 15095–15104 (2003).

133. M. Laurberg, H. Asahara, A. Korostelev, J. Zhu, S. Trakhanov, H. F. Noller, Structural basis for translation termination on the 70S ribosome. *Nature*. **454**, 852–857 (2008).

134. Y. Shimizu, ArfA recruits RF2 into stalled ribosomes. *Journal of Molecular Biology*. **423**, 624–631 (2012).

135. D. Kurita, Y. Chadani, A. Muto, T. Abo, H. Himeno, ArfA recognizes the lack of mRNA in the mRNA channel after RF2 binding for ribosome rescue. *Nucleic acids research*. **42**, 13339–52 (2014).

136. N. R. James, A. Brown, Y. Gordiyenko, V. Ramakrishnan, Translational termination without a stop codon. *Science*. **354**, 1437–1440 (2016).

137. C. Ma, D. Kurita, N. Li, Y. Chen, H. Himeno, N. Gao, Mechanistic insights into the alternative translation termination by ArfA and RF2. *Nature*. **541**, 550–553 (2016).

138. F. Zeng, Y. Chen, J. Remis, M. Shekhar, J. C. Phillips, E. Tajkhorshid, H. Jin, Structural basis of co-translational quality control by ArfA and RF2 bound to ribosome. *Nature*. **541**, 554–557 (2017).

139. G. Demo, E. Svidritskiy, R. Madireddy, R. Diaz-Avalos, T. Grant, N. Grigorieff, D. Sousa, A. A. Korostelev, Mechanism of ribosome rescue by ArfA and RF2. *eLife*. **6**, e23687 (2017).

140. P. Huter, C. Müller, B. Beckert, S. Arenz, O. Berninghausen, R. Beckmann, D. N. Wilson, Structural basis for ArfA–RF2-mediated translation termination on mRNAs lacking stop codons. *Nature*. **541**, 546–549 (2017).

141. Y. Chadani, K. Ono, K. Kutsukake, T. Abo, Escherichia coli YaeJ protein mediates a novel ribosome-rescue pathway distinct from SsrA- and ArfA-mediated pathways. *Mol. Microbiol.* **80**, 772–785 (2011).

142. T. Baba, T. Ara, M. Hasegawa, Y. Takai, Y. Okumura, M. Baba, K. A. Datsenko, M. Tomita, B. L. Wanner, H. Mori, *Molecular systems biology*, in press, doi:10.1038/msb4100050.

143. M. G. Gagnon, S. V. Seetharaman, D. Bulkley, T. a. Steitz, Structural Basis for the Rescue of Stalled Ribosomes: Structure of YaeJ Bound to the Ribosome. *Science*. **335**, 1370–1372 (2012).

144. Y. Handa, N. Inaho, N. Nameki, YaeJ is a novel ribosome-associated protein in Escherichia coli that can hydrolyze peptidyl–tRNA on stalled ribosomes. *Nucleic Acids Res*. **39**, 1739–1748 (2011).

145. S. Y. Lee, S. C. Bailey, D. Apirion, Small stable RNAs from Escherichia coli: evidence for the existence of new molecules and for a new ribonucleoprotein particle containing 6S RNA. *Journal of Bacteriology*. **133**, 1015–1023 (1978).

146. S. K. Jain, M. Gurevitz, D. Apirion, A Small RNA That Complements Mutants in the RNA Processing Enzyme Ribonuclease P. *Journal of Molecular Biology*. **162**, 515–533 (1982).

147. A. K. Chauhan, D. Apirion, The gene for a small stable RNA (10Sa RNA) of Escherichia coli. *Molecular Microbiology*. **3**, 1481–1485 (1989).

148. J. S. Tyagi, A. K. Kinger, Identification of the 10Sa RNA structural gene of Mycobacterium tuberculosis. *Nucleic Acids Research*. **20**, 138 (1991).

149. C. Ushida, H. Himeno, T. Watanabe, A. Muto, tRNA-like structures in 10Sa RNAs of Mycoplasma capricolum and Bacillus subtilis. *Nucleic Acids Research*. **22**, 3392–3396 (1994).

150. C. Zwieb, N. Larsen, J. Wower, The tmRNA database (tmRDB). *Nucleic Acids Research*. **26**, 166–167 (1998).

151. B.-K. Oh, D. Apirion, 10Sa RNA, a small stable RNA of Escherichia coli, is functional. *Molec. Gen. Genet.* **229**, 52–56 (1991).

152. J. E. Trempy, J. E. Kirby, S. Gotflesman, Alp Suppression of Lon : Dependence on the slpA Gene. *Journal of Bacteriology*. **176**, 2061–2067 (1994).

153. Y. Komine, M. Kitabatake, T. Yokogawa, K. Nishikawa, H. Inokuchi, A tRNA-like structure is present in 10Sa RNA, a small stable RNA from Escherichia coli. *Proc. Natl Acad. Sci. USA*. **91**, 9223–9227 (1994).

154. Y. Komine, M. Kitabatake, H. Inokuchi, 10Sa RNA Is Associated with 70S Ribosome Particles in Escherichia coli. *Journal of Biochemistry*. **119**, 463–467 (1996).

155. T. Tadaki, M. Fukushima, C. Ushida, H. Himeno, A. Muto, Interaction of 10Sa RNA with ribosomes in Escherichia coli. *FEBS Letters*. **399**, 223–226 (1996).

156. K. C. Keiler, P. R. Waller, R. T. Sauer, Role of a peptide tagging system in degradation of proteins synthesized from damaged messenger RNA. *Science*. **271**, 990–993 (1996).

157. A. Miczak, A. K. Chauhan, D. Apirion, Two new genes located between 2758 and 2761 kilobase pairs on the Escherichia coli genome. *Journal of Bacteriology*. **173**, 3271–3272 (1991).

158. A. W. Karzai, M. M. Susskind, R. T. Sauer, SmpB, a unique RNA-binding protein essential for the peptide-tagging activity of SsrA (tmRNA). *EMBO J.* **18**, 3793–3799 (1999).

159. K. C. Keiler, L. Shapiro, K. P. Williams, tmRNAs that encode proteolysis-inducing tags are found in all known bacterial genomes: A two-piece tmRNA functions in Caulobacter. *Proceedings of the National Academy of Sciences of the United States of America*. **97**, 7778–7783 (2000).

160. M. N. Subbarao, D. Apirion, A precursor for a small stable RNA (10Sa RNA) of Escherichia coli. *Molecular Genetics and Genomics*. **217**, 499–504 (1989).

161. S. Lin-Chao, C. L. Wei, Y. T. Lin, RNase E is required for the maturation of ssrA RNA and normal ssrA RNA peptide-tagging activity. *Proceedings of the National Academy of Sciences of the United States of America*. **96**, 12406–12411 (1999).

162. Z. Li, S. Pandit, M. P. Deutscher, 3′ Exoribonucleolytic trimming is a common feature of the maturation of small, stable RNAs in Escherichia coli. *PNAS*. **95**, 2856–2861 (1998).

163. E. Ranaei-siadat, C. Fabret, B. Seijo, F. Dardel, H. Grosjean, S. Nonin-lecomte, RNA-methyltransferase TrmA is a dual-specific enzyme responsible for C5-methylation of uridine in both tmRNA and tRNA. *RNA Biology*. **10**, 582–578 (2013).

164. B. Felden, K. Hanawa, J. F. Atkins, H. Himeno, A. Muto, R. F. Gesteland, J. A. McCloskey, P. F. Crain, Presence and location of modified nucleotides in Escherichia coli tmRNA: structural mimicry with tRNA acceptor branches. *EMBO Journal*. **17**, 3188–3196 (1998).

165. B. Felden, H. Himeno, A. Muto, J. P. McCutcheon, J. F. Atkins, R. F. Gesteland, Probing the structure of the Escherichia coli 10Sa RNA (tmRNA). *RNA*. **3**, 89–103 (1997).

166. K. P. Williams, D. P. Bartel, Phylogenetic analysis of tmRNA secondary structure. *RNA*. **2**, 1306–1310 (1996).

167. Y. Bessho, R. Shibata, S. Sekine, K. Murayama, K. Higashijima, C. Hori-Takemoto, M. Shirouzu, S. Kuramitsu, S. Yokoyama, Structural basis for functional mimicry of long-variable-arm tRNA by transfer-messenger RNA. *PNAS*. **104**, 8293–8298 (2007).

168. F. Weis, P. Bron, E. Giudice, J.-P. Rolland, D. Thomas, B. Felden, R. Gillet, tmRNA–SmpB: a journey to the centre of the bacterial ribosome. *EMBO J*. **29**, 3810–3818 (2010).

169. N. Nameki, T. Tadaki, H. Himeno, A. Muto, Three of four pseudoknots in tmRNA are interchangeable and are substitutable with single-stranded RNAs. *FEBS Letters*. **470**, 345–349 (2000).

170. K. P. Williams, Integration sites for genetic elements in prokaryotic tRNA and tmRNA genes: sublocation preference of integrase subfamilies. *Nucleic acids research*. **30**, 866–75 (2002).

171. C. Gaudin, X. Zhou, K. P. Williams, B. Felden, Two-piece tmRNA in cyanobacteria and its structural analysis. *Nucleic Acids Research*. **30**, 2018–2024 (2002).

172. S. M. Sharkady, K. P. Williams, A third lineage with two-piece tmRNA. *Nucleic Acids Res.* **32**, 1–8 (2004).

173. Y. Shimizu, T. Ueda, The role of SmpB protein in trans-translation. *FEBS Letters*. **514**, 74–77 (2002).

174. K. Takada, C. Takemoto, M. Kawazoe, T. Konno, K. Hanawa-suetsugu, S. Lee, M. Shirouzu, S. Yokoyama, A. Muto, H. Himeno, In vitro trans-translation of Thermus thermophilus: Ribosomal protein S1 is not required for the early stage of trans-translation. *RNA*. **13**, 503–510 (2007).

175. D. Kurita, A. Muto, H. Himeno, Chapter 20 In Vitro Trans-Translation Assays. *Methods in Molecular Biology*. **905**, 311–325 (2012).

176. S. Barends, a W. Karzai, R. T. Sauer, J. Wower, B. Kraal, Simultaneous and functional binding of SmpB and EF-Tu-GTP to the alanyl acceptor arm of tmRNA. *Journal of molecular biology*. **314**, 9–21 (2001).

177. N. Nameki, H. Takaku, H. Himeno, A. Muto, G. Kawai, Interaction Analysis between tmRNA and SmpB from Thermus thermophilus. *J. Biochem.* **138**, 729–739 (2005).

178. N. Ivanova, M. Lindell, M. Pavlov, L. Holmberg Schiavone, E. G. H. Wagner, M. Ehrenberg, Structure probing of tmRNA in distinct stages of trans-translation. *RNA (New York, N.Y.)*. **13**, 713–722 (2007).

179. E. Ranaei-siadat, C. Mérigoux, B. Seijo, L. Ponchon, J. Saliou, J. Bernauer, S. Sanglier-Cianferani, F. Dardel, P. Vachette, S. Nonin-Lecomte, In vivo tmRNA protection by SmpB and pre-ribosome binding conformation in solution. *RNA*. **20**, 1607–1620 (2014).

180. G. Dong, J. Nowakowski, D. W. Hoffman, Structure of small protein B: the protein component of the tmRNA-SmpB system for ribosome rescue. *EMBO Journal*. **21**, 1845–1854 (2002).

181. T. Someya, N. Nameki, H. Hosoi, S. Suzuki, H. Hatanaka, M. Fujii, T. Terada, M. Shirouzu, Y. Inoue, T. Shibata, S. Kuramitsu, S. Yokoyama, G. Kawai, T. L. James, Solution structure of a tmRNA-binding protein, SmpB, from Thermus thermophilus. *FEBS Letters*. **535**, 94–100 (2003).

182. S. Gutmann, P. W. Haebel, L. Metzinger, M. Sutter, B. Felden, N. Ban, Crystal structure of the transfer-RNA domain of transfer-messenger RNA in complex with SmpB. *Nature*. **424**, 699–703 (2003).

183. M. Hallier, J. Desreac, B. Felden, Small protein B interacts with the large and the small subunits of a stalled ribosome during trans-translation. *Nucleic Acids Research*. **34**, 1935–1943 (2006).

184. T. Wiegert, W. Schumann, SsrA-Mediated Tagging in Bacillus subtilis. *Journal of Bacteriology*. **183**, 3885–3889 (2001).

185. Y.-M. Hou, P. Schimmel, A simple structural feature is a major determinant of the identity of a transfer RNA. *Nature*. **333**, 140–145 (1988).

186. K. Hanawa-Suetsugu, M. Takagi, H. Inokuchi, H. Himeno, A. Muto, SmpB functions in various steps of trans-translation. *Nucleic acids research*. **30**, 1620–1629 (2002).

187. J. Rudinger-Thirion, R. Giegé, B. Felden, Aminoacylated tmRNA from Escherichia coli interacts with prokaryotic elongation factor Tu. *RNA*. **5**, 989–992 (1999).

188. S. Barends, J. Wower, B. Kraal, Kinetic Parameters for tmRNA Binding to Alanyl-tRNA Synthetase and Elongation Factor Tu from Escherichia coli. *Biochemistry*. **39**, 2652–2658 (2000).

189. M. Valle, R. Gillet, S. Kaur, A. Henne, V. Ramakrishnan, J. Frank, Visualizing tmRNA entry into a stalled ribosome. *Science*. **300**, 127–130 (2003).

190. C. Neubauer, R. Gillet, A. C. Kelley, V. Ramakrishnan, Decoding in the absence of a codon by tmRNA and SmpB in the Ribosome. *Science*. **335**, 1366–1369 (2012).

191. M. Valle, R. Gillet, S. Kaur, A. Henne, V. Ramakrishnan, J. Frank, Visualizing tmRNA entry into a stalled ribosome. *Science*. **300**, 127–130 (2003).

192. Y. Jacob, S. M. Sharkady, K. Bhardwaj, a. Sanda, K. P. Williams, Function of the SmpB Tail in Transfer-messenger RNA Translation Revealed by a Nucleus-encoded Form. *Journal of Biological Chemistry*. **280**, 5503–5509 (2005).

193. T. R. Sundermeier, D. P. Dulebohn, H. J. Cho, A. W. Karzai, A previously uncharacterized role for small protein B (SmpB) in transfer messenger RNA-mediated trans-translation. *Proc. Natl Acad. Sci. USA*. **102**, 2316–2321 (2005).

194. Y. Shimizu, T. Ueda, SmpB Triggers GTP Hydrolysis of Elongation Factor Tu on Ribosomes by Compensating for the Lack of Codon-Anticodon Interaction during Trans-translation Initiation. *Journal of Biological Chemistry*. **281**, 15987–15996 (2006).

195. M. R. Miller, Z. H. U. Liu, D. J. Cazier, G. M. Gebhard, S. R. Herron, H. S. Zaher, R. Green, A. R. Buskirk, The role of SmpB and the ribosomal decoding center in licensing tmRNA entry into stalled ribosomes. *RNA*. **17**, 1727–1736 (2011).

196. D. Kurita, A. Muto, H. Himeno, Role of the C-terminal tail of SmpB in the early stage of trans-translation. *RNA*. **16**, 980–990 (2010).

197. M. R. Miller, Z. H. U. Liu, D. J. Cazier, G. M. Gebhard, S. R. Herron, H. S. Zaher, R. Green, A. R. Buskirk, The role of SmpB and the ribosomal decoding center in licensing tmRNA entry into stalled ribosomes. *RNA*. **17**, 1727–1736 (2011).

198. F. Weis, P. Bron, J.-P. Rolland, D. Thomas, B. Felden, R. Gillet, Accommodation of tmRNA-SmpB into stalled ribosomes: a cryo-EM study. *RNA (New York, N.Y.)*. **16**, 299–306 (2010).

199. K. Cheng, N. Ivanova, S. H. W. Scheres, M. Y. Pavlov, J. M. Carazo, H. Hebert, M. Ehrenberg, M. Lindahl, tmRNA·SmpB complex mimics native aminoacyl-tRNAs in the A site of stalled ribosomes. *Journal of Structural Biology*. **169**, 342–348 (2009).

200. D. J. F. Ramrath, H. Yamamoto, K. Rother, D. Wittek, M. Pech, T. Mielke, J. Loerke, P. Scheerer, P. Ivanov, Y. Teraoka, O. Shpanchenko, K. H. Nierhaus, C. M. T. Spahn, The complex of tmRNA–SmpB and EF-G on translocating ribosomes. *Nature*. **485**, 526–529 (2012).

201. N. Ivanova, M. Y. Pavlov, M. Ehrenberg, tmRNA-induced Release of Messenger RNA from Stalled Ribosomes. *Journal of Molecular Biology*. **350**, 897–905 (2005).

202. A. W. Karzai, R. T. Sauer, Protein factors associated with the SsrA-SmpB tagging and ribosome rescue complex. *Proceedings of the National Academy of Sciences of the United States of America*. **98**, 3040–3044 (2001).

203. Z.-F. Cheng, M. P. Deutscher, Purification and Characterization of the Escherichia Coli Exoribonuclease Rnase R Comparison with Rnase II. *J. Biol. Chem.* **277**, 21624–21629 (2002).

204. R. G. Matos, C. Bárria, R. N. Moreira, S. Barahona, S. Domingues, C. M. Arraiano, The importance of proteins of the RNase II/RNB-family in pathogenic bacteria. *Frontiers in microbiology*. **4**, 1–4 (2014).

205. J. Richards, P. Mehta, A. W. Karzai, RNase R degrades non-stop mRNAs selectively in an SmpB-tmRNA-dependent manner. *Molecular Microbiology*. **62**, 1700–1712 (2006).

206. R. N. Moreira, S. Domingues, S. C. Viegas, M. Amblar, C. M. Arraiano, Synergies between RNA degradation and trans-translation in Streptococcus pneumoniae: cross regulation and co-transcription of RNase R and SmpB. *BMC Microbiology*. **12** (2012).

207. Y. Yamamoto, T. Sunohara, K. Jojima, T. Inada, H. Aiba, SsrA-mediated trans-translation plays a role in mRNA quality control by facilitating degradation of truncated mRNAs. *RNA*. **9**, 408–418 (2003).

208. D. R. Tanner, J. D. Dewey, M. R. Miller, A. R. Buskirk, Genetic analysis of the structure and function of transfer messenger RNA pseudoknot 1. *Journal of Biological Chemistry*. **281**, 10561–10566 (2006).

209. I. K. Wower, C. Zwieb, J. Wower, Escherichia coli tmRNA lacking pseudoknot 1 tags truncated proteins in vivo and in vitro. *RNA*. **15**, 128–137 (2009).

210. K. P. Williams, K. A. Martindale, D. P. Bartel, Resuming translation on tmRNA : a unique mode of determining a reading frame. **18**, 5423–5433 (1999).

211. S. Lee, M. Ishii, T. Tadaki, A. Muto, H. Himeno, Determinants on tmRNA for initiating efficient and precise trans-translation: some mutations upstream of the tag-encoding sequence of Escherichia coli tmRNA shift the initiation point of trans-translation in vitro. *RNA*. **7**, 999–1012 (2001).

212. T. Watts, D. Cazier, D. Healey, A. Buskirk, SmpB Contributes to Reading Frame Selection in the Translation of Transfer–Messenger RNA. *Journal of Molecular Biology*. **391**, 275–281 (2009).

213. T. Konno, D. Kurita, K. Takada, A. Muto, H. Himeno, A functional interaction of SmpB with tmRNA for determination of the resuming point of trans -translation. *RNA*. **13**, 1723–1731 (2007).

214. S. Gottesman, E. Roche, Y. Zhou, R. T. Sauer, The ClpXP and ClpAP proteases degrade proteins with carboxy-terminal peptide tails added by the SsrA-tagging system. *Genes and Development*. **12**, 1338–1347 (1998).

215. C. Herman, D. Thévenet, P. Bouloc, G. C. Walker, R. D'Ari, Degradation of carboxy-terminal-tagged cytoplasmic proteins by the Escherichia coli protease HflB (FtsH). *Genes and Development*. **12**, 1348–1355 (1998).

216. J. M. Flynn, I. Levchenko, M. Seidel, S. H. Wickner, R. T. Sauer, T. A. Baker, Overlapping recognition determinants within the ssrA degradation tag allow modulation of proteolysis. *Proceedings of the National Academy of Sciences of the United States of America*. **98**, 10584–10589 (2001).

217. D. Dulebohn, J. Choy, T. Sundermeier, N. Okan, A. W. Karzai, *Trans-translation: The tmRNA-mediated surveillance mechanism for ribosome rescue, directed protein degradation, and nonstop mRNA decay* (2007), vol. 46 of *Biochemistry*.

218. B. Janssen, C. Hayes, The tmRNA ribosome rescue system. *Advances in protein chemistry and structural biology*. **86**, 151–191 (2012).

219. I. Levchenko, M. Seidel, R. T. Sauer, T. A. Baker, A Specificity-Enhancing Factor for the ClpXP Degradation Machine. *Science*. **289**, 2354–2356 (2000).

220. D. M. Retallack, D. I. Friedman, A role for a small stable RNA in modulating the activity of DNA-binding proteins. *Cell Press*. **83**, 227–235 (1995).

221. K. C. Keiler, Biology of trans-Translation. *Annual Review Microbiology*. **62**, 133–151 (2008).

222. A. Muto, A. Fujihara, K. Ito, J. Matsuno, C. Ushida, H. Himeno, Requirement of transfer-messenger RNA for the growth of Bacillus subtilis under stresses. *Genes to Cells*. **5**, 627–635 (2000).

223. Y. Komine, M. Kitabatake, T. Yokogawa, K. Nishikawa, H. Inokuchi, A tRNA-like structure is present in 10Sa RNA, a small stable RNA from Escherichia coli. *Proceedings of the National Academy of Sciences of the United States of America*. **91**, 9223–7 (1994).

224. W. H. McClain, K. Foss, Changing the identity of a tRNA by introducing a G-U wobble pair near the 3' acceptor end. *Science*. **240**, 793–796 (1988).

225. C. Francklyn, K. Musier-Forsyth, P. Schimmel, Small RNA helices as substrates for aminoacylation and their relationship to charging of transfer RNAs. *European Journal of Biochemistry*. **206**, 315–321 (1992).

226. C. Francklyn, P. Schimmel, Aminoacylation of RNA minihelices with alanine. *Nature*. **337**, 478–481 (1989).

227. M. E. Saks, Sampson, J. N. Abelson, The transfer RNA identity problem: a search for rules. *Science*. **263**, 191–197 (1994).

228. S. Barends, J. Wower, B. Kraal, Kinetic Parameters for tmRNA Binding to Alanyl-tRNA Synthetase and Elongation Factor Tu from Escherichia coli. *Biochemistry*. **39**, 2652–2658 (2000).

229. C. Neubauer, R. Gillet, A. C. Kelley, V. Ramakrishnan, Decoding in the absence of a codon by tmRNA and SmpB in the Ribosome. *Science*. **335**, 1366–1369 (2012).

230. T. M. Schmeing, The Crystal Structure of the Ribosome Bound to EF-Tu and Aminoaacyl-tRNA. **688**, 688–695 (2010).

231. H. Wolf, G. Chinali, A. Parmeggiani, Mechanism of the Inhibition of Protein Synthesis by Kirromycin. *European Journal of Biochemistry*. **75**, 67–75 (1977).

232. N. Ivanova, M. Y. Pavlov, B. Felden, M. Ehrenberg, Ribosome rescue by tmRNA requires truncated mRNAs. *J. Mol. Biol.* **338**, 33–41 (2004).

233. D. Kurita, M. R. Miller, A. Muto, A. R. Buskirk, H. Himeno, Rejection of tmRNA·SmpB after GTP hydrolysis by EF-Tu on ribosomes stalled on intact mRNA. *RNA (New York, N.Y.)*. **20**, 1706–1714 (2014).

234. K. Takada, C. Takemoto, M. Kawazoe, T. Konno, K. Hanawa-suetsugu, S. Lee, M. Shirouzu, S. Yokoyama, A. Muto, H. Himeno, In vitro trans -translation of Thermus thermophilus : Ribosomal protein S1 is not required for the early stage of trans -translation, 503–510 (2007).

235. S. E. Walker, K. Fredrick, Preparation and evaluation of acylated tRNAs. *Methods*. **44**, 81–86 (2008).

236. R. Jünemann, J. Wadzack, F. J. Triana-Alonso, J. U. Bittner, J. Caillet, T. Meinnel, K. Vanatalu, K. H. Nierhaus, In vivo deuteration of transfer RNAs: overexpression and large-scale purification of deuterated specific tRNAs. *Nucleic acids research*. **24**, 907–13 (1996).

237. E. Schmitt, M. Panvert, S. Blanquet, Y. Mechulam, Crystal structure of methionyl-tRNAfMet transformylase complexed with the initiator formyl-methionyl-tRNAfMet. *EMBO J.* **17**, 6819–26 (1998).

238. M. R. Miller, A. R. Buskirk, An unusual mechanism for EF-Tu activation during tmRNA-mediated ribosome rescue. *RNA*. **20**, 228–235 (2014).

239. S. Nonin-Lecomte, N. Germain-Amiot, R. Gillet, M. Hallier, L. Ponchon, F. Dardel, B. Felden, Ribosome hijacking: a role for small protein B during trans-translation. *EMBO Rep.* **10**, 160–165 (2009).

240. N. Fischer, P. Neumann, L. V. Bock, C. Maracci, Z. Wang, A. Paleskava, A. L. Konevega, G. F. Schröder, H. Grubmüller, R. Ficner, M. V. Rodnina, H. Stark, The pathway to GTPase activation of elongation factor SelB on the ribosome. *Nature*. **540**, 80–85 (2016).

241. Y. Zhang, S. Hong, A. Ruangprasert, G. Skiniotis, C. M. Dunham, Alternative Mode of E-Site tRNA Binding in the Presence of a Downstream mRNA Stem Loop at the Entrance Channel. *Structure*. **26**, 437-445.e3 (2018).

242. G. Z. Yusupova, M. M. Yusupov, J. H. D. Cate, H. F. Noller, The Path of Messenger RNA through the Ribosome. *Cell*. **106**, 233–241 (2001).

243. Y. Shimizu, a Inoue, Y. Tomari, T. Suzuki, T. Yokogawa, K. Nishikawa, T. Ueda, Cell-free translation reconstituted with purified components. *Nature biotechnology*. **19**, 751–5 (2001).

244. R. Fernandez-Leiro, S. Scheres, A pipeline approach to single-particle processing in RELION. *bioRxiv*, 078352 (2016).

245. X. Li, P. Mooney, S. Zheng, C. R. Booth, M. B. Braunfeld, S. Gubbens, D. A. Agard, Y. Cheng, Electron counting and beam-induced motion correction enable near-atomic-resolution single-particle cryo-EM. *Nat Methods*. **10**, 584–590 (2013).

246. K. Zhang, Gctf: Real-time CTF determination and correction. *J. Struct. Biol.* **193**, 1–12 (2016).

247. S. H. W. Scheres, Semi-automated selection of cryo-EM particles in RELION-1.3. *J. Struct. Biol.* **189**, 114–122 (2015).

248. E. F. Pettersen, T. D. Goddard, C. C. Huang, G. S. Couch, D. M. Greenblatt, E. C. Meng, T. E. Ferrin, UCSF Chimera—A visualization system for exploratory research and analysis. *J Comput Chem.* **25**, 1605–1612 (2004).

249. P. Emsley, B. Lohkamp, W. G. Scott, K. Cowtan, Features and development of Coot. *Acta Crystallogr D*. **66**, 486–501 (2010).

250. A. Brown, F. Long, R. A. Nicholls, J. Toots, P. Emsley, G. Murshudov, Tools for macromolecular model building and refinement into electron cryo-microscopy reconstructions. *Acta Crystallogr D*. **71**, 136–153 (2015).

251. W. L. Delano, The PyMOL Molecular Graphics System. *http://www.pymol.org* (2002) (available at https://ci.nii.ac.jp/naid/10020095229/).

252. P. D. Adams, P. V. Afonine, G. Bunkóczi, V. B. Chen, I. W. Davis, N. Echols, J. J. Headd, L.-W. Hung, G. J. Kapral, R. W. Grosse-Kunstleve, A. J. McCoy, N. W. Moriarty, R. Oeffner, R. J. Read, D. C. Richardson, J. S. Richardson, T. C. Terwilliger, P. H. Zwart, PHENIX: a comprehensive Python-based system for macromolecular structure solution. *Acta Crystallogr D*. **66**, 213–221 (2010).

253. V. B. Chen, W. B. Arendall, J. J. Headd, D. A. Keedy, R. M. Immormino, G. J. Kapral, L. W. Murray, J. S. Richardson, D. C. Richardson, MolProbity: all-atom structure validation for macromolecular crystallography. *Acta Crystallogr D*. **66**, 12–21 (2010).

254. P. V. Cornish, D. N. Ermolenko, H. F. Noller, T. Ha, Spontaneous Intersubunit Rotation in Single Ribosomes. *Molecular Cell*. **30**, 578–588 (2008).

255. T. M. Schmeing, P. B. Moore, T. A. Steitz, Structures of deacylated tRNA mimics bound to the E site of the large ribosomal subunit. *RNA*. **9**, 1345–1352 (2003).

256. A. Savelsbergh, V. I. Katunin, D. Mohr, F. Peske, M. V. Rodnina, W. Wintermeyer, An Elongation Factor G-Induced Ribosome Rearrangement Precedes tRNA-mRNA Translocation. *Molecular Cell*. **11**, 1517–1523 (2003).

257. D. N. Ermolenko, H. F. Noller, mRNA translocation occurs during the second step of ribosomal intersubunit rotation. *Nature Structural & Molecular Biology*. **18**, 457–462 (2011).

258. S. M. Studer, J. S. Feinberg, S. Joseph, Rapid Kinetic Analysis of EF-G-dependent mRNA Translocation in the Ribosome. *Journal of Molecular Biology*. **327**, 369–381 (2003).

259. D. J. F. Ramrath, H. Yamamoto, K. Rother, D. Wittek, M. Pech, T. Mielke, J. Loerke, P. Scheerer, P. Ivanov, Y. Teraoka, O. Shpanchenko, K. H. Nierhaus, C. M. T. Spahn, The complex of tmRNA–SmpB and EF-G on translocating ribosomes. *Nature*. **485**, 526–529 (2012).

260. Y. Gao, M. Selmer, C. M. Dunham, A. Weixlbaumer, A. C. Kelley, The structure of the ribosome with elongation factor G trapped in the post-translocational state. *Science*. **326**, 694–699 (2009).

261. K. Cheng, N. Ivanova, S. H. W. Scheres, M. Y. Pavlov, J. M. Carazo, H. Hebert, M. ans Ehrenberg, M. Lindahl, tmRNA·SmpB complex mimics native aminoacyl-tRNAs in the A site of stalled ribosomes. *Journal of Structural Biology*. **169**, 342–348 (2009).

262. Y. Shimizu, T. Ueda, in *PURE Technology*, Y. Endo, K. Takai, T. Ueda, Eds. (Humana Press, Totowa, NJ, 2010; https://doi.org/10.1007/978-1-60327-331-2_2), *Methods Mol Biol*, pp. 11–21.

263. J. R. Peacock, R. R. Walvoord, A. Y. Chang, M. C. Kozlowski, H. Gamper, Y.-M. Hou, Amino acid-dependent stability of the acyl linkage in aminoacyl-tRNA. *RNA*. **20**, 758–764 (2014).

264. K. Venkataraman, H. Zafar, A. W. Karzai, Distinct tmRNA sequence elements facilitate RNase R engagement on rescued ribosomes for selective nonstop mRNA decay. *Nucleic Acids Res.* **42**, 11192–11202 (2014).

265. D. Camenares, D. P. Dulebohn, A. Svetlanov, A. W. Karzai, Active and Accurate trans-Translation Requires Distinct Determinants in the C-terminal Tail of SmpB Protein and the mRNA-like Domain of Transfer Messenger RNA (tmRNA). *Journal of Biological Chemistry*. **288**, 30527–30542 (2013).

266. C. M. Hudson, B. Y. Lau, K. P. Williams, Ends of the line for tmRNA-SmpB. *Front. Microbiol.* **5**, 1–9 (2014).

267. X. Bai, E. Rajendra, G. Yang, Y. Shi, S. H. Scheres, Sampling the conformational space of the catalytic subunit of human γ-secretase. *eLife*. **4** (2015), doi:10.7554/eLife.11182.

268. K. L. Triman, in *Advances in Genetics* (Academic Press, 2007; http://www.sciencedirect.com/science/article/pii/S0065266006580046), vol. 58, pp. 89–119.

269. K. L. Triman, A. Peister, R. A. Goel, Expanded Versions of the 16S and 23S Ribosomal RNA Mutation Databases (16SMDBexp and 23SMDBexp). *Nucleic Acids Res*. **26**, 280–284 (1998).

270. O. Rackham, J. W. Chin, A network of orthogonal ribosome·mRNA pairs. *Nature Chemical Biology*. **1**, 159–166 (2005).

271. L. Gold, Posttranscriptional Regulatory Mechanisms in Escherichia Coli. *Annual Review of Biochemistry*. **57**, 199–233 (1988).

272. H. Chen, M. Bjerknes, R. Kumar, E. Jay, Determination of the optimal aligned spacing between the Shine – Dalgarno sequence and the translation initiation codon of Escherichia coli m RNAs. *Nucleic Acids Res*. **22**, 4953–4957 (1994).

273. L. Wang, A. Brock, B. Herberich, P. G. Schultz, Expanding the Genetic Code of Escherichia coli. *Science*. **292**, 498–500 (2001).

274. J. W. Chin, T. A. Cropp, J. C. Anderson, M. Mukherji, Z. Zhang, P. G. Schultz, An Expanded Eukaryotic Genetic Code. *Science*. **301**, 964–967 (2003).

275. K. Sakamoto, A. Hayashi, A. Sakamoto, D. Kiga, H. Nakayama, A. Soma, T. Kobayashi, M. Kitabatake, K. Takio, K. Saito, M. Shirouzu, I. Hirao, S. Yokoyama, Site-specific incorporation of an unnatural amino acid into proteins in mammalian cells. *Nucleic Acids Res*. **30**, 4692–4699 (2002).

276. R. Furter, Expansion of the genetic code: Site-directed p-fluoro-phenylalanine incorporation in Escherichia coli. *Protein Science*. **7**, 419–426 (1998).

277. K. Wang, H. Neumann, S. Y. Peak-Chew, J. W. Chin, Evolved orthogonal ribosomes enhance the efficiency of synthetic genetic code expansion. *Nature Biotechnology*. **25**, 770–777 (2007).

278. H. Neumann, K. Wang, L. Davis, M. Garcia-Alai, J. W. Chin, Encoding multiple unnatural amino acids via evolution of a quadruplet-decoding ribosome. *Nature*. **464**, 441–444 (2010).

279. K. Wang, A. Sachdeva, D. J. Cox, N. M. Wilf, K. Lang, S. Wallace, R. A. Mehl, J. W. Chin, Optimized orthogonal translation of unnatural amino acids enables spontaneous protein double-labelling and FRET. *Nature Chemistry*. **6**, 393–403 (2014).

280. S. D. Fried, W. H. Schmied, C. Uttamapinant, J. W. Chin, Ribosome Subunit Stapling for Orthogonal Translation in E. coli. *Angewandte Chemie International Edition*. **54**, 12791–12794 (2015).

281. C. Orelle, E. D. Carlson, T. Szal, T. Florin, M. C. Jewett, A. S. Mankin, Protein synthesis by ribosomes with tethered subunits. *Nature*. **524**, 119–124 (2015).

282. K. Kitahara, T. Suzuki, The Ordered Transcription of RNA Domains Is Not Essential for Ribosome Biogenesis in Escherichia coli. *Molecular Cell*. **34**, 760–766 (2009).

283. E. Afonina, N. Chichkova, S. Bogdanova, A. Bogdanov, 30S ribosomal subunits with fragmented 16S RNA: a new approach for structure and function study of ribosomes. *Biochimie*. **73**, 777–787 (1991).

284. T. Yokoyama, T. Suzuki, Ribosomal RNAs are tolerant toward genetic insertions: evolutionary origin of the expansion segments. *Nucleic Acids Res*. **36**, 3539–3551 (2008).

285. A. A. Szewczak, T. R. Cech, An RNA internal loop acts as a hinge to facilitate ribozyme folding and catalysis. *RNA* (1997).

286. W. H. Schmied, Z. Tnimov, C. Uttamapinant, C. D. Rae, S. D. Fried, J. W. Chin, Controlling orthogonal ribosome subunit interactions enables evolution of new function. *Nature*. **564**, 444 (2018).

287. S. Ude, J. Lassak, A. L. Starosta, T. Kraxenberger, D. N. Wilson, K. Jung, Translation Elongation Factor EF-P Alleviates Ribosome Stalling at Polyproline Stretches. *Science*. **339**, 82–85 (2013).

288. L. K. Doerfel, I. Wohlgemuth, C. Kothe, F. Peske, H. Urlaub, M. V. Rodnina, EF-P Is Essential for Rapid Synthesis of Proteins Containing Consecutive Proline Residues. *Science*. **339**, 85–88 (2013).

289. G. Blaha, R. E. Stanley, T. A. Steitz, Formation of the First Peptide Bond: The Structure of EF-P Bound to the 70S Ribosome. *Science*. **325**, 966–970 (2009).

Publications

Rae, Christopher D., Yuliya Gordiyenko, and V. Ramakrishnan. 2019. "How a circularized tmRNA moves through the ribosome." *Science* 363 (6428): 740–744.

Huang, Yueyang, John N. Alumasa, Lauren T. Callaghan, R. Samuel Baugh, **Christopher D. Rae**, Kenneth C. Keiler, and Shauna M. McGillivray. 2019. "A small-molecule inhibitor of trans-translation synergistically interacts with cathelicidin antimicrobial peptides to impair survival of Staphylococcus aureus." *Antimicrobial Agents and Chemotherapy* 63 (4): e02362-18.

Schmied, Wolfgang H., Zakir Tnimov, Chayasith Uttamapinant, **Christopher D. Rae**, Stephen D. Fried, and Jason W. Chin. 2018. "Controlling orthogonal ribosome subunit interactions enables evolution of new function." *Nature* 564 (7736): 444–448.